Universidad de Cantabria

E.T.S Ingenieros de Caminos, Canales y Puertos

Dpto. de Ciencias y Técnicas del Agua y del Medio Ambiente

Doctoral Thesis

Modelado Numérico y Estadístico de la Componente Meteorológica del Nivel del Mar a Escala Regional y Global

---

Numerical and Statistical Modelling of the Atmospheric Surge at Regional and Global Scale

---

Author:
Alba Cid Carrera

Supervisors:
Dra. Sonia Castanedo Bárcena
Dr. Raúl Medina Santamaría

Environmental Hydraulics Institute "IH Cantabria"

June 2015

Always look on the bright side of life

Monty Python's Life of Brian

Preface

The general objective of this thesis is to further enhance our knowledge in one of the variables that determine the sea level: the atmospheric surge.

The atmospheric surge is defined as the component of the sea level that is driven by the wind stress and the pressure gradients. In this thesis, the study of the atmospheric surge is faced from different approaches that include the numerical modelling, the statistical modelling and the analysis of the extreme events.

First, a numerical model was used to simulate the atmospheric surge in an area covering Southern Europe that includes the Mediterranean Sea, the Iberian Atlantic Ocean and the Canary Islands region. Two high resolution databases were developed for this area using two different atmospheric forcings, which enabled us to test the sensitivity of the surge to the forcing resolution. The results of this dynamical simulation were validated with tide gauges at coastal areas and with satellite measures throughout all the domain, and then used to study the surge variability in terms of seasonality and trends.

In a next step, an extreme analysis was applied to the simulated surge to also describe the characteristics of the surge in terms of extreme events (storm surges). The extreme values were selected, from one of the hourly databases mentioned above, using the Peak Over Threshold method (POT). Following, a time-dependent statistical model was used to characterise the long term trends of the magnitude, duration and number of storm surges that occur every year, as well as to estimate the 50-year return level. Finally, the correlation of the storm surges and the North Atlantic Oscillation was also studied.

Lastly, the atmospheric surge was estimated from a statistical point of view. The numerical modelling requires a high computational effort, and hence, when the time coverage or the spatial extent under study is large, a different approach should be considered. In this chapter of the thesis, we use a multivariate regression model to statistically reconstruct surge levels from the 20th Century Reanalysis. This is done by finding the relationship between the atmospheric fields (mean sea level pressures) and the surge. This statistical simulation allowed us to developed a global atmospheric surge database that covers the period from the end of the XIX century to the present.

According to the general objective of this thesis, the study of the atmospheric surge from these different viewpoints, contributed to a better understanding of this sea level component, giving insights of their characteristics at different temporal and spatial scales, and also about the advantages and shortcomings of the different simulation methods.

Acknowledgements

A pesar de la "presión social" para que escriba unos agradecimientos al estilo clásico, tengo la cabeza muy dura y poca facilidad para compartir mis sentimientos; así que me limitaré a agradecer a mis directores, Sonia y Raúl, la oportunidad que me concedieron para iniciar este doctorado, la confianza depositada y la ayuda proporcionada durante todos estos años, y que ha dado lugar a esta tesis. No puedo no mencionar a Fer, que aunque será parte del tribunal, ha aportado tanto a esta tesis que merecería que su nombre figurase junto al de los directores. Tampoco puedo obviar a todos aquellos compañeros, y que en muchas ocasiones son también amigos, que me han echado una mano en todo este proceso. Para terminar, agradeceros a las (y los) que sabéis que formáis una parte importante de mi vida, simplemente ese hecho, que seáis parte de mi.

Contents

List of Figures

List of Tables

Adicado a miña familia

Resumen en castellano

De acuerdo con la normativa de estudios de doctorado de la Universidad de Cantabria en relación a los requerimientos exigidos para aquellas tesis redactadas en un idioma diferente al español, aprobada por Junta de Gobierno de 12 de marzo de 1999 y actualizada a 18 de diciembre de 2013, a continuación se presenta un resumen suficientemente extenso del documento original redactado en inglés.

1 Introducción

1.1 Motivación y antecedentes

Se denomina marea meteorológica a la componente meteorológica del nivel del mar, que se define como la variación de nivel debida a los efectos de la presión y el viento sobre la superficie del mar. La marea meteorológica juega un papel importante en la variación del nivel del mar y, a diferencia de otras componentes del nivel del mar, como la marea astronómica que tiene un comportamiento determinista, la marea meteorológica depende de los gradientes de presión y de la tensión superficial viento, es por tanto una variable estocástica que necesario analizar a partir de datos disponibles o a partir de su modelado.

La magnitud de la marea meteorológica es variable a lo largo del planeta; los niveles más elevados se encuentran en las costas del norte de Europa, pudiendo alcanzar valores superiores a 1 m. Aunque la marea meteorológica también tiene efecto en el medio de mares y océanos, es en la costa donde adquiere mayor importancia puesto que el efecto del viento contribuye a acumular el agua hacia la costa con una magnitud inversamente proporcional a la profundidad. Por tanto, en océano abierto son los gradientes de presión los que más influyen en el nivel de la marea meteorológica, mientras que cerca de la costa es el viento el que juega un papel fundamental.

Las zonas costeras son por tanto especialmente vulnerables a la variabilidad climática y a los cambios en el nivel del mar. Para analizar los posibles impactos en la costa, es necesario disponer de series largas de datos que describan esta variable. Desafortunadamente, los datos de mareógrafos no cubren todas las costas de nuestro planeta, y además no suelen consistir en un registro continuo en el tiempo, sino que contienen huecos debido a paradas de mantenimiento o a fallos, sobre todo durante eventos extremos. Por otro lado, los mareógrafos registran el nivel total, es decir, incluyen el nivel debido a la marea

astronómica, a la meteorológica, así como el debido a la componente estérica (variaciones debidas a cambios en el volumen del agua asociados a cambios en la temperatura) y al aporte de masa (debido al derretimiento del hielo). Existen métodos, como el análisis armónico (Pawlowicz et al., 2002), que permiten separar la componente astronómica de la señal total, quedando el "residuo", que es la variación de nivel debida a la componente meteorológica, al aporte de masa y a la señal estérica (aunque estas últimas son de pequeña magnitud en el corto plazo). En resumen, obtener la señal correspondiente a la marea meteorológica a partir de los datos de mareógrafos no es una tarea simple y requiere un procedimiento cuidadoso.

Para salvar las limitaciones que tiene el estudio de la marea meteorológica a partir de datos de mareógrafos, el modelado de esta componente del nivel del mar se ha convertido en una de las herramientas más útiles para generar bases de datos homogéneas y de larga duración. En la tesis, esto se aborda desde dos perspectivas diferentes: el modelado numérico y el modelado estadístico.

Existen numerosos modelos de circulación oceánica capaces de reproducir procesos oceánicos, entre ellos la marea meteorológica. Estos modelos necesitan como datos de partida, información relativa a la presión atmosférica a nivel del mar y a la velocidad y dirección del viento, así como información sobre la batimetría de la zona de estudio; con estos datos y resolviendo las ecuaciones de gobierno de las ondas largas, los modelos numéricos son capaces de reproducir la variación del nivel del mar debida a los gradientes de presión atmosférica y a la tensión que el viento ejerce sobre la superficie del mar. La dificultad del uso de modelos numéricos reside en la adecuada elección del valor de los parámetros necesarios para la resolución de las ecuaciones que definen el modelo. Normalmente se lleva a cabo un proceso de calibración y validación que permite determinar la exactitud de los resultados, mediante por ejemplo, la comparación con los registros de mareógrafos.

Una alternativa a los modelos numéricos son los modelos estadísticos, que se basan en encontrar la relación existente entre la marea meteorológica y el forzamiento atmosférico que la origina. Una vez establecida esta relación estadística, es posible reconstruir la señal de la marea meteorológica a partir de los campos atmosféricos, lo que resulta en un ahorro considerable de tiempo y recursos computacionales.

Otra opción que nos permite obtener un valor aproximado de la marea meteorológica es el uso de la relación del barómetro inverso, que básicamente relaciona el nivel del mar, con cambios en la presión atmosférica media en superficie. La relación del barómetro inverso expone que por cada milibar de disminución (aumento) de la presión con respecto a la presión media, se produce un aumento (descenso) del nivel del mar de 1 cm. Esto se conoce como aproximación estática, ya que sólo tiene en cuenta la presión, despreciando

los efectos del viento. Por tanto, esta relación puede ser válida lejos de la costa, mientras que cerca, donde los efectos del viento son muy importantes, la relación del barómetro inverso no es capaz de representar correctamente la marea meteorológica.

El paso siguiente, una vez que se disponen de bases de datos homogéneas y de larga duración, es el análisis de los eventos extremos de marea meteorológica, que como ya se ha mencionado, son uno de los fenómenos que más pueden afectar a las regiones costeras.

Esta tesis está por tanto orientada a ahondar en el estudio que los efectos del viento y la presión tienen sobre la variación del nivel del mar; esto es, la marea meteorológica.

1.2   Objetivos de la tesis

El objetivo general de la tesis es profundizar en el conocimiento de la marea meteorológica, tanto en términos de su modelado como en el estudio de sus niveles extremos. Para alcanzar este objetivo general, se plantean tres objetivos específicos:

- **Explorar la habilidad de los modelos numéricos para simular la marea meteorológica**, creando dos nuevas bases de datos de alta resolución para el sur de Europa, y comprobar la sensibilidad de los resultados a la resolución del forzamiento atmosférico.

- **Analizar los niveles extremos de marea meteorológica**, estudiando cambios de largo de plazo en la intensidad, la frecuencia y la duración de los eventos extremos, y analizando la sensibilidad de los extremos a la Oscilación del Atlántico Norte (NAO).

- **Explorar la habilidad de los modelos estadísticos para reproducir la marea meteorológica**, utilizando un reanálisis atmosférico para reconstruir estadísticamente la marea meteorológica, generando una base de datos global que se extiende en el tiempo desde el año 1871 al 2010.

1.3   Organización de la tesis

La estructura de la tesis se organiza como sigue:

El capítulo 1, describe la motivación que ha llevado al desarrollo de esta tesis y proporciona una visión general sobre el estado del conocimiento en este campo para facilitar la comprensión de los siguientes capítulos. Los siguientes tres capítulos (capítulos 2, 3 y 4) dan respuesta a los objetivos específicos arriba planteados. Cada capítulo está compuesto

de un pequeño resumen, una introducción, la descripción de la metodología y los datos usados, así como la presentación de los resultados obtenidos y las conclusiones extraídas. Cada capítulo constituye en sí mismo una versión editada de artículos publicados, o enviados para su revisión, en revistas científicas indexadas dentro del SCI (Science Citation Index). Finalmente, el capítulo 5 proporciona unas conclusiones generales y marca las futuras líneas de investigación.

A continuación se proporciona una breve descripción del contenido de cada capítulo, que será ampliada en los apartados 2, 3 y 4 de este resumen en castellano:

- **Capítulo 2. Modelado numérico de la marea meteorológica en el sur de Europa: Base de datos GOS**

  En este capítulo se desarrollan, mediante modelado numérico, dos bases de datos de marea meteorológica llamadas GOS 1.1 y GOS 2.2 (Global Ocean Surges, por sus siglas en inglés). Estas dos bases de datos se diferencian en los campos atmosféricos utilizados como forzamiento por el modelo. En un caso, el forzamiento atmosférico es SeaWind I que consiste en un downscaling dinámico, de 30 km de resolución espacial, del reanálisis global NCEP. En el segundo caso, el forzamiento que se utiliza es SeaWind II, downscaling dinámico del reanálisis global ERA-interim, y que en este caso posee una resolución espacial de 15 km. En este apartado se describe el modelo numérico utilizado (modelo ROMS) y su configuración, así como también se validan los resultados obtenidos con datos de mareógrafos y de satélites. Comparar los resultados de GOS 1.1 y GOS 2.1 permitirá comprobar la sensibilidad de la marea meteorológica al forzamiento atmosférico. Al final de este capítulo, se analiza también la variabilidad estacional y las tendencias de largo plazo.

- **Capítulo 3. Cambios de largo plazo en la intensidad, frecuencia y duración de los eventos extremos de marea meteorológica en el sur de Europa**

  En este capítulo, se parte de la base de datos GOS 1.1 para estudiar las características de los eventos extremos de marea meteorológica. En concreto, mediante el uso de un modelo estadístico de extremos no estacionario, se caracterizan los cambios en la frecuencia (tasa de ocurrencia anual), intensidad (magnitud de los extremos) y duración de los eventos extremos. Estos extremos se seleccionan utilizando la técnica de excedencias sobre un umbral (Peak Over Threshold) y se modelan combinando la distribución generalizada de pareto (Generalized Pareto Distribution) y el proceso de Poisson. En este apartado también estudiaremos la relación de los extremos de marea meteorológica con la Oscilación del Atlántico Norte, ya que la NAO es uno de los principales causantes de las variaciones de largo plazo en el área noratlántica.

- **Capítulo 4. Reconstrucción estadística global de la marea marea meteorológica a partir del reanálisis *20th Century Reanalysis (1871-2010)***

En este capítulo, describimos la metodología para la generación de una base de datos global de marea meteorológica mediante técnicas estadísticas. En un primer paso, se obtiene la relación estadística entre una base de datos global de marea meteorológica desarrollada por AVISO (DAC, Dynamic Atmospheric Correction) y su forzamiento, que son campos atmosféricos del reanálisis global ERA-interim. En un siguiente paso, la relación estadística obtenida (basada en regresión lineal múltiple) se utiliza para reconstruir el nivel de marea meteorológica a nivel global, partiendo de los datos atmosféricos de otro reanálisis que abarca desde 1871 a 2010 (20th Century Reanalysis).

2 Modelado numérico de la marea meteorológica en el sur de Europa: Base de datos GOS

Este apartado constituye un resúmen del artículo de investigación publicado en la revista Climate Dynamics por Cid, A., Castanedo, S., Abascal, A. J., Menéndez, M., y Medina, R. en 2014 con el título "A high resolution hindcast of the meteorological sea level component for Southern Europe: the GOS dataset". doi: 10.1007/s00382-013-2041-0

2.1 Introducción

Existe un creciente interés en el estudio del efecto que la presión atmosférica y el viento producen sobre la superficie del mar, sobre todo debido a su importante contribución al nivel del mar durante eventos de inundación. Las zonas que se ven más afectadas son las zonas costeras, que a su vez son especialmente vulnerables al cambio y la variabilidad climática. La marea meteorológica, causada principalmente por bajas presiones y viento fuerte, se ve afectada por cambios en los patrones climáticos (Flather et al., 1998; Lowe et al., 2001; Woth et al., 2006). Para analizar y entender estos cambios, se necesitan series temporales largas de los niveles de marea meteorológica. Desafortunadamente, los datos reales que proporcionan las redes de medida (mareógrafos principalmente) son escasos y presentan limitaciones en cuanto a las escalas temporales y espaciales que cubren. Es más, los datos provenientes de mareógrafos normalmente presentan periodos donde no hay datos registrados, lo que introduce incertidumbre y dificulta el estudio. Para salvar estas limitaciones, los modelos numéricos se han convertido en una de las herramientas más útiles para generar bases de datos de alta resolución espacial y temporal.

Recientemente, muchos estudios han tratado de entender y cuantificar los cambios en la marea meteorológica mediante el uso de bases de datos numéricas. Estas bases de datos pueden utilizarse de la misma manera que las observaciones para un amplio abanico de estudios, que analizan por ejemplo valores extremos (Flather et al., 1998; Marcos et al., 2009), variabilidad decadal (Butler et al., 2007), frecuencia de eventos extremos de marea meteorológica (Bernier and Thompson, 2006) o los efectos del cambio climático sobre esta componente del nivel del mar (Flather, 2000; Jordà et al., 2012; Wang et al., 2008).

Para un dominio espacial similar al presentado en este capítulo de la tesis (sur de Europa), Sebastião et al. (2008) desarrollaron una base de datos de nivel del mar que incluye la señal astronómica y la meteorológica. Por otro lado, Ratsimandresy et al. (2008) presentaron una base de datos de marea meteorológica para el Mediterráneo.

Hoy en día, para reproducir adecuadamente los fenómenos de mesoescala, los esfuerzos se centran en aumentar la resolución del forzamiento atmosférico (Brown et al., 2010; Eric Jones and Davies, 2006; Wang et al., 2008). Esto nos indica que para reproducir de forma precisa la marea meteorológica son necesarios datos atmosféricos de alta resolución. En este estudio, se utilizan dos forzamientos diferentes que nos permitirán investigar la sensibilidad del los resultados al campo atmosférico. Del uso de dos forzamientos distintos, resulta la generación de dos bases de datos diferentes de marea meteorológica. Los dos conjuntos de datos se engloban dentro de la base de datos GOS (Global Ocean Surge). Estas bases de datos representan la variación del nivel del mar debido al viento y la presión de forma continua en el tiempo, no son sólo simulaciones específicas durante tormentas.

2.2   Descripción de la base de datos

La base de datos GOS se ha desarrollado utilizando el modelo ROMS (Regional Ocean Modeling System, Haidvogel et al. 2008; Shchepetkin and McWilliams 2005). El dominio espacial va desde los 25°a los 46°N en latitud y desde los -20°a los 37°E en longitud, con una resolución espacial de $1/8°(\sim 14$ km). La batimetría se extrae de ETOPO 2, que es una base de datos topográfica y batimétrica global de 2 min de resolución (Smith and Sandwell, 1997).

El modelo ROMS se ejecuta con configuración 2D y la variación de nivel del mar obtenida de la relación del barómetro inverso se impone como señal en los contornos. Como forzamiento atmosférico se usan dos bases de datos diferentes: *SeaWind I* (30 km de resolución horizontal) y *SeaWind II* (15 km de resolución horizontal). Estos datos atmosféricos se han obtenido mediante un downscaling dinámico de los reanalisis NCEP y ERA-interim, respectivamente, y han sido validados exhaustivamente mediante observaciones (más detalles en Menendez et al. 2014). Estos forzamientos de resolución temporal horaria, se han interpolado a la resolución espacial de la malla de ROMS (1/8°).

En resumen, se han desarrollado dos bases de datos de marea meteorológica:

1. GOS 1.1 que es una base de datos horaria con resolución espacial de 1/8°desde 1948 a 2009 forzado con SeaWind I (30 km).

2. GOS 2.1 que posee la misma resolución espacial y temporal pero está forzado con SeaWind II y cubre el periodo 1989-2009 (15 km).

2.3 Validación de la base de datos

Los niveles de marea meteorológica obtenidos con el modelo ROMS se han comparado con datos de 58 mareógrafos distribuidos a lo largo del dominio de cálculo. La validación también se ha hecho con datos de altímetro para cubrir áreas donde no existen datos de mareógrafos. En el caso de la validación con mareógrafos, se ha utilizado la librería t-tide (Pawlowicz et al., 2002) para separar la componente de marea astronómica y poder comparar la señal resultante (residuo) con los datos simulados numéricamente. Esta validación se ha hecho comparando con el punto GOS más cercano al mareógrafo y obteniendo parámetros estadísticos que cuantifican el ajuste de los datos (coeficiente de correlación ρ y error cuadrático medio $RMSE$). Los resultados de la validación con mareógrafos pueden verse en la Fig.1 y Fig.2
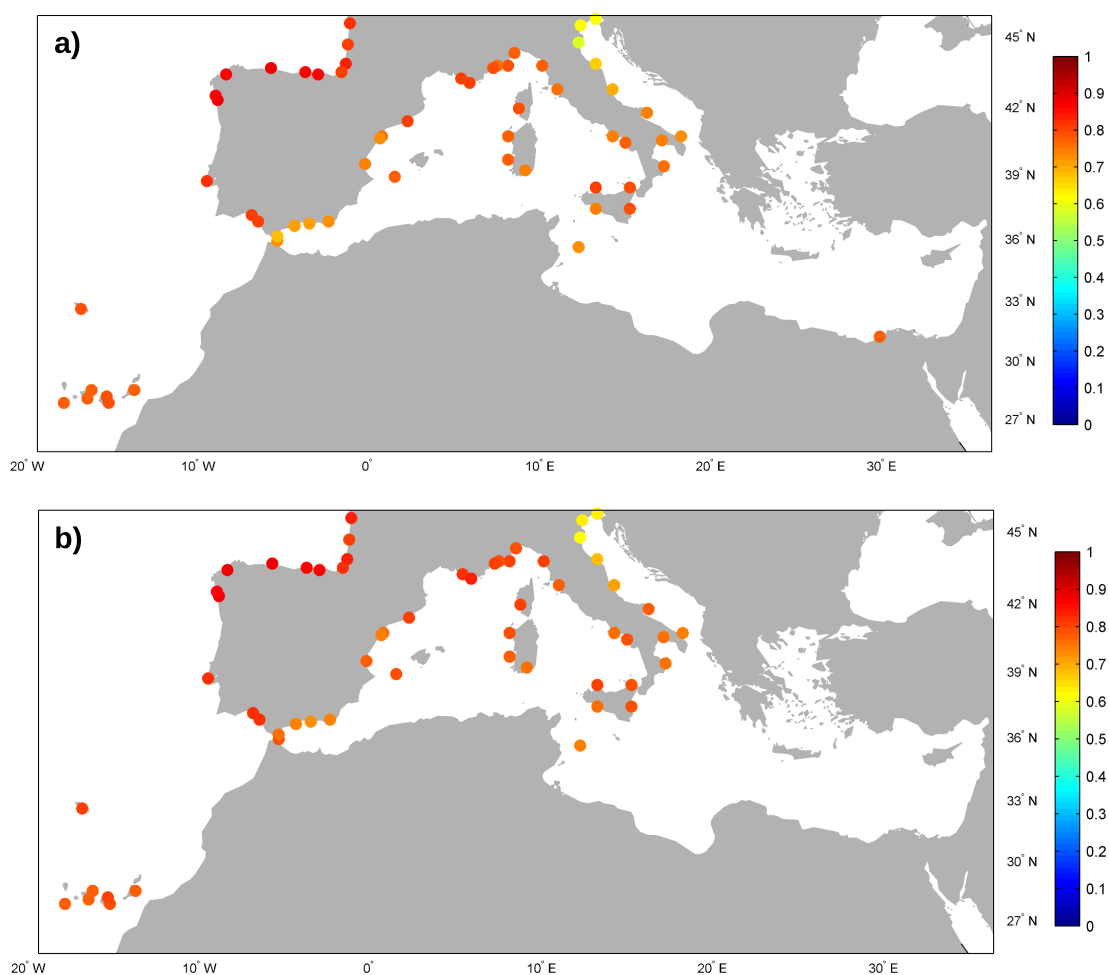
Figura 1: Coeficiente de correlación (ρ) entre la señal de marea meteorológica de los mareógrafos y de las bases de datos GOS. a) GOS 1.1 b) GOS 2.1.

Tal y como se recoge en las Fig.1 y 2, el coeficiente de correlación es mayor de 0.8 en la parte Atlántica del dominio (llegando a 0.85 en los mareógrafos situados en la costa norte de la Península Ibérica) y de alrededor de 0.75 en la zona del Mediterráneo. El
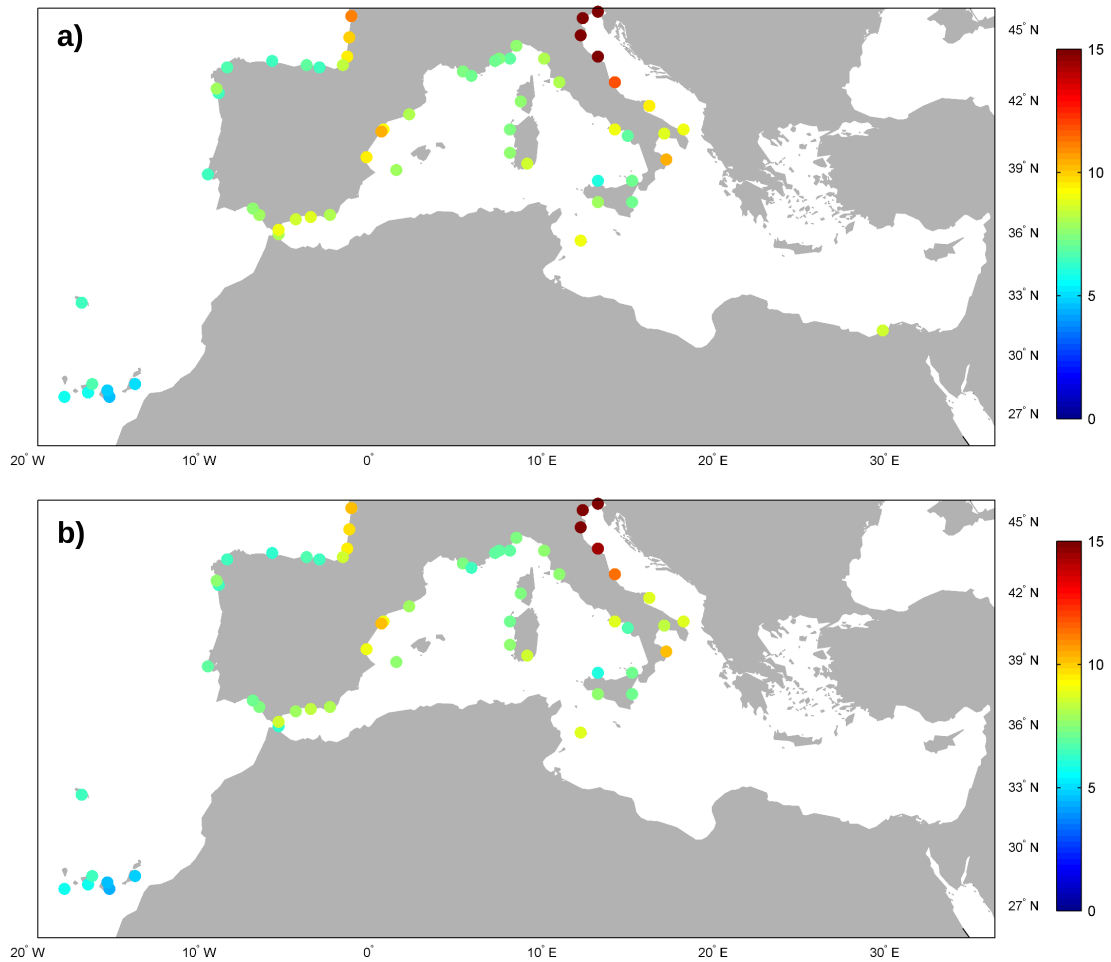
Figura 2: Error cuadrático medio (*RMSE*) entre la señal de marea meteorológica de los mareógrafos y de las bases de datos GOS. Las unidades son cm. a) GOS 1.1 b) GOS 2.1.

RMSE alcanza valores máximos de unos 10 cm, lo que representa un 10 % de error con respecto a la variabilidad máxima registrada por el mareógrafo. Una excepción es la zona del Adriático Norte, donde se obtienen correlaciones menores y errores mayores, debido probablemente a que es una zona somera donde la batimetría y los parámetros de fricción usados en el modelado numérico juegan un papel determinante.

Por otra parte, hay que mencionar que la señal de un mareógrafo y la de GOS no representan exactamente los mismos fenómenos físicos, por lo que deben existir diferencias en la comparación. La variación del nivel en GOS se debe estrictamente a los gradientes de presión y a la tensión superficial del viento, mientras que de la serie de nivel del mareógrafo sólo se ha eliminado la componente astronómica, es decir, permanecen las variaciones debidas a procesos locales como la señal estérica y la influencia de ríos.

De las Fig.1 y 2 también se concluye que los resultados de la validación son muy similares para GOS 1.1 y GOS 2.1, por lo que, en este caso, la influencia de la resolución

del forzamiento atmosférico en los resultados de marea meteorológica es prácticamente despreciable. Sin embargo, habría que comprobar si a escala más local (zonas costeras, estuarios...) la resolución del forzamiento afecta más significativamente a los resultados.

En cuanto a la validación con satélites, se han utilizado datos de anomalías de nivel del mar (distribuidos por Aviso, `http://www.aviso.altimetry.fr/en/data/products/sea-surface-height-products/global/sla.html`) a los que se ha añadido la señal correspondiente a la marea meteorológica (DAC, Dynamic Atmospheric Correction, también distribuida por Aviso), previamente eliminada en el procesado de los datos de satélite pero que también proporciona Aviso (`http://www.aviso.altimetry.fr/en/data/products/auxiliary-products/atmospheric-corrections.html`). Para la comparación con los datos numéricos, se ha dividido el dominio en zonas de 1°x 1°y en cada una de ellas se comparan los datos de satélite con los datos del nodo más cercano de GOS. El análisis estadístico se hace para cada una de las zonas y para el periodo 1992-2009, puesto que los datos de satélite comienzan en 1992. Aunque la validación se ha realizado para las dos bases de datos GOS, los resultados son muy similares y sólo se muestra la figura correspondiente a GOS 2.1 (Fig.3).

Como puede observarse en la Fig.3, el ajuste entre los datos de satélite y los numéricos (GOS 2.1) es bueno, obteniendo valores de ρ superiores a 0.75 en todo el dominio y valores máximos de $RMSE$ de 8 cm en el Atlántico y 10 cm en el Mediterráneo, con excepción del Adriático Norte, el Golfo de Gabes y el Mar Egeo. En estas 3 zonas someras y semi-encerradas, la menor precisión de los resultados se puede explicar en términos de la limitación de datos disponible (como por ejemplo la batimetría) o de la descripción de procesos físicos (por ejemplo los coeficientes de fricción). Algunos autores (e.g. García-Lafuente et al. 2004; Marcos and Tsimplis 2007) sugieren que la señal estérica es más importante en el Mediterráneo que en el Atlántico, lo que explicaría la diferencia en el $RMSE$ encontrada entre esas dos áreas.

2.4 Variabilidad de la marea meteorológica

En este apartado, se hace un análisis de la variabilidad y las tendencias a largo plazo de la marea meteorológica de GOS. Para ello, se analizan medias mensuales y estacionales y se obtienen las tendencias mediante un ajuste lineal en cada punto de la malla. Investigamos las tendencias durante dos periodos, uno de más largo plazo desde 1948 a 2009 (GOS 1.1) y otro más reciente de 1989 a 2009 (GOS 2.1). Las tendencias para el periodo 1948-2009 son negativas en todo el dominio aunque de pequeña magnitud, con valores máximos de -0.35 mm/año. Para el periodo 1989-2009 las tendencias son positivas y de mayor magnitud a lo largo de todo el dominio. El sector Atlántico presenta tendencias
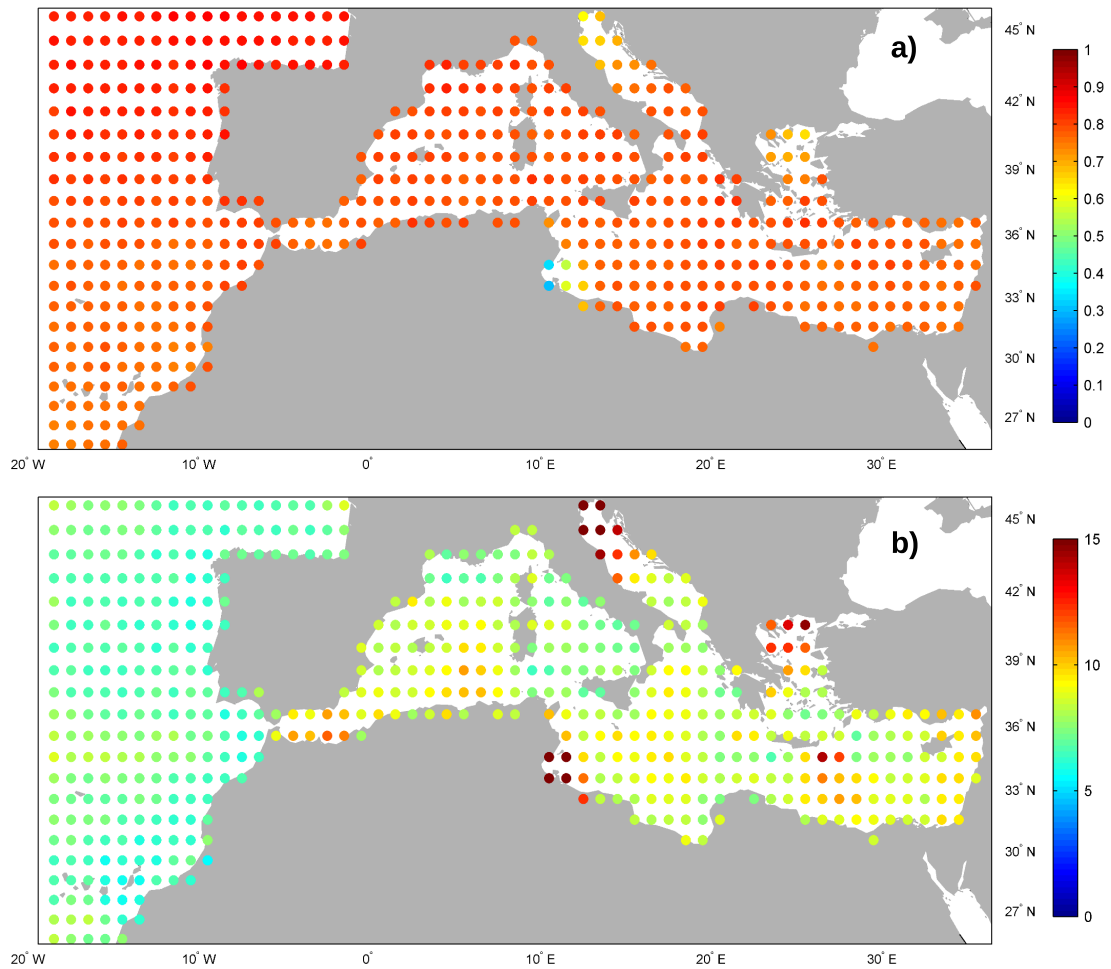
Figura 3: Comparación entre GOS 2.1 y los datos de altímetro. a) Coeficiente de correlación (ρ), b) Error cuadrático medio en cm (RMSE)

más o menos uniformes de 0.5 mm/año mientras que en el Mediterráneo existe más variación espacial, con valores entre 0.6 y 1.5 mm/año. Gomis et al. (2008) calcularon las tendencias para distintos periodos y también obtuvieron tendencias de signo distinto en función del periodo analizado: negativas para el periodo 1958-2001 y positivas para un periodo más reciente (1993-2001).

2.5 Conclusiones

El principal objetivo de este estudio ha sido la generación de dos bases de datos de marea meteorológica de alta resolución espacial (1/8°) y temporal (1 hora) para el sur de Europa. Esto se ha llevado a cabo mediante el uso del modelo numérico ROMS, con el que se han creado dos bases de datos distintas, y donde la diferencia reside en el forzamiento atmosférico utilizado: SeaWind I que tiene 30 km de resolución horizontal y es un downscaling dinámico del reanálisis NCEP; y Seawind II, de 15 km de resolución

y obtenido mediante downscaling dinámico de ERA-interim. Esto ha dado lugar a GOS 1.1 (1948-2009) y GOS 2.1 (1989-2009), respectivamente.

Las diferencias en la validación de ambas bases de datos son mínimas, por lo que la influencia de la resolución del forzamiento atmosférico en los resultados de marea meteorológica no es significativa. Sin embargo, hay que tener en cuenta que ambos forzamientos son ya de alta resolución, mientras que en estudios de otros autores como Wakelin and Proctor (2002) donde sí ven una clara influencia, los forzamientos que comparan tienen muy diversas resoluciones espaciales y temporales.

La validación con datos de satélite ha permitido la identificación de ciertas áreas donde las bases de datos GOS no representan correctamente el nivel de marea meteorológica, identificación que no hubiese sido posible sólo con la validación con mareógrafos, puesto que son zonas sin medidas disponibles. En estas zonas, GOS sobrestima los datos de satélite. Si la razón de estas diferencias estuviese en que el forzamiento atmosférico no tiene suficiente resolución, la marea meteorológica debería verse subestimada (Wakelin and Proctor, 2002) y no al contrario. Es por esto que la falta de exactitud detectada en las áreas relativamente someras y semi-encerradas, se deba probablemente a la batimetría o los parámetros de fricción usados, como ya mencionó Pascual et al. (2008).

Finalmente, con la estimación de las tendencias de largo plazo se comprobó que el periodo utilizado para calcular las tendencias determina el signo de las mismas. La tendencia de los últimos 20 años (1989-2009) es positiva en todo el dominio, mientras que en el más largo plazo (1948-2009) se obtienen tendencias negativas, como también obtuvo Gomis et al. (2008).

3 Cambios de largo plazo en la intensidad, frecuencia y duración de los eventos extremos de marea meteorológica en el sur de Europa

Este apartado constituye un resúmen del artículo de investigación publicado en la revista Climate Dynamics por Cid, A., Menéndez, M., Castanedo, S., Abascal, A. J., Méndez, F.J., and Medina, R. en 2015 con el título "Long-term changes in the frequency, intensity and duration of extreme storm surge events in southern Europe". doi: 10.1007/s00382-015-2659-1

3.1 Introducción

Las áreas costeras son especialmente vulnerables a la variabilidad climática y a cambios en el nivel del mar. Concretamente, los extremos de nivel del mar tienen efectos inmediatos en la costa. Estos extremos se producen normalmente por la combinación de la pleamar astronómica con extremos de marea meteorológica. Mientras que la marea astronómica es una componente determinista del nivel del mar, la marea meteorológica depende del forzamiento atmosférico, por tanto, para estudiar futuros riesgos en la costa es necesario analizar esta variable no determinista desde un punto de vista estadístico.

Los primeros estudios en relación con el análisis extremal, definían los niveles asociados a determinados periodos de retorno ajustando toda la serie de datos a la función de distribución elegida. Este método tiene el inconveniente de que proporciona una estimación de los extremos poco fiable, ya que la mayoría de los datos ajustados están alejados de la cola de la distribución. Recientemente, se han utilizado diferentes aproximaciones estadísticas para estudiar eventos extremos, tanto en términos del método de selección de extremos como en el modelo de extremos elegido. El método de máximos anuales (AMM, Annual Maxima Method) y la función generalizada de extremos (GEV, Generalized Extreme Value distribution) es la aproximación elegida por Bernier and Thompson (2006) para calcular periodos de retorno de extremos de nivel del mar en el noroeste Atlántico. Marcos et al. (2009) seleccionaron los 10 extremos más intensos del año (r-largest method) y los ajustaron a la función generalizada de Pareto (GPD, Generalized Pareto Distribution) constante en el tiempo para así obtener los niveles asociados a periodos de retorno, mientras que para estimar las tendencias usaron percentiles anuales. El método de AMM tiene la desventaja de agrupar una muestra pequeña de eventos extremos y de no considerar todos los extremos absolutos en el análisis. El método de r-largest no tiene el inconveniente de seleccionar una muestra pequeña de datos pero sí de seleccionar un número fijo de eventos extremos en cada periodo. Esto podría ocasionar que se

considerasen eventos extremos en el análisis que sin embargo no son extremos absolutos del total de datos. Méndez et al. (2006) utilizaron una versión dependiente del tiempo del modelo de máximos sobre un umbral (POT, Peak Over Threshold) para analizar las tendencias en la intensidad y la frecuencia de extremos de oleaje. La dependencia temporal del modelo estadístico también fue introducida por Marcos et al. (2011), donde seleccionaron los extremos con el método de los r-largest eventos extremos al año y permitieron variabilidad temporal en los parámetros de la función de distribución con el objetivo de estudiar los cambios en los extremos de marea meteorológica para distintos escenarios de cambio climático.

3.2   Descripción de la base de datos

Los eventos extremos de marea meteorológica se han seleccionado a partir de la base de datos numérica GOS 1.1 descrita en el capítulo anterior (Cid et al. 2014), aunque actualizada hasta finales de 2013. Como ya se ha mencionado, esta base de datos recoge la variación del nivel del mar debida a los gradientes de presión y a la tensión del viento en superficie, de forma horaria durante 66 años (1948-2013) y con una resolución espacial de aproximadamente 14 km (1/8°).

3.3   Modelo de valores extremos

El primer paso en el análisis de eventos extremos consiste en la selección de los mismos. En este estudio, la selección se hace con la técnica POT, de manera que se seleccionan todos los eventos que superen un determinado umbral. El umbral elegido es el percentil del 99.5 %, de forma que todos los niveles de marea meteorológica que estén por encima de este umbral, y estén separados por al menos 3 días de diferencia entre ellos (para asegurar la independencia entre eventos), serán considerados en el análisis extremal. La elección del valor del umbral es un punto clave para la correcta modelización de los extremos. Si el umbral es muy bajo, causará un sesgo (bias) en la cola de la distribución asintótica, es decir, se estarán considerando como extremos, eventos que en realidad no lo son, y por tanto las asunciones del modelo no se cumplirán. Si por el contrario el umbral es muy alto, la varianza será muy grande puesto que se estarán considerando muy pocos datos en el análisis. El umbral seleccionado en este estudio asegura una media de 2 eventos extremos al año, lo que respeta las asunciones del modelo.

Una vez seleccionados los extremos, se utiliza el método POT dependiente del tiempo para estimar las tendencias de largo plazo y los niveles de marea meteorológica asociados al periodo de retorno de 50 años. Este método combina la GPD para estudiar la magnitud de las excedencias sobre el umbral y la distribución de Poisson (P) para estudiar la tasa

de ocurrencia de las mismas. Para que el modelo GPD-P sea dependiente del tiempo y poder estimar tendencias, se permite que el parámetro de Poisson y el parámetro de escala de Pareto sean linealmente dependientes del tiempo.

Para analizar si las tendencias obtenidas se deben en parte a la variabilidad decadal-interanual, se estima la relación estadística entre el índice NAO y la frecuencia y magnitud de los extremos de marea meteorológica. Para ello se introduce el índice mensual de la NAO como covariable en el modelo.

3.4 Resultados

La descripción espacial de las variables analizadas se refleja en la Fig.4. Como se puede observar, existe un gradiente latitudinal en el valor del umbral (Fig.4a), siendo este superior a 30 cm a partir de los 40°N y disminuyendo progresivamente hacia el sur, con valores de aproximadamente 10 cm alrededor de las Islas Canarias. Se aprecia también como las magnitudes aumentan en la plataforma continental debido a la sobre-elevación producida por el viento (claramente apreciable en la zona de la costa francesa). En el Mediterráneo, el valor del umbral es en general mayor en la cuenca oeste; los valores más grandes se localizan en 5 zonas semi-encerradas: Golfo de León, Golfo de Gabes, Mar Adriático, Golfo de Sirte y Mar Egeo. Es también en estas zonas, junto con el Mar de Alborán y la zona más este de la cuenca Mediterránea, donde se encuentra el mayor número de eventos extremos (Fig.4b), alcanzando valores de 5 extremos/año. La zona Atlántica experimenta un menor número de eventos extremos, con aproximadamente 2 extremos/año. La Fig.4c muestra la duración media de los eventos, donde se aprecian claramente dos patrones diferentes: la zona Atlántica con duraciones de aproximadamente un día y la zona Mediterránea con duraciones máximas de 15 horas.

Una vez descritas las variables a analizar, se aplica el modelo GPD-P para estimar las tendencias en las 3 variables. Como se observa en la Fig.5a, las tendencias en magnitud son generalmente positivas, aunque no significativas, en la mayor parte del dominio; una excepción son el sur de Grecia, el noroeste de Génova y la zona más este del Mediterráneo, con tendencias de 1 mm/año, y el Mar de Alborán y sur de Sicilia con valores de 0.5 mm/año. La Fig.5b muestra las tendencias en la frecuencia que, si nos fijamos sólo en las significativas, son negativas en todo el dominio con excepción del sur de Grecia donde se registra un incremento del 1.5 %. Los mayores valores de decrecimiento, en torno a un 2 %, se encuentran en la zona centro-sur del Mediterráneo (como por ejemplo el Golfo de Sirte), donde las tendencias son de un -2 %. Las tendencias en la duración se muestran en la Fig.5c, donde se observa un decrecimiento general en el Atlántico y un crecimiento
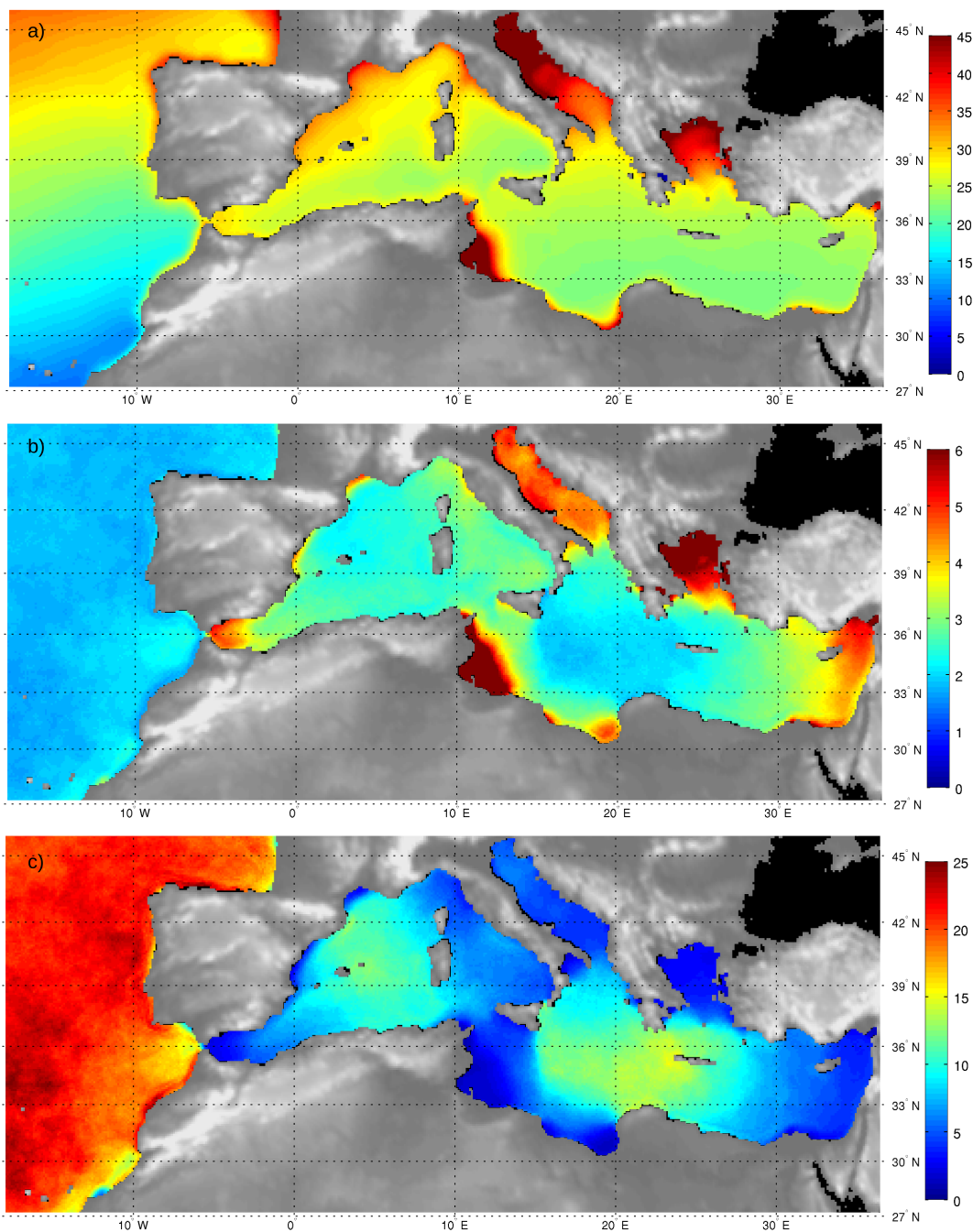
Figura 4: Descripción de los extremos de marea meteorológica. a) valor del umbral del 99.5 % (cm). b) número medio de eventos extremos al año. c) duración media de los eventos extremos (horas).

en el Mediterráneo. Sin embargo, estas tendencias son significativas principalmente en la zona este del Mediterráneo, donde los incrementos pueden llegar a 1.5 horas/año.
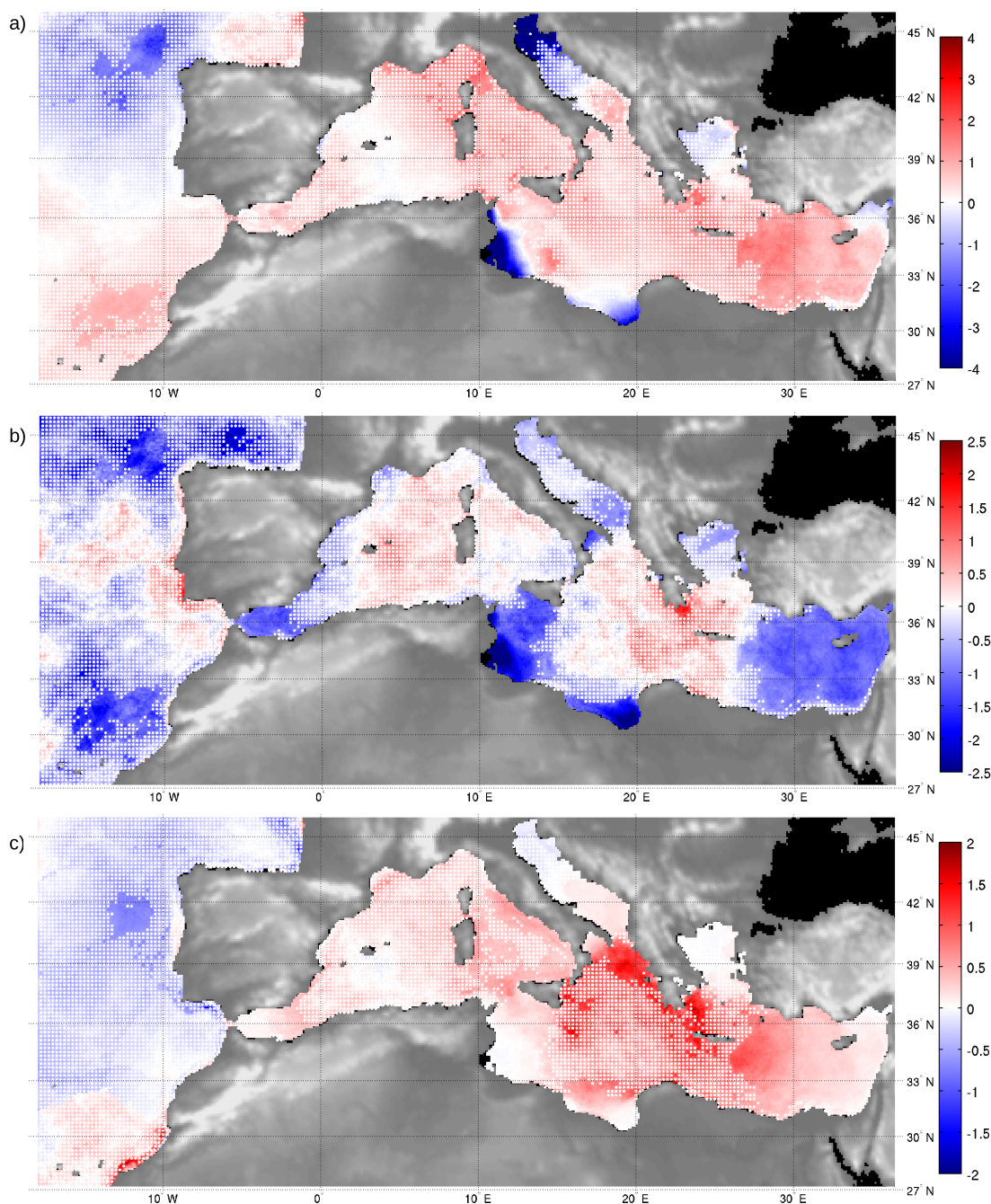
Figura 5: Distribución espacial de las tendencias de largo plazo. Los puntos blancos representan áreas donde la significancia de las tendencias es inferior al 90 %. a) Tendencias en la intensidad (mm/año), obtenidas mediante un ajuste lineal del nivel asociado al periodo de retorno de 50 años. b) Tendencias en la frecuencia (%), obtenidas del parámetro de Poisson dependiente del tiempo y expresado en porcentaje relativo al número total de eventos. c) Tendencias en la duración (horas/año).

Tal y como se deduce de la Fig.5, la mayoría del sur de Europa no presenta tendencias significativas en los extremos de marea meteorológica. Esto puede ser debido a que

estos eventos extremos se vean más afectados por la variabilidad inter-anual o decadal que por variaciones climáticas de mayor escala temporal. La variabilidad atmosférica en la zona está muy influida por la NAO, es por ello que se ha investigado la relación de la marea meteorológica con este índice climático. Concretamente, como se muestra en la Fig.6, se ha analizado la sensibilidad entre el índice mensual de la NAO y la frecuencia y magnitud de los eventos extremos. Se observa que la relación encontrada es mayoritariamente negativa, tanto en términos de intensidad como de frecuencia, lo cual significa que los extremos de marea meteorológica son más frecuentes e intensos cuando la fase de la NAO es negativa. Este es el resultado esperado, puesto que las fases negativas de la NAO se caracterizan por una desviación en la dirección de las tormentas hacia latitudes más bajas y por un debilitamiento del anticiclón sobre las azores, lo que ocasiona un aumento del nivel del mar relacionado con el barómetro inverso. Otro aspecto a destacar es que la NAO influye más en la frecuencia de los extremos que en su magnitud, ya que en su relación con la frecuencia se observan significancias mayores al 90 % en todo el dominio, lo que no ocurre en el caso de la magnitud.

El modelo de extremos utilizado ha permitido también estimar el nivel asociado al periodo de retorno de 50 años, no sólo teniendo en cuenta la magnitud de los eventos extremos sino también su frecuencia

3.5   Conclusiones

El principal objetivo de este estudio ha consistido en establecer el marco estadístico para el estudio de eventos extremos de marea meteorológica. El uso de un modelo de extremos dependiente del tiempo y donde el número de eventos extremos por periodo no se establece de antemano, ha permitido estimar las tendencias de largo plazo en las tres variables consideradas (magnitud, frecuencia y duración). La principal conclusión es que las tendencias no son, en general, significativas, lo que ha llevado a analizar otras fuentes de variabilidad que afecten a la marea meteorológica a una escala de tiempo menos amplia. Para ello se ha analizado la influencia de la NAO en los extremos, encontrando una alta sensibilidad de los mismos a este índice climático, sobre todo en su frecuencia.
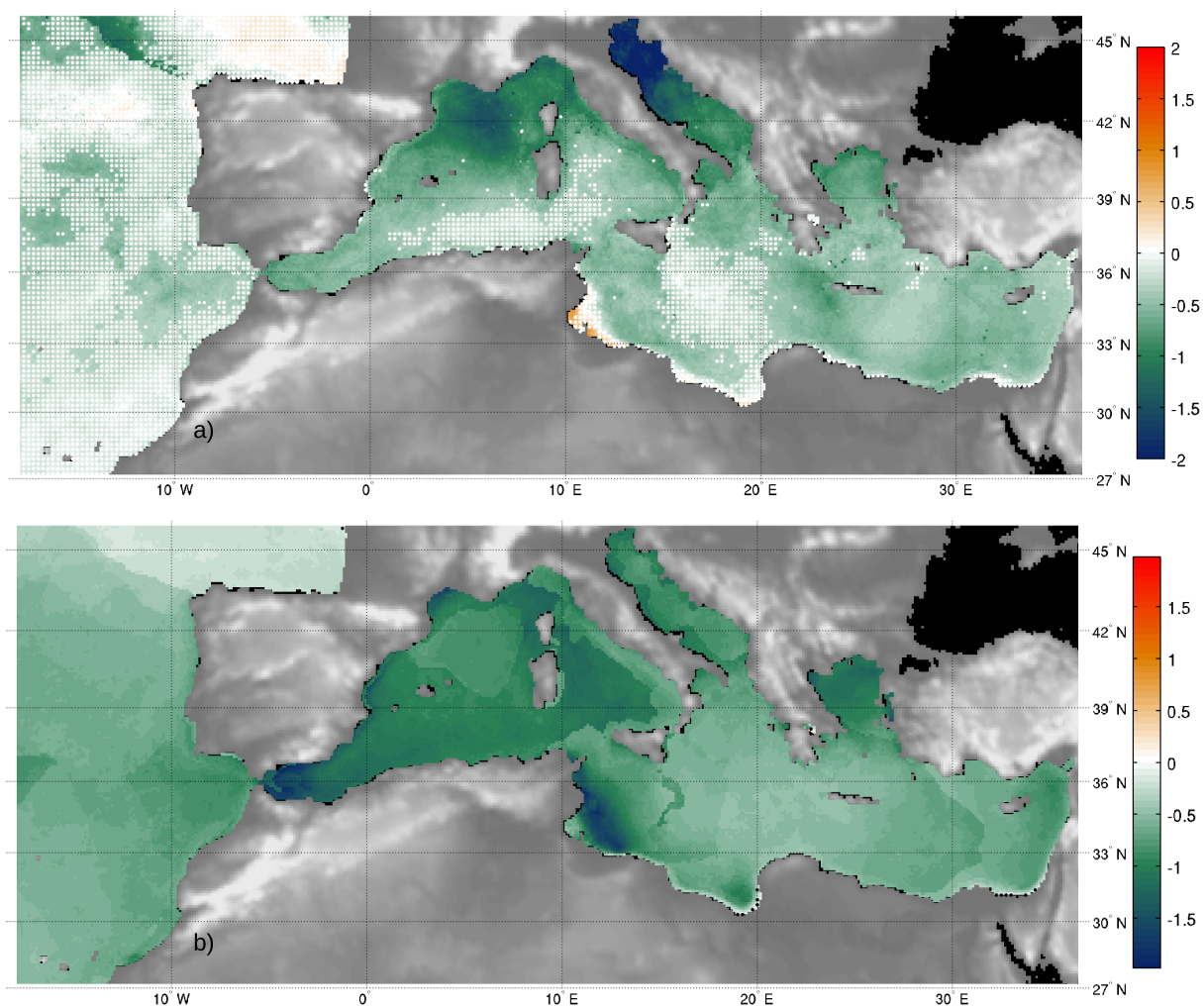
Figura 6: a) Sensibilidad de la intensidad de los extremos a la NAO (cm/ud. índice).
b) Sensibilidad de la frecuencia de los extremos a la NAO (eventos al año/ud. índice).
Los puntos blancos representan áreas donde la significancia es inferior al 90 %.

4 Reconstrucción estadística global de la marea marea meteorológica a partir del reanálisis *20th Century Reanalysis (1871-2010)*

Este apartado constituye un resúmen del artículo de investigación enviado a la revista Global and Planetary Change por Cid, A., Camus, P., Castanedo, S., Méndez, F.J., and Medina, R. en 2015 con el título "Global reconstructed daily surge levels from the 20th Century Reanalysis (1871-2010)".

4.1 Introducción

La marea meteorológica presenta una gran variabilidad espacial a lo largo del globo, sin embargo hasta ahora su análisis se ha centrado en la zona sur de Europa. En este apartado se desarrolla una base de datos de marea meteorológica a escala global, mediante reconstrucción estadística.

Existen distintas técnicas de modelado estadístico ampliamente utilizadas en climatología o en otras variables oceánicas. Las técnicas de downscaling estadístico se pueden clasificar en: funciones de transferencia, tipos de tiempo (weather types) o generadores de tiempo estocásticos (Giorgi et al., 2001). Con respecto al clima marítimo, las funciones de transferencia (o modelos de regresión) han sido aplicadas por Wang et al. (2012) para reconstruir la altura de ola significante a escala global. Por otro lado, Camus et al. (2014b) y Espejo et al. (2014) aplicaron una técnica basada en tipos de tiempo para reproducir el clima marítimo. En cuanto a la marea meteorológica, Dangendorf et al. (2014) compararon el comportamiento a largo plazo de esta variable con la reconstrucción de la misma a partir de campos de viento por medio de una formulación empírico-estadística (Müller-Navarra and Giese, 1999).

En este estudio, en primer lugar se establece la relación estadística que existe entre la base de datos de marea meteorológica global (Dynamic Atmospheric Correction de AVISO, DAC) y el forzamiento atmosférico que la origina (campos de presión del reanálisis ERA-interim). Una vez que este modelo estadístico está calibrado y validado, se usarán los campos atmosféricos de otro reanálisis, que comienza a final del siglo XIX (20th Century Reanalysis, 20CR), para así poder reconstruir la marea meteorológica a escala global y para un periodo de tiempo largo (1871-2010).

4.2 Descripción de las bases de datos

La base de datos de marea meteorológica consiste en la *Dynamic Atmospheric Correction* (DAC, `http://www.aviso.altimetry.fr/`). Es una base de datos generada numéricamente que empieza en septiembre de 1992, con una resolución espacial de 0.25° x 0.25° y temporal de 6 horas, y que utiliza datos de viento y presión procedentes del reanálisis ERA-interim.

El reanálisis atmosférico ERA-interim (Dee et al., 2011) consiste en campos 6-horarios de vientos y presiones (entre otras variables) con una resolución espacial de 0.75°, y que abarca desde 1979 hasta la actualidad, aunque en este estudio utilizaremos sólo los datos del periodo coincidente con DAC (1992-2014). Ambas bases de datos son las que se han utilizado en este estudio para calibrar y validar el modelo estadístico.

Por otro lado, se han empleado los datos de presión atmosférica a nivel del mar (SLP) del 20th Century Reanalysis (Compo et al., 2011). Éstos tienen una resolución espacial de 2° y temporal de 6 horas, y cubren el periodo entre 1871 y 2010. Estos son los datos que se han utilizado para la reconstrucción estadística.

4.3 Metodología del modelo estadístico

El objetivo de la reconstrucción estadística es estimar los niveles de marea meteorológica (predictando) a partir de condiciones atmosféricas locales (predictor) mediante una relación estadística. En concreto, la estimación de niveles máximos diarios de marea meteorológica a partir condiciones atmosféricas medias diarias.

La resolución espacial de la reconstrucción está condicionada por los 2° de resolución del 20CR, por ello, tanto DAC como ERA-interim se han reorganizado con esta resolución espacial. El predictando es por tanto la serie temporal de máximos diarios de marea meteorológica cada 2°. El predictor consiste en la SLP media diaria y los gradientes de la misma, en un área de 4° x 4° alrededor del predictando. Por tanto, el predictor está formado por 9 datos de SLP y 9 datos de gradiente de SLP, lo que hace un total de 18 componentes. Para reducir la dimensionalidad se aplica un análisis de componentes principales y se seleccionan las componentes que explican el 95 % de la varianza. A continuación se ajusta el modelo de regresión lineal, estimando en cada punto el nivel de marea meteorológica como una combinación de las componentes principales (PCs) más importantes del predictor. Como se observa en la Ec.1, para una determinada localización (x_i), los niveles se pueden estimar como una combinación de n PCs, que varían a lo largo del dominio.

$$MareaMeteorologica(x_i,t) = a_i + b_{1,i} \times PC_{(1)}(x_i,t) + b_{2,i} \times PC_{(2)}(x_i,t) + ... + b_{n,i} \times PC_{(n)}(x_i,t)$$
$$(1)$$

donde n es el número de PCs que se utilizan en la reconstrucción y $a_i, b_{1,i}, ..., b_{n,i}$ son los coeficientes obtenidos del modelo de regresión.

Una vez definido el modelo estadístico, se obtienen las PCs del predictor del reanálisis 20CR, para así, utilizando los coeficientes obtenidos en la Ec.1, reconstruir la marea meteorológica en todo el globo.

4.4   Validación del modelo estadístico y reconstrucción global

Una vez llevada a cabo la reconstrucción global de la marea meteorológica utilizando los predictores de 20CR, se selecciona el periodo coincidente con DAC (periodo de control) para comprar los resultados de la reconstrucción con los datos originales de DAC. En la Fig.7 se muestra la calidad de la reconstrucción por medio de tres parámetros estadísticos: el coeficiente de correlación (ρ), el error cuadrático medio (RMSE), y el RMSE relativo a la máxima variabilidad de la marea meteorológica en la zona. Se observa que las correlaciones son superiores a 0.7 en todo el globo, siendo especialmente altas en las zonas extra-tropicales del Hemisferio Norte. Las mayores diferencias se localizan en la zona de Indonesia, norte de Sudamérica y costas de Siberia. En la franja ecuatorial las correlaciones son en general menores. Este patrón espacial se explica porque la dinámica oceánica en latitudes altas tiene unas escalas espaciales y temporales menores, y el predictor propuesto en este estudio tiene mayor habilidad para reconstruir la marea meteorológica en estas zonas que en las zonas tropicales. En la Fig.7b se muestra el error absoluto y se observa que los mayores errores (de unos 10 cm) se encuentran en el Hemisferio Norte, específicamente en zonas semi-encerradas como la Bahía de Hudson o el Mar del Norte, y también a lo largo de las costas de Siberia y Rusia. Esto es debido a que en las zonas de aguas poco profundas, y especialmente en zonas semi-encerradas, la marea meteorológica está muy influida por las condiciones locales de viento; por tanto, sería necesario un predictor con mayor resolución espacial para mejorar los resultados en esas zonas. Al analizar el error relativo (Fig.7c) se observa que las mayores discrepancias (en torno a un 10 %) se localizan en la zona ecuatorial, errores que no se detectan en la figura del error absoluto puesto que los niveles de marea meteorológica en esta zona son muy pequeños, y por tanto también lo son sus errores.

A parte de esta comparación espacial, se han seleccionado también 6 puntos (puntos rojos en la Fig.8) para poder visualizar la comparación temporal entre las series original y reconstruida durante el periodo de control. Esto se muestra en la Fig.9, donde, excepto
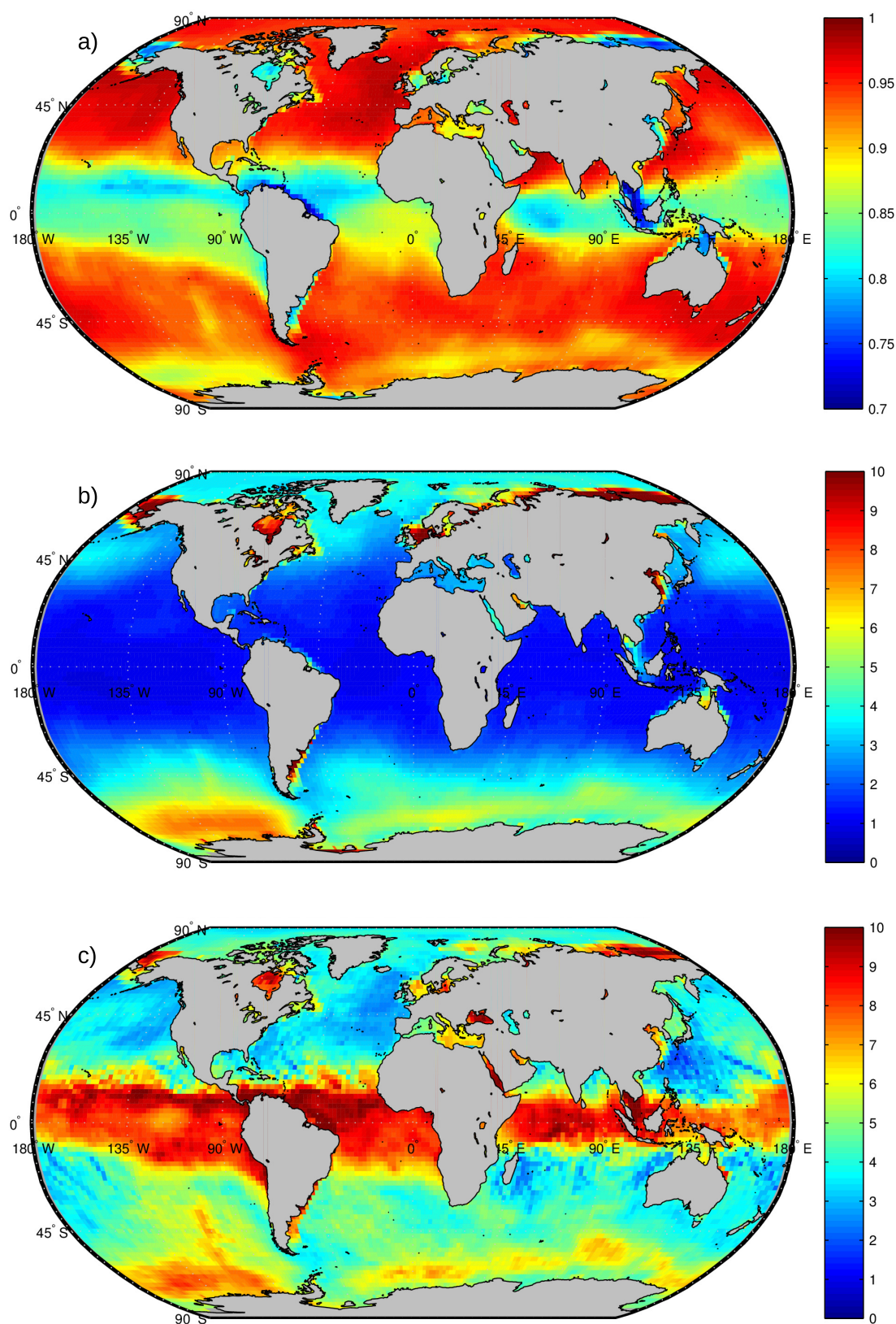
Figura 7: Comparación espacial, durante el periodo de control, entre los niveles de DAC y los niveles reconstruidos a partir de los predictores de 20CR. a) coeficiente de correlación (ρ). b) RMSE (cm). c) RMSE relativo a la máxima variabilidad de la marea meteorológica (%).

para los puntos 4 y 6, se aprecia una buena concordancia tanto en términos de correlación como de errores. En los puntos 4 y 6 se observan extremos de marea meteorológica que no están presentes en la base de datos original; después de un breve estudio se ha comprobado que esos puntos se localizan en zonas de paso de huracanes, y que esos extremos que se aprecian en la reconstrucción se corresponden con huracanes históricos. De esto se deduce que el reanálisis 20CR es mejor asimilando información relativa a huracanes que ERA-interim.
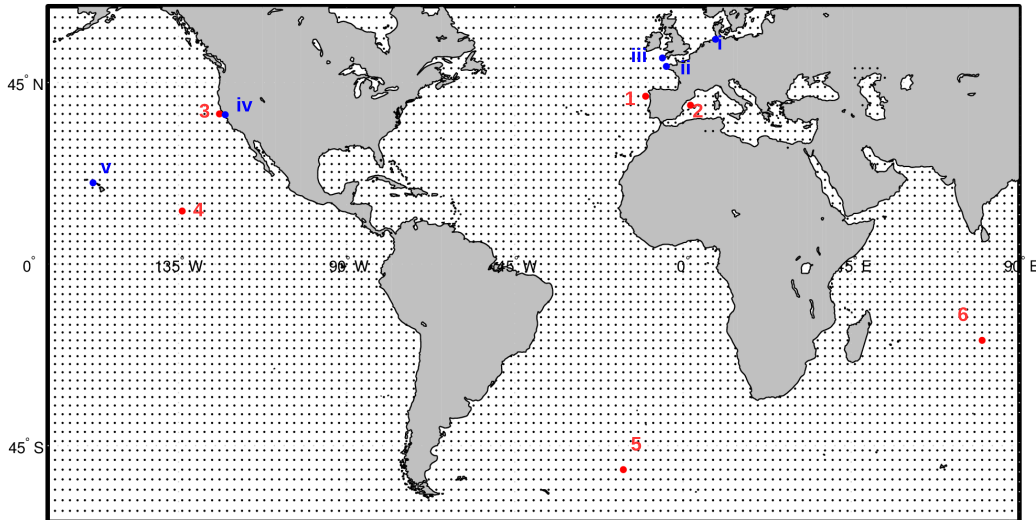
Figura 8: En los puntos rojos es donde se compararán los datos originales de DAC y los reconstruidos con 20CR. En los puntos azules se comparará la marea meteorológica reconstruida con datos de mareógrafos. Los puntos negros muestran la resolución espacial de 2°.

Por otro lado, también se han comparado los datos reconstruidos con datos de mareógrafos en las localizaciones marcadas con un punto azul en la Fig.8. En la Fig.10, se muestra la comparación temporal para finales del siglo XIX o principios del XX, y como se observa, las mejores concordancias se aprecian en el caso de Brest ($\rho = 0,92$, $RMSE = 4cm$) y Newlyn ($\rho = 0,91$, $RMSE = 5cm$); en Honolulu ($\rho = 0,74$, $RMSE = 2cm$) se observan periodos donde la concordancia no es buena, pero como ya se ha mencionado, la exactitud del modelo en estas zonas es inferior, debido a su vez a que la magnitud de la marea meteorológica en estas zonas es muy pequeña.

La distribución espacial de niveles de marea meteorológica se muestra en la Fig.11. Se ha calculado el percentil del 99.5% para dos periodos de tiempo, el periodo de control (1992-2010) y para todo el periodo reconstruido (1871-2010). Los niveles mayores se alcanzan en zonas costeras del norte de Europa, donde los valores pueden alcanzar más de 1 metro. Lo contrario sucede en la zona ecuatorial, donde el nivel es incluso negativo, debido a
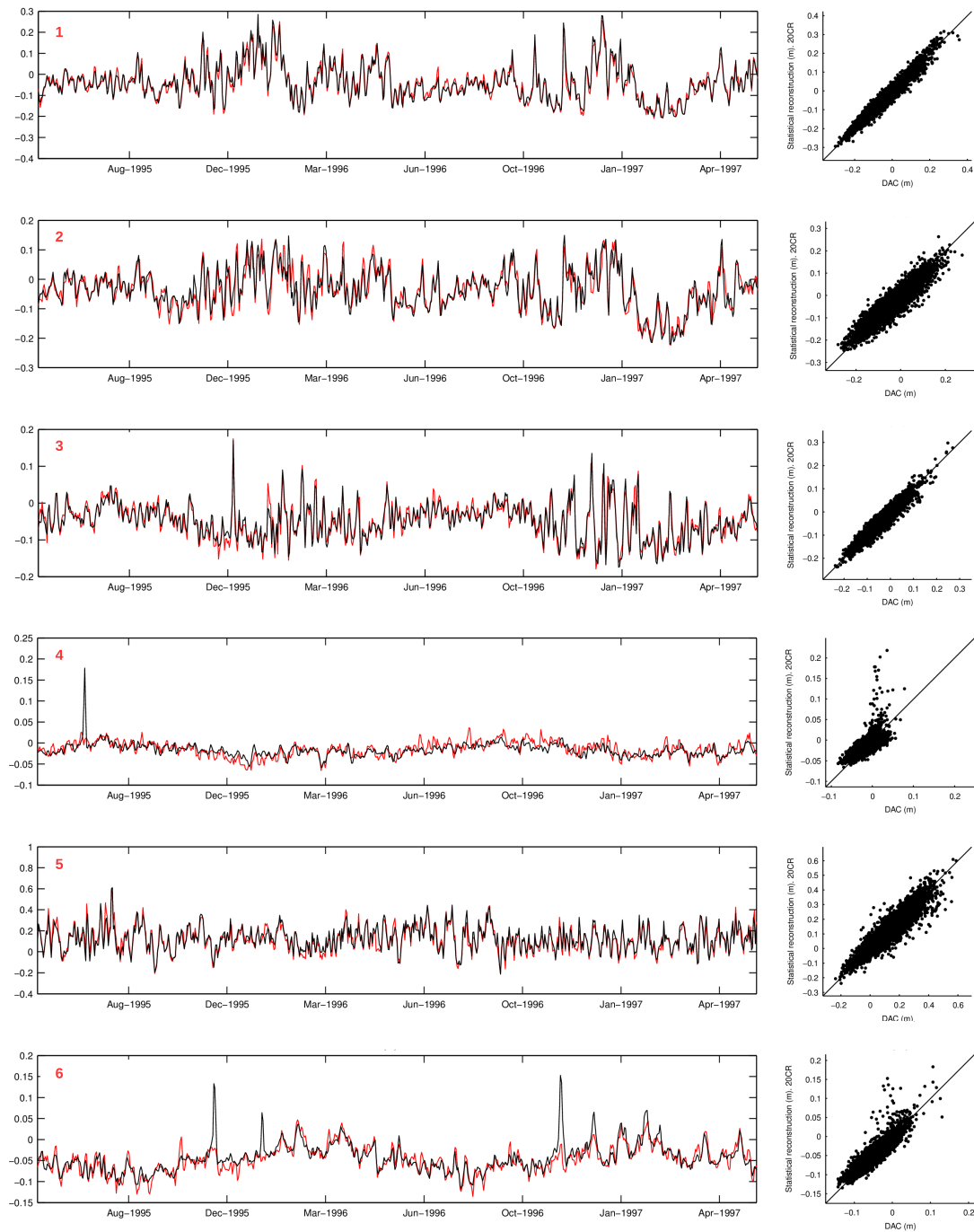
Figura 9: Series temporales de nivel de marea meteorológica (m) en los 6 puntos definidos en la Fig.8. Las líneas rojas representan los datos originales de DAC, las negras son la reconstrucción a partir de los predictores de 20CR. (1): $\rho = 0.97$ $RMSE = 1.84$ cm; (2): $\rho = 0.93$ $RMSE = 2.81$ cm; (3): $\rho = 0.95$ $RMSE = 1.65$ cm; (4): $\rho = 0.81$ $RMSE = 1.43$ cm; (5): $\rho = 0.94$ $RMSE = 4.34$ cm; (6): $\rho = 0.91$ $RMSE = 1.42$ cm
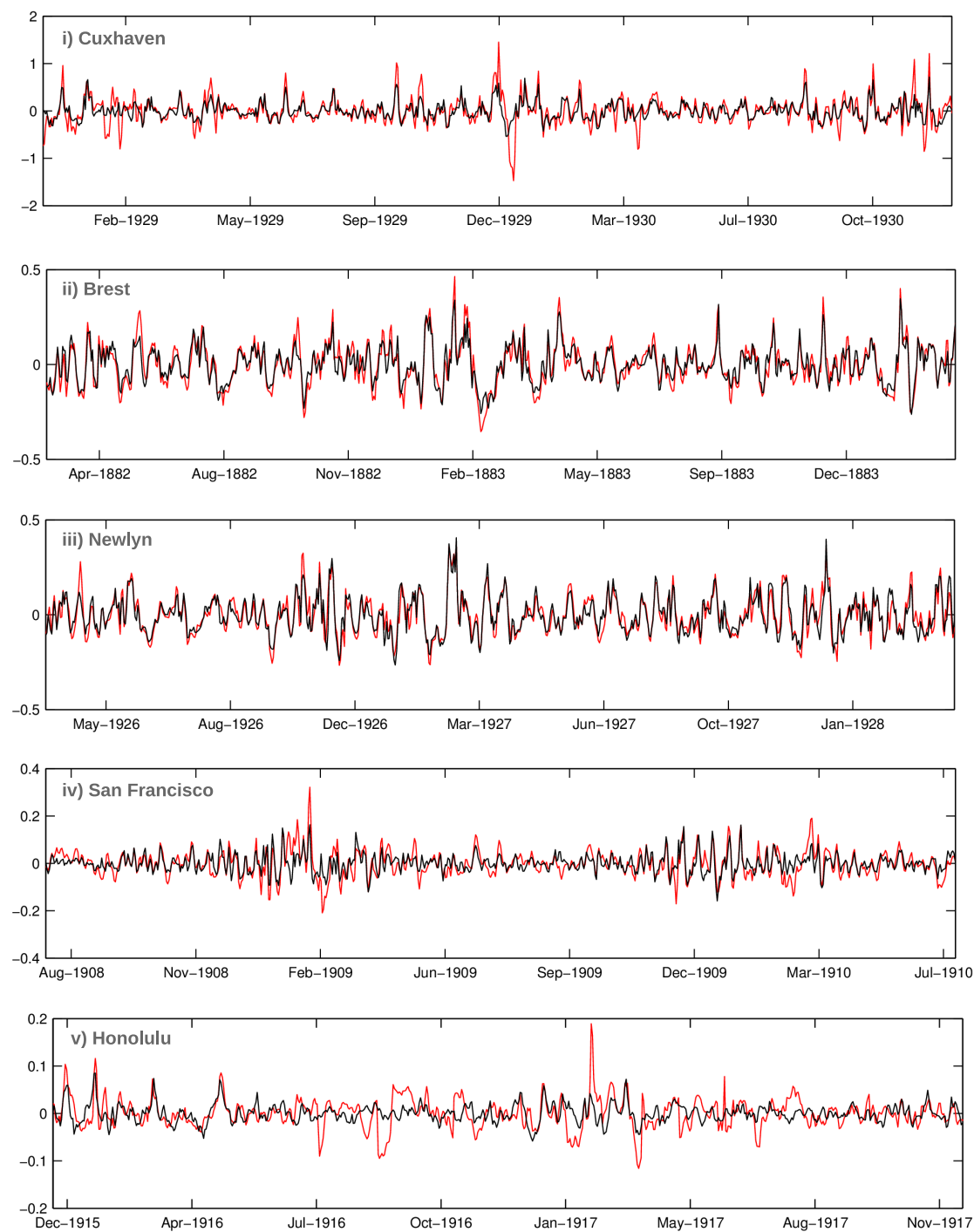
Figura 10: Comparación de la marea meteorológica reconstruida (línea negra) con el registro del mareógrafo (línea roja) en 5 localizaciones (puntos azules de la Fig.8).

que son zonas con condiciones anticiclónicas prácticamente permanentes. La zona extra-tropical del Hemisferio Sur registra valores relativamente altos (más de 60 cm); esto se debe a las condiciones de viento altamente energéticas que existen en esta zona y a a su vez, a condiciones generales de bajas presiones. De la Fig.11 también se concluye que al tener en cuenta todo el periodo disponible, el valor del percentil del 99.5 % disminuye, esto se aprecia claramente en la zona antártica y alrededor de Canadá y las costas del Ártico. Se estima que la actividad ciclónica extra-tropical ha aumentado ligeramente en el Hemisferio Norte, aunque esta afirmación genera controversia (Dangendorf et al., 2014). Sin embargo, sí se ha incrementado significativamente en el Hemisferio Sur (Wang et al., 2013), lo que concuerda con los resultados mostrados en esta figura.
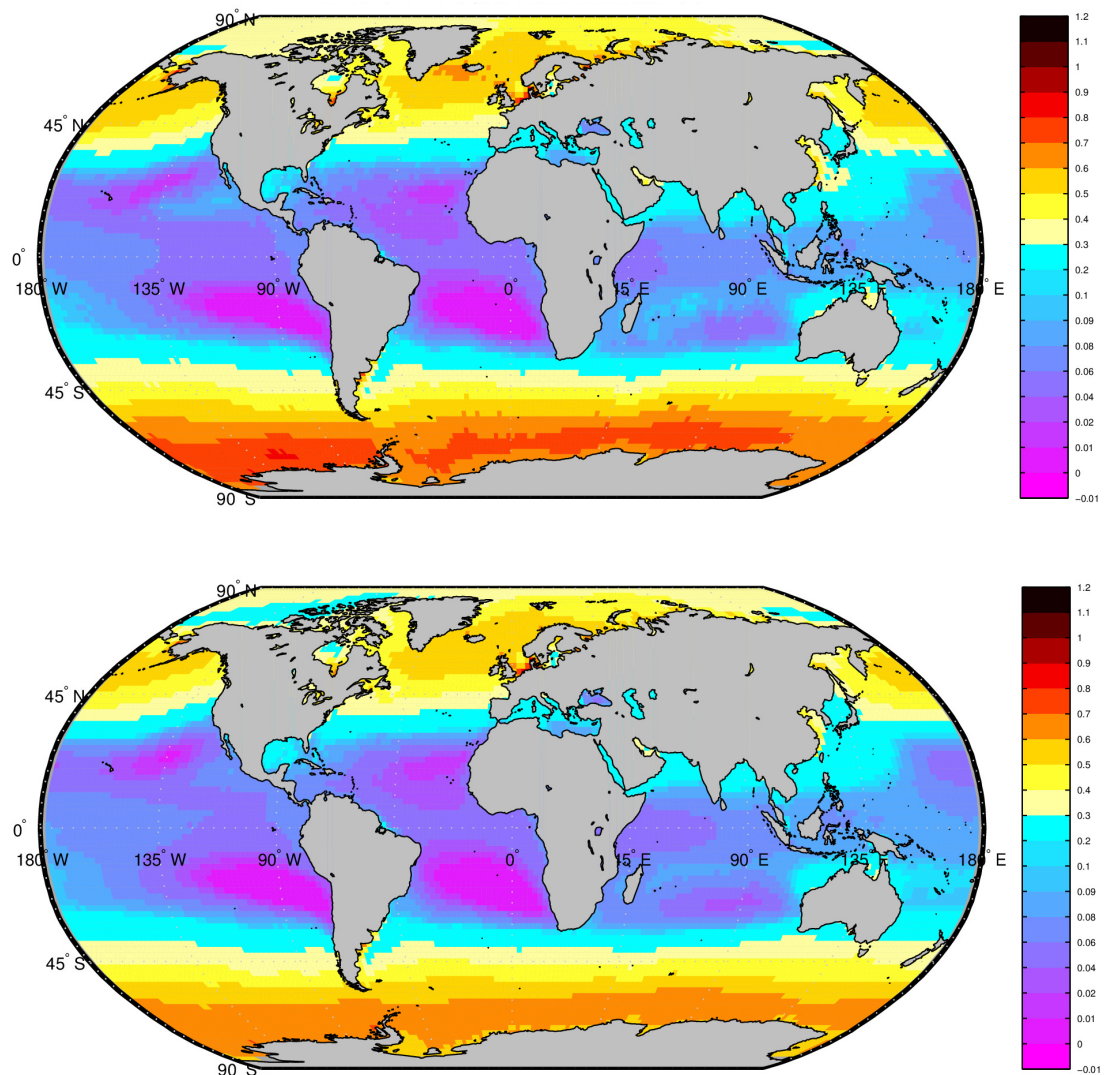
Figura 11: Valor del percentil del 99.5 % (m) de la reconstrucción estadística utilizando 20CR para el periodo 1992-2010 (panel superior) y para el periodo completo de 20CR (panel inferior).

4.5 Conclusiones

El principal objetivo de este estudio ha consistido en generar una base de datos global de marea meteorológica para el periodo 1871-2010. Esto se ha conseguido mediante reconstrucción estadística, utilizando un modelo de regresión lineal multivariado que utiliza como predictores datos de SLP y gradientes extraídos del reanálisis *20th Century Reanlysis*. De la comparación entre los niveles reconstruidos y los originales, se concluye que en el Hemisferio Sur la concordancia es ligeramente inferior, debido a que la calidad del 20CR es inferior en este hemisferio. Alrededor de la zona tropical, se ha encontrado que la reconstrucción sobrestima los datos originales, esto es consecuencia de que el 20CR asimila mejor la información relativa a los ciclones tropicales, dando lugar por tanto a niveles extremos que no están presentes en los datos originales. En zonas semi-encerradas sería necesario aumentar la resolución del predictor para capturar mejor la variabilidad atmosférica y mejorar así la precisión de los resultados. La pequeña magnitud de la marea meteorológica y la mayor escala espacial y temporal de la dinámica oceánica en la zona ecuatorial, dificulta una reconstrucción estadística precisa por parte del modelo numérico. Finalmente, de la comparación con mareógrafos se ha comprobado que el modelo es capaz de reproducir la marea meteorológica lejos del periodo utilizado para calibrar y validar el modelo, como se ha comprobado para periodos desde finales del siglo XIX.

5 Conclusiones generales y futuras líneas de investigación

5.1 Resumen de aportaciones

El objetivo principal de esta tesis ha consistido en ampliar el conocimiento sobre una componente muy importante del nivel del mar: la marea meteorológica. Este objetivo general se ha alcanzado por medio de la consecución de tres objetivos más específicos:

1. **Estudiar la marea meteorológica desde el punto de vista del modelado numérico**. Se han desarrollado dos bases de datos de alta resolución, espacial y temporal, y se han validado los resultados con medidas de mareógrafos y satélites. Se ha analizado la influencia que la resolución del forzamiento atmosférico tiene sobre los resultados de marea meteorológica, y también se han obtenido la variabilidad y las tendencias a largo plazo.

2. **Estudiar los extremos de marea meteorológica mediante el uso de un modelo estadístico variable en el tiempo**. Se ha presentado un marco estadístico para analizar los cambios en los extremos de marea meteorológica. Se ha utilizado la técnica de excedencias sobre un umbral para seleccionar los eventos extremos y caracterizar su intensidad, frecuencia y duración. Así mismo, se ha utilizado el modelo GPD-P dependiente del tiempo para estimar las tendencias de largo plazo y calcular también el nivel asociado al periodo de retorno de 50 años. Finalmente, se ha comprobado la sensibilidad de los extremos de marea meteorológica a la NAO.

3. **Estudiar la marea meteorológica desde el punto de vista del modelado estadístico**. Se ha desarrollado una base de datos global de marea meteorológica mediante el uso de un modelo estadístico. Se ha establecido la relación entre el forzamiento atmosférico (campos de presión superficiales) y la marea meteorológica utilizando un modelo de regresión lineal multivariada. Una vez definida la relación estadística, se han utilizado los campos del *20th Century Reanalysis* para reconstruir la marea meteorológica desde finales del siglo XIX hasta el año 2010 a escala global.

5.2 Conclusiones

En esta sección se resumen las principales conclusiones de la tesis.

1. **Estudio de la marea meteorológica desde el punto de vista del modelado numérico.**

- La comparación de la marea meteorológica con 58 mareógrafos y con datos de satélite ha permitido una amplia validación espacial. En la validación con mareógrafos se han obtenido coeficientes de correlación superiores a 0.8 en la zona atlántica y de alrededor de 0.75 en el Mar Mediterráneo. Los errores cuadráticos medios (RMSE) son inferiores o cercanos a 10 cm en todas las localizaciones con mareógrafos.

- El uso de datos de satélite en la validación ha permitido la identificación de zonas específicas donde los resultados de la simulación no son fiables, y que de otra manera no hubiesen podido ser detectados debido a la ausencia de mareógrafos en esas zonas.

- Estas zonas tienen características espaciales comunes, ya que todas ellas son áreas relativamente someras y semi-encerradas. En estas zonas, las características locales cobran mucha importancia; un ejemplo es el fuerte viento del sureste ("Siroco") que sopla en el mar Adriático y que se acentúa debido a la orografía de la zona, lo que ocasiona variaciones en el nivel del mar que no se ven representadas en un estudio regional.

- En este estudio se ha comparado la señal de GOS con el residuo de los mareógrafos, que además de la marea meteorológica también contiene información relativa a la componente estérica y al aporte de masa. Estas últimas podrían ser de mayor magnitud en el Mediterráneo, lo que implicaría un menor grado de ajuste en la validación, tal y como se ha observado.

- El análisis de la sensibilidad de los resultados a la resolución del forzamiento atmosférico, ha indicado que la marea meteorológica no se ve a penas influida ya que no se aprecian mejoras en los resultados al utilizar un forzamiento con 15 km de resolución espacial en lugar de 30 km. A pesar de esta primera conclusión, sería necesario comprobar si a escala más local, como las zonas costeras o estuarinas, se aprecia una influencia de la resolución del forzamiento.

- El análisis de la tendencias en la marea meteorológica muestra que el signo de las mismas es diferente en función del periodo que se analice. Para el periodo 1948-2009, sólo se identifican tendencias de signo negativo, mientras que si analizamos los últimos 20 años (1989-2009) las tendencias son todas de signo positivo.

2. **Estudio los extremos de marea meteorológica mediante un modelo estadístico dependiente del tiempo.**

- El uso del modelo de extremos GPD-P dependiente del tiempo ha permitido analizar las variaciones en la intensidad, frecuencia y duración de los eventos extremos de marea meteorológica.

- El valor del umbral del 99.5 % muestra un gradiente norte-sur, con valores mayores al norte y magnitudes menores al sur. El número medio de eventos extremos al año es menor en el Atlántico que en el Mediterráneo, mientras que las duraciones son mayores en el Atlántico que en el Mediterráneo.

- En la mayoría del dominio analizado, las tendencias no son significativas en ninguna de las tres variables analizadas. Una excepción, son las zonas del Mar de Alborán, la zona más Este del mar Mediterráneo, el norte del Mar Adriático y los Golfos de Gabes y Sirte.

- Cuando se han comparado las tendencias obtenidas en este estudio con las obtenidas por otros autores, se ha puesto de manifiesto que existen una gran variedad de métodos y periodos de tiempo utilizados para estimarlas. Es por ello que hacer conclusiones generales sobre las tendencias es un aspecto complejo, pues depende del periodo de tiempo en el que se ha llevado a cabo el análisis.

- Se han encontrado correlaciones negativas entre el índice NAO y los extremos de marea meteorológica, tanto en el número de eventos extremos como en su magnitud; lo que indica que en fases de NAO negativas los eventos extremos son más intensos y más frecuentes.

- En este estudio se ha comprobado la relación de la NAO con la frecuencia y magnitud de los extremos, pero existen otros índices climáticos, como por ejemplo el Índice de Oscilación del Mediterráneo (MOI) o el patrón del Atlántico Este (EA), que podrían influir en la variabilidad de la marea meteorológica en el sur de Europa.

- El nivel asociado al periodo de retorno de 50 años muestra un patrón espacial similar al del umbral del 99.5 %, aunque las magnitudes son obviamente mayores.

3. **Estudio de la marea meteorológica desde el punto de vista del modelado estadístico.**

- El modelo estadístico ha mostrado una alta capacidad para reproducir la marea meteorológica a lo largo de todo el globo, especialmente en las áreas extra-tropicales. Alrededor del área ecuatorial y en zonas semi-encerradas, la precisión del modelo estadístico es inferior, aun así, las correlaciones mínimas están en torno a 0.7 y los errores relativos máximos en torno al 10 %. Esto se

debe a que en las zonas semi-encerradas la resolución del predictor debería ser mayor para capturar correctamente la variabilidad atmosférica; en las zonas ecuatoriales, la magnitud de la marea meteorológica es tan pequeña que el modelo estadístico tiene dificultades en reproducirla correctamente.

- El reanálisis atmosférico utilizado para la reconstrucción (20th Century Reanalysis), presenta menor calidad en el Hemisferio Sur, es por ello que al comparar los resultados reconstruidos con los datos de marea meteorológica originales, la concordancia es mayor en el Hemisferio Norte.

- Existe una sobrestimación de la señal de marea meteorológica en ciertas zonas tropicales. Se ha encontrado que estas áreas están situadas en zonas de paso de ciclones tropicales, y el reanálisis 20CR asimila mejor la información relativa a los ciclones que ERA-interim.

- El percentil del 99.5% muestra que los valores más altos de marea meteorológica se localizan en las costas del norte Europa, con valores superiores a 1 m.

- La comparación con mareógrafos ha mostrado que el modelo estadístico proporciona buenos resultados fuera del periodo de control, tal y como muestra la comparación con 5 mareógrafos que tienen registros desde finales del siglo XIX o principios del XX.

- A pesar de que la fiabilidad del 20CR para periodos anteriores a mediados del siglo XX es un tema sobre el que no hay consenso pleno dentro de la comunidad científica, en esta primera validación con mareógrafos se han encontrado buenas concordancias para esa época en 5 mareógrafos distribuidos por el Hemisferio Norte.

- Como resultado de este trabajo, se cuenta con una base de datos de marea meteorológica a escala global con una resolución horizontal de 2° para el periodo 1871-2010. Esta base de datos está disponible para ser utilizada por la comunidad científica.

5.3 Futuras líneas de investigación

El estudio llevado a cabo durante esta tesis ha conducido al planteamiento de las siguientes líneas de investigación:

- Con respecto al modelado numérico, se propone analizar en profundidad el motivo o motivos por los que el resultado del modelado de la marea meteorológica es menos preciso en el Mar Mediterráneo que en la zona Atlántica. Se debería comprobar si

en las zonas semi-encerradas, un incremento de la resolución de la batimetría o la elección de otro valor para, por ejemplo, los parámetros de fricción, sería suficiente para mejorar la calidad de los resultados, o si por el contrario existen fenómenos físicos como las "seiches"que no se están reproduciendo correctamente.

- En el análisis extremal, se ha comprobado la relación de la NAO con la frecuencia y la magnitud de los extremos de marea meteorológica, pero se necesita ahondar más en el estudio de los patrones atmosféricos y su influencia sobre la marea meteorológica para dar explicación a resultados encontrados en este estudio, por ejemplo, el motivo por el cual los eventos extremos son más frecuentes en el Mediterráneo.

- Con respecto al modelado estadístico, se propone comprobar cómo la resolución del predictor atmosférico, especialmente en las zonas costeras donde la marea meteorológica es mayor, afecta a los resultados. Por otro lado, la aplicación del modelo estadístico para predecir la marea meteorológica derivada de distintos escenarios de cambio climático es algo que ya estamos llevando a cabo.

Chapter 1

Introduction

1.1. Motivation and background

The two most important components of the sea level, as can be seen from Fig.1.1, are the astronomical tide (tide) and the atmospheric surge, the latter especially important during storms (storm surge). The combination of both is called storm tide and it is the main driver of the variations in the sea level.

The atmospheric surge is defined as the sea level variation due to the effect of the pressure gradients and the wind stress over the sea surface. It is an important contributor to the sea level variability, and unlike other sea level components, as the astronomical tide which has a deterministic behaviour, the surge depends on the atmospheric pressure and wind, and hence, it is necessary to analyse this variable from available measures or in the absence of them, from its modelling.
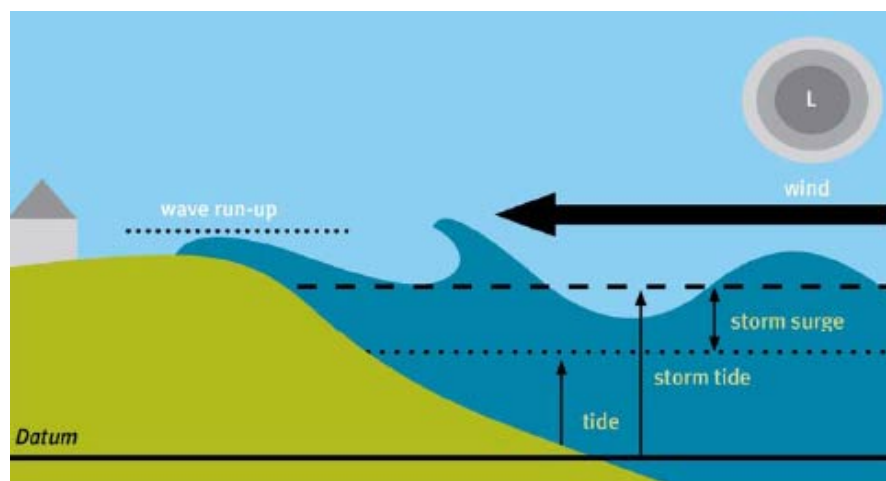
Figure 1.1: Diagram of the two most important components of the sea level: tide and surge. (source: `http://www.mfe.govt.nz/node/18466`)

The importance of the atmospheric surge is spatially variable along the world; the biggest magnitudes are located along the Northern European coasts, where they can reach values of above 1 m. Although surges also affect the sea level in the open ocean, they become extremely important at the coast, where the wind contributes to pile water towards the land. Therefore, in the open ocean, pressure gradients are the main drivers of the surge, while close to the coast the wind component gains strength. This is illustrated in Fig.1.2 for an extreme storm surge (hurricane storm surge).
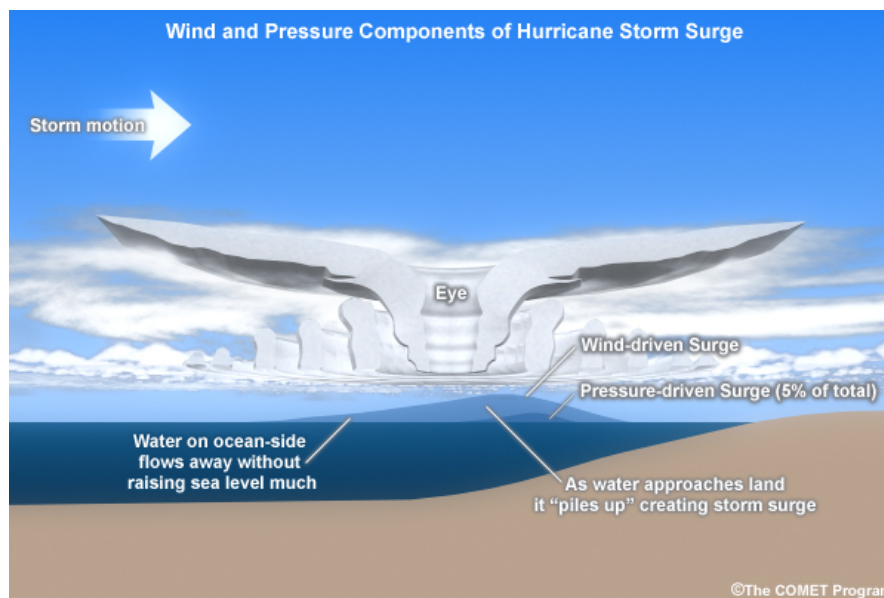
Figure 1.2: Importance of the wind and pressure in the storm surge. (source: `http://www.nhc.noaa.gov/surge/`)

As emerge from the above, coastal areas are specially vulnerable to climate variability and changes in sea level. Particularly, extreme sea level events have immediate impacts on the coast. During the past century, strong surge events have caused considerable damage to properties and even loss of life. One of the major contributors to these extreme sea levels in coastal regions is the atmospheric surge, specially during storm events (storm surges); positive surge events are added to tidal levels, increasing the risk of coastal flooding by extreme water levels.

Therefore, it is important in the general coastal planning and in flood risk assessment, to try to foresee surge impacts on the coast. For this purpose, long time series describing this variable are required. Unfortunately, real data provided by measurement networks are scarce and present severe limitations, both in terms of spatial and temporal coverage. Moreover, observations usually contain gaps and are irregularly sampled, which difficult their analysis. Even so, one way of studying the atmospheric surge is from measures recorded at tide gauges. Tide gauges measure the total sea level, which includes the astronomical tide component; the surge component; the steric component,

that represents changes in the sea level volume due to variations in the water density (changes in its temperature); and changes in the mass component (volume changes due mainly to melting of land supported ice). There are various methods to separate the tidal component from the total sea level signal, e.g. spectral analysis (Bromirski et al., 2003) or the classical harmonic analysis (Pawlowicz et al., 2002). The remaining signal after separating the astronomical tide is called non-tidal residual, and it is formed by the surge, the steric signal and the mass signal, although the latest have generally a small magnitude in the short term.

The shortcomings of working with tide gauges are, as already said, that measures are not continuous in time, and especially during extreme events, they can stop working due to failures or breaking. Shifts in the datum are also frequent, so extracting the surge signal from tide gauges is not a straightforward task and requires a careful analysis. Moreover, most of the world areas are ungauged, and thus, it is needed to find other sources of information that provide atmospheric surge data, as for example numerical models. In any case, tide gauges will always be a valuable tool to, for example, validate the results obtained from other methods.

To overcome the limitations of analysing the atmospheric surge from tide gauge records, the modelling of the atmospheric surge has become one of the most useful tools for generating long-term and high resolution (in time and space) databases. In the present thesis, this objective is approached from two different perspectives: the numerical modelling and the statistical modelling.

There are numerous ocean circulation models that are able to simulate ocean processes, including atmospheric surges. They need atmospheric inputs of the wind stress and pressure gradients over the simulation domain, as well as a description of the sea floor (bathymetric information) in order to reproduce the sea level variation due to these forcings. The difficulty of using numerical models lies in choosing the appropriate combination of parameters that are involved in the model equations, and which will allow us to obtain reliable results. A calibration-validation process is generally followed when performing a numerical simulation, and comparing the numerical results with, e.g. tide gauge measures, will enabled us to check the accuracy of the results.

An alternative to numerical models are statistical models. Statistical models, work by finding a statistical relationship between the atmospheric surge and the atmospheric forcing that drives the surge; once this relationship is established, the surge can be reconstructed from the atmospheric fields, saving a lot of time and computational resources.

One final option to estimate the atmospheric surge is by the inverse barometer relationship, which basically relates the surge level with changes in mean sea level pressure, causing an increase (decrease) of 1 cm in the sea level every 1 millibar of decrease (increase) in the sea level pressure. This is called a static approximation, since it only takes into account the pressure effect over the sea level, neglecting wind effects. It can be a valid approximation far away from the coast, where the wind effects are less important, but close to the coast it does not represent properly the atmospheric surge.

Once we have long-term surge data, the focus is on the analysis of the extreme events, the other aspect we want to address in this research since, as already said, storm surges are one of the major hazards in coastal regions.

This research, is therefore intended to shed light on the increasing interest that the effect of wind and pressure have on the sea surface, that is, the atmospheric surge.

1.2. State of the art

In this section we provide a brief description of the context that involves the three main aspects that we address in this thesis: The numerical modelling, the statistical modelling and the analysis of extreme events.

1.2.1. Numerical modelling

In recent years, many studies have aimed at understanding and quantifying changes in the atmospheric surge by means of numerically generated databases. These databases are useful for a wide variety of studies:

Flather et al. (1998) performed a 2D simulation of the atmospheric surge for the northwest European continental shelf and then used it to address extreme values. A similar study was carried out by Marcos et al. (2009) for Southern Europe, where they used the numerical database generated by Ratsimandresy et al. (2008) to compare the obtained extreme events with those obtained from tide gauges. Bernier and Thompson (2006) also used a numerical model for studying extreme events, specifically, the frequency of storm surges in the Northwest Atlantic. Butler et al. (2007) addressed decadal variations of storm surge elevations from both tide gauges and the outputs of a numerical model.

Climate change effects on storm surges have also been studied from numerical models, for instance, Wang et al. (2008) used the same numerical model that we apply in this thesis to address changes in the number and magnitude of storm surges over Irish waters. Lowe

et al. (2001) studied the storm surge behaviour under a future climate change scenario around United Kingdom, using a numerical model. Woth et al. (2006) applied and ensemble of storm surge extremes, obtained from four different regional climate models, to study changes in storm surge statistics at the North Sea.

Specifically for a similar domain to the one we analyse in the first part of this thesis (Southern Europe), Ratsimandresy et al. (2008) performed an atmospheric surge hindcast, later extended in time by Jordà et al. (2012). These hindcasts were performed for the period 1958-2001 (extended to 2008) using a barotropic model (HAMSOM model, Backhaus 1985) driven with wind and pressure fields created by means of dynamical downscaling from the global reanalysis NCEP, using the limited area model (LAM) REMO (Jacob and Podzun, 1997).

Nowadays, in order to reproduce mesoscale phenomena, efforts are directed towards increasing the resolution of the atmospheric forcing fields in atmospheric surge numerical simulations (Brown et al., 2010; Eric Jones and Davies, 2006; Wang et al., 2008). Thus, high resolution atmospheric fields are required for simulating more accurately this sea level component. In the present thesis we use two different atmospheric fields to test the sensibility of the surge to the forcing resolution.

1.2.2. Statistical modelling

An alternative to the numerical modelling is the statistical modelling, especially when we are interested in reproduce the atmospheric surge signal in a wide domain and for a long period of time, as it is the case in the last part of this thesis (global domain and 140 years of hourly data). The use of a statistical approach will save us a lot of effort, both in terms of computational resources and time.

In climate or other ocean variables, different techniques of statistical reconstruction are widely used, however its application to the atmospheric surge has been less explored. Generally, statistical downscaling techniques can be classified into: transfer functions, weather-type approaches and stochastic weather generators (Giorgi et al., 2001).

Regarding marine climate, linear transfer functions (regression models) have been applied to downscale the significant wave height at global (Wang et al., 2012) and at regional scale (Casas-Prat et al., 2014). Also, a weather-type model has been proposed to downscale multivariate wave climate (Camus et al. 2014b, Espejo et al. 2014).

Apart from wave climate, statistical techniques have been used for Calafat and Gomis (2009) to reconstruct the sea level using a reduced space optimal interpolation analysis for the Mediterranean Sea. For atmospheric surges specifically, Dangendorf et al. (2014)

compared in the North Sea, the long-term behaviour of surges to that of reanalysis wind fields by means of a statistical-empirical formulation (Müller-Navarra and Giese, 1999).

As can be seen, the application of statistical downscaling approaches is usually limited to specific locations; in this thesis, we extend its use to a global scale.

1.2.3. Extreme events analysis

It has already been stated that coastal areas are specially vulnerable to climate variability and changes in sea level. Particularly, extreme sea level events have immediate impacts on the coast. These extreme events are generally driven by the combination of high tides and storm surges. While astronomical tide is a deterministic component of the sea level, the storm surge depends on the atmospheric forcing; hence, in order to study future risks on the coast, it is necessary to analyse this non-deterministic variable from a statistical point of view.

First works regarding extreme analysis, defined return levels by fitting the whole data set to a distribution model. This simple method has the inconvenient of providing unreliable extreme estimates due to the fact that most of the sample values are far away from the tail. Recently, different statistical approaches have been used in the study of extreme episodes, both in terms of the extreme selection method and the extreme value model used. The Annual maxima method (AMM) and Generalized Extreme Value (GEV) distribution is the approach chosen by Bernier and Thompson (2006) to calculate the return period of extreme sea levels in the northwest Atlantic. The 10 largest value per year (r-largest method) were selected by Marcos et al. (2009) and fitted to a steady Generalized Pareto Distribution (GPD) to obtain extreme sea level return periods, while trends were estimated by annual percentiles. The Annual Maxima Method has the disadvantage of gathering a small extreme sample that could disregard extremes in the remaining data. The r-largest model overcomes the limitation of the small amount of data but also has the inconvenient of defining a specific number of extremes per period. This could lead to consider events in the analysis that are not absolute extremes of the whole data set. Méndez et al. (2006) used a time-dependent version of the Peak Over Threshold (POT) model to examine trends in the intensity and frequency of extreme wave events. Temporal dependency was also included by Marcos et al. (2011) in their study of the storm surge changes under different climate change scenarios. In this case, they selected the extremes as the r-largest values per year and allowed time-variability in the parameters of the distribution function.

In this thesis, we select the extreme events using a POT technique, which enable us not to limit the number of extremes to a certain amount, but to consider all the events

above a specific threshold. Following, the use of a time-dependent GPD-Poisson model allow us to estimate long term trends and returning storm surge levels.

1.3. Objectives of the thesis

The general objective of this thesis is to deepen the knowledge of the atmospheric surge, both in terms of its modelling and the study of its extremes. To achieve this general objective, three specific goals will be addressed:

- **Test the ability of numerical models to simulate the atmospheric surge**, creating and validating two new high-resolution surge databases for southern Europe, and exploring the sensitivity of the modelled surge to the atmospheric forcing resolution.

- **Study extreme surge events**, assessing long-term changes in the intensity, frequency and duration of the extreme events, and analysing the sensitivity of the extremes to the North Atlantic Oscillation.

- **Test the ability of statistical models to reproduce the atmospheric surge**, using an atmospheric reanalysis to statistically generate a global surge database that spans from 1871 to 2010.

These objectives have been accomplished and the results have been published in peer-reviewed journals. Next section describes the chapters and the specific papers that this thesis has led to.

1.4. Layout of the thesis

The structure of the thesis is organised as follows:

The present chapter (chapter 1), describes the motivation for this research and provides some background for a better understanding of the next sections. At the end of this chapter, the specific objectives outlined above and the sections where they are addressed, are described.

The following three chapters (chapters 2, 3 and 4) address the specific objectives of the thesis. Each of the chapters includes an abstract, an introduction, a description of the methodology and the data used, as well as the results and some conclusions, constituting an edited version of the articles published in or submitted to SCI journals.

Finally, the last chapter (chapter 5) summarises all conclusions obtained from the present thesis and also suggests future research topics as a continuation of this work.

Following, a brief abstract of the research carried out at each chapter is described:

1.4.1.   Chapter 2. A high resolution hindcast of the meteorological sea level component for Southern Europe: the GOS dataset

In this chapter, two surge databases named GOS 1.1 and GOS 2.1 (Global Ocean Surges), obtained by means of a numerical model, are presented. They differ in the atmospheric data used as an input for the numerical modelling. In one case, the atmospheric forcing is SeaWind I (dynamical downscaling from NCEP reanalysis at 30 km of spatial resolution), and the other one is forced with SeaWind II (dynamical downscaling from ERA-interim reanalysis at 15 km of horizontal resolution). In this paper, it is described the numerical model used to simulate the atmospheric surge and its configuration (ROMS model), as well as the validation of the results, using tide gauges and satellite information. Comparing surge levels from GOS 1.1 and GOS 2.1 enables us to test the sensitivity of the surge to the atmospheric field resolution. At the end of the chapter, seasonal variability and long term trends using the GOS dataset are also estimated.

The work developed in this chapter has led to the next publication:

Cid, A., Castanedo, S., Abascal, A. J., Menéndez, M., and Medina, R. (2014). A high resolution hindcast of the meteorological sea level component for Southern Europe: the GOS dataset. Climate Dynamics, 43(7-8), 1–18. doi:10.1007/s00382-013-2041-0

1.4.2.   Chapter 3. Long-term changes in the frequency, intensity and duration of extreme storm surge events in southern Europe

In this chapter, we use the numerical surge database GOS 1.1, described in the afore-mentioned paper (chapter 2), to study the characteristics of extreme storm surge events. Specifically, we use a non-stationary statistical model to address changes in the frequency (occurrence rate per year), intensity (magnitude of the extremes) and duration of extreme storm surge events. Extreme events are selected using a Peak Over Threshold (POT) approach and modelled by combining the Generalized Pareto Distribution (GPD) and the Poisson (P) process. In this paper we also study the relationship of the storm surges with the North Atlantic Oscillation (NAO) index, since NAO is one of the main drivers of the long-term variability in the North Atlantic area.

The work developed in this chapter has led to the next publication:

Cid, A., Menéndez, M., Castanedo, S., Abascal, A. J., Méndez, F. J., and Medina, R. (2015). Long-term changes in the frequency, intensity and duration of extreme storm surge events in southern Europe. Climate Dynamics. doi: 10.1007/s00382-015-2659-1

1.4.3. Chapter 4. Global reconstructed daily surge levels from the 20th Century Reanalysis (1871-2010)

In this chapter, we present a global surge database obtained by means of a statistical modelling. In a first step, we obtain the statistical relationship between a global surge database named developed by AVISO (DAC, Dynamic Atmospheric Correction), that starts in the nineteens, and their forcing (atmospheric fields from ERA-interim). In a second step, the statistical relationship, based on multiple linear regression, is used to reconstruct surges from a different atmospheric forcing (20th Century Reanalysis), that starts in the late XIX century. Therefore, the results of this work provide surge values at a global scale and for 140 years (1871-2010).

The work developed in this chapter has been submitted to Global and Planetary Change:

Cid, A., Camus, P., Castanedo, S., Méndez, F. J., and Medina, R. (2015). Global reconstructed daily surge levels from the 20th Century Reanalysis (1871-2010).

Chapter 2

A High resolution hindcast of the meteorological sea level component for Southern Europe: The GOS dataset

Abstract

Two sets of 62-year (1948–2009) and 21-year (1989–2009) high-resolution hindcasts of the meteorological sea level component have been developed for Southern Europe using the Regional Ocean Model System (ROMS) of Rutgers University. These new databases, named *GOS 1.1* and *GOS 2.1*, are a valuable tool for a wide variety of studies, such as those related to a better understanding of sea level variability, flooding risk and coastal engineering studies. The model domain encloses Southern Europe, including the Mediterranean Sea and the Atlantic coast, with a horizontal resolution of 1/8° (~14 km). In order to study the effect of the atmospheric forcing resolution, ROMS is driven with two different regional atmospheric forcings: SeaWind I (30 km of horizontal resolution) and SeaWind II (15 km of horizontal resolution). Both are the result of a dynamical downscaling from global atmospheric reanalysis: NCEP global reanalysis and ERA-Interim global reanalysis, respectively. As a result, two surge data sets are obtained: GOS 1.1 (forced with SeaWind I) and GOS 2.1 (forced with SeaWind II). Surge elevations calculated by ROMS are compared with in situ measurements from

tide gauges in coastal areas and with open ocean satellite observations. The validation procedure, testing outcomes from GOS 1.1 and GOS 2.1 against observations, shows the capability of the model to simulate accurately the sea level variation induced by the meteorological forcing. A description of the surge in terms of seasonality and long term trends is also made. The climate variability analysis reveals clear seasonal patterns in the Mediterranean Sea basins. A long-term negative trend for the period 1948–2009 is found, whilst positive trends are computed for the last 20 years (GOS 2.1).

2.1. Introduction

There is an increasing interest in studying the sea surface response to the atmospheric pressure and wind forcing due to its important contribution to sea level during flood events. Coastal areas are particularly vulnerable to climate variability and change. Storm surges, which are primarily caused by low pressure and strong winds, are affected by changes in climate patterns (Flather et al., 1998; Lowe et al., 2001; Woth et al., 2006). As a consequence, coastal flooding and management practices could also be affected. In order to understand these changes, long time series describing these phenomena are required. Unfortunately, real data provided by measurement networks are scarce and presents severe limitations, both in terms of spatial and temporal coverage. Moreover, observations usually contain gaps and irregular sampling, which introduces difficulties and uncertainties into the study. In order to overcome these limitations, numerical models have become one of the most useful tools for generating long- term and high resolution (in time and space) databases. Numerical models have the advantage of being able to generate long-time series of atmospheric and ocean variables for periods when no observation is available. This makes surge hindcasts a relevant tool in many scientific and engineering studies.

In recent years, many studies have aimed at understanding and quantifying changes in storm surge by means of numerically generated databases. These databases can be analysed in the same way as observations for a wide variety of studies addressing extreme values (Flather et al., 1998; Marcos et al., 2009), decadal variations (Butler et al., 2007), frequency of storm surges (Bernier and Thompson, 2006) or climate change effects on storm surge (Flather and Williams, 2000; Jordà et al., 2012; Wang et al., 2008).

With respect to Southern Europe, Sebastião et al. (2008) has performed a sea level hindcast for the Atlantic coast of Europe (including astronomic and meteorological effects). There is also the hindcast presented by Ratsimandresy et al. (2008) for the Mediterranean Sea. Both hindcasts were performed for the period 1958–2001 using a barotropic model (HAMSOM model (Backhaus, 1985)) with a grid size of 10' in longitude and 15'

in latitude. In both cases, the model was driven with wind and pressure fields with a resolution of 0.5° 9 0.5°. These atmospheric fields were created by means of dynamical downscaling from the global reanalysis NCEP, using the limited area model (LAM) REMO (Jacob and Podzun, 1997). There is also a new study on storm surge for the Mediterranean Sea, with focus on the Italian coast, where a model coupling waves, astronomical tide and storm surge has been developed (Ferrarin et al., 2013). In this work, the atmospheric data fields are produced by a meteorological model chain, from global to local scale.

Nowadays, in order to reproduce mesoscale phenomena, efforts are directed towards increasing the resolution of the atmospheric forcing fields in storm surge numerical simulations (Brown et al., 2010; Eric Jones and Davies, 2006; Wang et al., 2008). Thus, high resolution atmospheric fields are required for simulating more accurately this sea level component. In this work, two different atmospheric forc- ings have been used in order to investigate the sensitivity of the results to the resolution of the atmospheric fields. This resulted in the generation of two high resolution surge hindcast for Southern Europe. The obtained regional data sets belong to the GOS (Global Ocean Surges) database (the American GOS dataset is described in Losada et al. 2013). These data sets represent the sea level variation due to wind and pressure for continuous series of meteorological fields, not only specific simulations during storms. Therefore, hereafter we will use the term storm surge when referring to the wind and atmospheric pressure contribution to the total sea level.

It is important to highlight that these hindcasts enclose the whole Southern European coast, including the Canary Islands region (see Fig.2.1). Up to now, none of the existing databases provide information that westward. This reveals the importance of the present work and its applicability to current studies in the area (for instance, coastal dynamic studies related to desalinization plants).

The European GOS data sets have been performed using the Regional Ocean Model System (ROMS) (Shchepetkin and McWilliams, 2005), and using two different atmospheric forcings: SeaWind I (30 km of horizontal resolution) and SeaWind II (15 km of horizontal resolution). These atmospheric fields have been obtained by a dynamical downscaling from NCEP and ERA-Interim global reanalysis, respectively, and they have been exhaustively validated with observations (more details in Menendez et al. 2014). The influence of the forcing resolution into the storm surge elevation is analysed by means of the comparison of both datasets with observed data.

Special attention is focused on the validation of the storm surge numerical results. Surge elevations calculated by ROMS model in the two runs are exhaustively compared with values measured by 58 tide gauges distributed across the domain. In areas where no

observations are available, validation is made by the use of altimetry data. As far as the authors' knowledge, validation of storm surge with satellite data has been previously done by Wang et al. (2008), only for Irish waters. Thus, this is the first attempt in validating the results from a storm surge numerical model using altimetry data in a large area, covering all Southern Europe. Satellite altimeter data were also used by Calafat and Gomis (2009) to reconstruct and validate sea level fields in the Mediterranean Sea. In this work a comparison between the model results and altimetry data is made all over the domain. The satellite validation is a step forward with respect to previous works, where validations were performed only with tide gauges, covering few locations of the whole domain.

The aim of this paper is not only the presentation of the two storm surge databases but also the analysis of the seasonal variability and long term trends using GOS hindcasts. Results show clear seasonal patterns as well as different trends when averaging different periods, as already suggested by Gomis et al. (2008).

The main objectives of this work are:

1. The description of the two data sets,

2. its validation with tide gauges and satellite data,

3. obtaining the influence of the forcing resolution on the storm surge results by comparing the two datasets and

4. the application of GOS database to study variability and trends.

The organization of this paper is as follows: The model description and configuration is described in Section 2.2. Section 4.4 is devoted to verify the modelling results by comparing them with satellite and tide gauge data. Seasonal patterns and estimated long-term trends of the meteorological sea level component are analysed in section 2.4. Finally, the main conclusions are summarized in section 4.6.
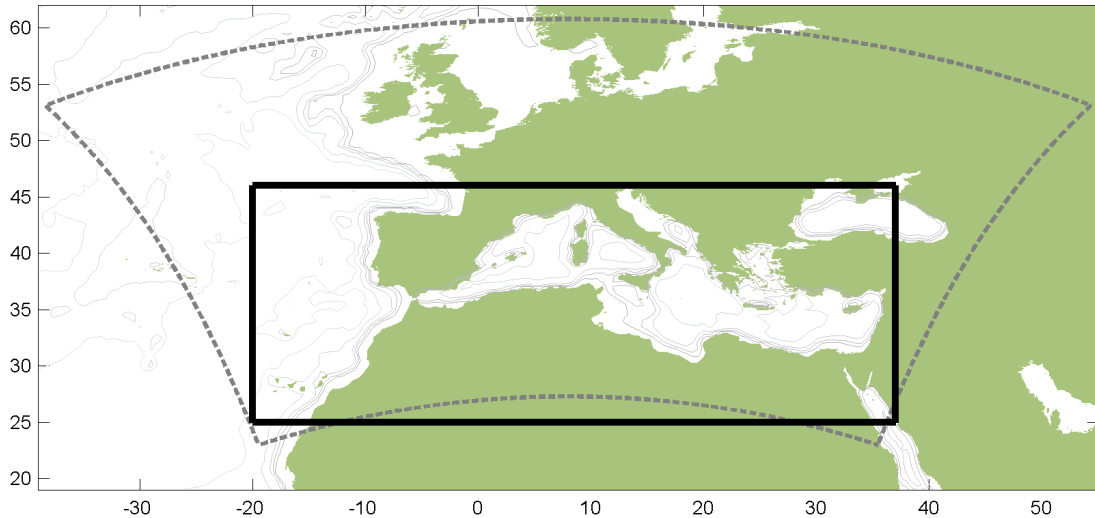
Figure 2.1: Grid domain of storm surge hindcast (black line) and atmospheric down-scaling (dashed gray line)

2.2. Model set-up

Storm surge has been simulated using the Regional Ocean Model System (ROMS) developed by Rutgers University. ROMS is a three-dimensional, free-surface, terrain-following ocean model that solves the Reynolds-averaged Navier-Stokes equations using the hydrostatic vertical momentum balance and Boussinesq approximation with a split-explicit time stepping algorithm (Haidvogel et al., 2008, 2000; Shchepetkin and McWilliams, 2005). It uses a horizontal curvilinear Arakawa C grid and vertical stretched terrain-following coordinates.

The model is set-up for Southern Europe covering the area shown in Fig.2.1, which spans from 25°N to 46°N in latitude and from 20°W to 37°E in longitude with a horizontal resolution of 1/8°. The bathymetry is extracted from the ETOPO 2 database, a global topography of 2 minutes resolution derived from depth soundings and satellite gravity observations (Smith and Sandwell, 1997).

In this study, ROMS model is run in barotropic mode. The inverted barometer effect is imposed at the open boundaries of the domain (North and West), using a free surface Chapman condition and 2D Flather condition for momentum. Note that non-linear energy transfer between tides and surges is very low off the Spanish coast (Carretero Albiach et al., 2000; Ratsimandresy et al., 2008), and the microtidal environment of the Mediterranean Sea reduces the nonlinear interaction between tides and storm surges (Lionello, 2012). Based on these features of the study area at this scale and resolution, it is possible to perform and independent model computation of residuals, without taking into account the nonlinear transfer of tidal energy. Bottom stress is given by a quadratic

bottom drag coefficient of 10-4. Horizontal viscosity is set using a lateral, harmonic, constant mixing coefficient of 500 m/s. The model is driven with hourly meteorological data of wind and atmospheric pressure provided by dynamical downscalings developed within the framework of the SeaWind project (more details in Menendez et al. 2014). The atmospheric downscaling was performed using the Research and Forecasting model with the Advanced Research dynamical solver (WRF-ARW) (Skamarock et al., 2008). SeaWind grid domain covers the European region and the whole Mediterranean Sea (see Fig.2.1). SeaWind dataset consist of two different atmospheric hindcasts: SeaWind I (30 km horizontal resolution for a period of 62 years) and SeaWind II (15 km horizontal resolution for a 21-year period). SeaWind I is based on the NCEP global reanalysis I (Kalnay et al., 1996) and SeaWind II is based on the ERA-Interim global reanalysis (Dee et al., 2011). Both downscalings were interpolated to the ROMS grid at 1/8°horizontal resolution.

As a summary, two storm surge hindcasts are performed: (1) GOS 1.1 which is an hourly dataset of 1/8°spatial resolution for the 1948-2009 period forced with SeaWind I; and (2) GOS 2.1 consisting of an hourly dataset of 1/8°spatial resolution for the 1989-2009 period forced with SeaWind II.

2.3. Hindcast validation

2.3.1. Tide gauges versus modelled data

Model results are validated using in-situ measurements from local tide gauges. This work makes use of tide gauge records from different sources: Puertos del Estado (PdE) (`www.puertos.es`), University of Hawaii Sea Level Center (UHSLC) (`http://uhslc.soest.hawaii.edu`), Système d'Observation du Niveau des Eaux Littorales (SONEL) (`http://www.sonel.org`) and Istituto Superiore per la Protezione e la Ricerca Ambientale (ISPRA) (`www.idromare.it`). Fig.2.2 illustrates the location of the tide gauge stations used in the validation, which cover a wide area within the computational domain, both in Atlantic and Mediterranean coast. Although there are several tide gauges along the east Adriatic and few more stations along the Turkey coast, they have not been considered because their length and quality are not adequate for a representative validation of the model results. A summary of the tide gauges data is presented in Table 2.1, including the name of the station, owner institution and available data periods. Observations as well as numerical simulations provide hourly data. Modelled time series are extracted at these locations (closest GOS grid point to the tide gauge) and compared with the observed residual (observed total elevation minus predicted tide)

from the in-situ measurements. Predicted tide at each tide gauge station is calculated using t-tide package (Pawlowicz et al., 2002). Each year is analysed separately, and in the case of too many gaps in the tide gauge time series for a specific year, the tidal analysis for that period is not performed. Tidal constituents included in the analysis are those with a noise-signal ratio greater than 2, except for the annual and semi-annual components that have not been removed because, as previous authors indicate (Pascual et al., 2008), the main contributors to this particular signals are thermosteric and meteorological rather than astronomical. The mean sea level of the entire time series at each station is subtracted from the non-tidal residuals to obtain storm surge anomalies. Mean level at each grid point of the numerical data is subtracted from the modelled series in order to also have 'anomalies' in the hindcast results. Throughout the rest of this paper when speaking about non-tidal residuals from tide gauges or simulated storm surge, we refer to anomalies.
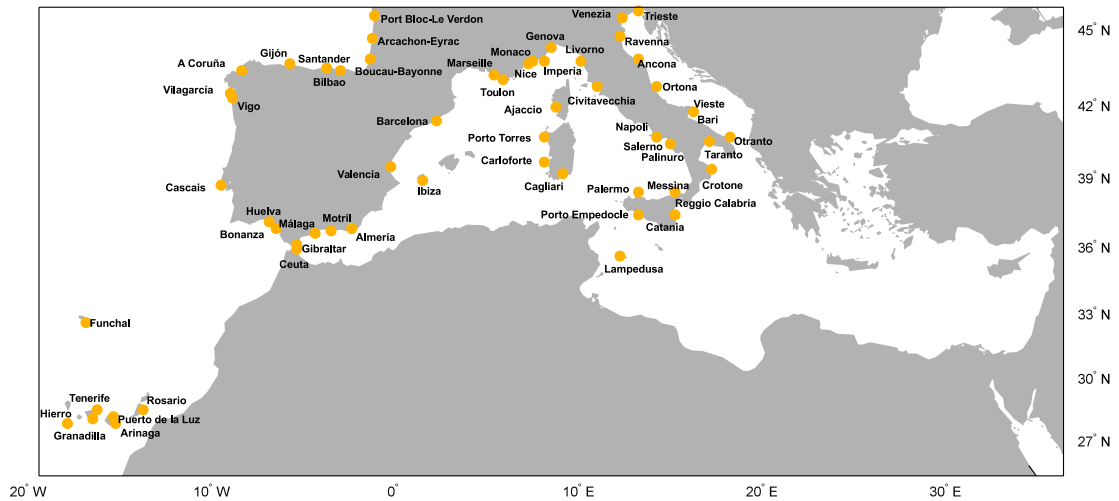
Figure 2.2: Location of the tide gauges used to validate the storm surge hindcasts.

Fig.2.3 shows the time series comparison for 3 stations in the Atlantic area (Santander, Huelva and Arinaga; a, b and c, respectively) and 3 stations in the Mediterranean basin (Genova, Porto Torres and Palermo; d, e and f, respectively). A period of 3 months (Jan-Mar) for the year 2004 is presented. The grey line represents the non-tidal residuals extracted from the tide gauges, while red and blue lines correspond to the storm surge hindcast (GOS 1.1 and GOS 2.1 respectively). The hourly time series comparison shows a good agreement, both in terms of magnitude and timing of the surge events. As can be seen, results from GOS 1.1 and GOS 2.1 are very similar.

In order to quantify the accuracy of the simulations, a statistical analysis is carried out. Key statistical parameters such as correlation factors and root mean square errors (RMSE) are calculated at each location. As an example, Fig.2.4 depicts the diagnostic plots for GOS 2.1 at the same stations mentioned in Fig.2.3 The panels show the scatter,
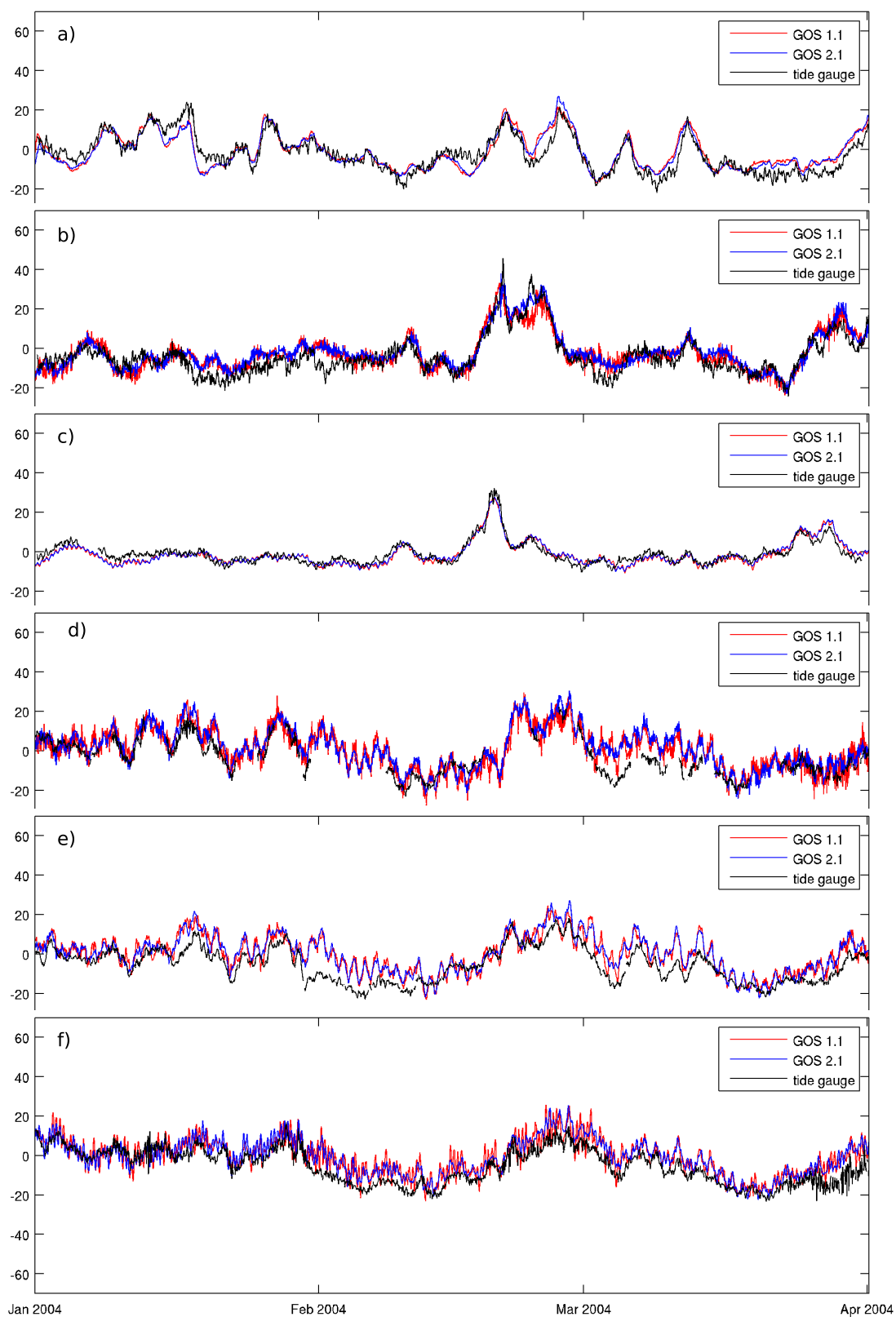
Figure 2.3: Storm surge comparison between model (GOS 1.1 in red and GOS 2.1 in blue) and tide gauge (grey) at six locations. a) Santander b) Huelva c) Arinaga d) Genova e) Porto Torres f) Palermo.

TIDE-GAUGE STATION	DATA PROVIDER	INITAL DATE	FINAL DATE	GOS 1.1 DATASET		GOS 2.1 DATASET	
				ρ	RMSE (cm)	ρ	RMSE (cm)
A Coruña	PdE	1992	2008	0.87	6.60	0.88	6.47
Ajaccio	SONEL	1981	2003	0.79	7.62	0.80	7.31
Almería	PdE	2006	2009	0.73	8.20	0.74	8.01
Ancona	ISPRA	1986	2011	0.66	15.07	0.68	14.35
Arcachon-Eyrac	SONEL	1967	2004	0.81	10.05	0.81	9.61
Arinaga	PdE	2003	2009	0.79	4.48	0.79	4.42
Barcelona	PdE	1992	2008	0.80	7.98	0.80	7.82
Bari	ISPRA	1979	2011	0.64	12.48	0.74	9.11
Bilbao	PdE	1992	2009	0.86	6.48	0.86	6.42
Bonanza	PdE	1992	2009	0.81	7.76	0.82	7.48
Boucau-Bayonne	SONEL	1967	2004	0.83	9.51	0.83	9.50
Cagliari	ISPRA	1986	2011	0.75	8.57	0.75	8.46
Carloforte	ISPRA	1988	2011	0.77	7.65	0.77	7.60
Cascais	UHSLC	1971	1999	0.82	6.55	0.82	6.99
Catania	ISPRA	1970	2011	0.79	7.17	0.79	7.18
Ceuta	UHSLC	1970	2006	0.72	8.11	0.79	6.30
Civitavecchia	ISPRA	1973	2012	0.75	8.16	0.77	7.67
Crotone	ISPRA	1991	2011	0.76	10.33	0.76	10.12
Funchal	UHSLC	1977	2005	0.79	6.51	0.80	6.46
Genova	ISPRA	1998	2011	0.78	7.66	0.80	7.28
Gibraltar	UHSLC	1970	1997	0.69	9.14	0.75	8.62
Gijón	PdE	1995	2009	0.88	6.38	0.88	6.32
Granadilla	PdE	2003	2009	0.77	5.69	0.77	5.64
Hierro	PdE	2003	2009	0.77	5.75	0.78	5.69
Huelva	PdE	1996	2009	0.81	7.51	0.82	7.16
Ibiza	PdE	2003	2009	0.78	7.75	0.78	7.57
Imperia	ISPRA	1986	2011	0.79	7.02	0.80	6.85
Lampedusa	ISPRA	1998	2011	0.73	8.95	0.73	8.79
Livorno	ISPRA	1972	2011	0.78	8.12	0.80	7.64
Málaga	PdE	1992	2009	0.72	8.61	0.74	7.92
Marseille	SONEL	1985	2004	0.81	7.30	0.82	7.42
Messina	ISPRA	1973	2012	0.79	6.79	0.79	6.72
Monaco	SONEL	1960	2004	0.76	7.27	0.79	6.88
Motril	PdE	2004	2008	0.72	8.83	0.73	8.41
Napoli	ISPRA	1986	2011	0.79	6.52	0.80	6.34
Nice	SONEL	1981	2004	0.79	7.10	0.80	6.90
Ortona	ISPRA	1986	2011	0.69	11.94	0.71	11.34
Otranto	ISPRA	1987	2011	0.72	9.05	0.74	8.71
Palermo	ISPRA	1992	2011	0.80	6.02	0.81	5.93
Palinuro	ISPRA	1987	2011	0.78	6.91	0.79	6.74
Port Bloc-Le Verdon	SONEL	1959	2004	0.82	11.24	0.83	10.15
Porto Empedocle	ISPRA	1973	2011	0.74	7.85	0.75	7.65
Porto Torres	ISPRA	1985	2011	0.77	7.34	0.78	7.24
Puerto de la Luz	UHSLC	1975	2006	0.80	4.73	0.80	4.59
Ravenna	ISPRA	1975	2011	0.59	18.72	0.62	17.35
Reggio Calabria	ISPRA	1998	2012	0.78	7.17	0.78	7.18
Rosario	PdE	2003	2009	0.78	5.00	0.78	4.92
Salerno	ISPRA	1991	2011	0.75	9.07	0.75	8.90
Santander	PdE	1992	2009	0.86	6.81	0.86	6.74
Taranto	ISPRA	1991	2011	0.74	8.83	0.76	8.22
Tenerife	PdE	1992	2009	0.78	6.59	0.78	6.49
Toulon	SONEL	1961	2004	0.81	7.25	0.83	6.46
Trieste	ISPRA	1988	2011	0.61	19.55	0.64	18.07
Valencia	PdE	1992	2006	0.75	9.46	0.77	8.93
Venezia	ISPRA	1986	2011	0.61	20.20	0.64	18.46
Vieste	ISPRA	1990	2011	0.75	9.38	0.77	8.88
Vigo	PdE	1992	2009	0.88	6.53	0.89	6.34
Vilagarcía	PdE	1997	2009	0.86	7.80	0.87	7.68

TABLE 2.1: Statistical parameters of comparison between observed and hindcasts (GOS 1.1 and GOS 2.1). The root mean square error (RMSE) and the correlation index (ρ) are displayed.

quantile-quantile plot, and statistical indices of observed versus modelled data. Colours indicate the sample density (red for high density and blue for low data density). The solid line corresponds to $y = x$ (modelled equal to observed data). 30 quantiles are estimated on a equally spaced Gumbel probability distribution, which allows a more detailed representation of the higher values. Solid circles show quantiles above the 90th percentile. The number of data in the dataset (NObs), RMSE and the correlation coefficient (ρ) are also shown. Correlation coefficients are significant at 95% confidence interval. It can be observed the good agreement reached between measured and hindcasted values. High correlations values (0.78-0.86) and small RMSE (4.42-7.28 cm) are obtained both

in Atlantic and Mediterranean coast. The majority of data (red areas in Fig.2.4) are around the bisector, although slight discrepancies can be seen at the upper tail of the quantiles. These discrepancies can be due to local effects related to the bathymetry that we are not able to reproduce at the resolution used in this study.

A summary of the statistical results obtained for both data set (GOS 1.1 and GOS 2.1) is shown in Table.2.1. The RMSE and the correlation index are presented for each tide-gauge station. The information gathered in this table is also presented in Fig.2.5 and Fig.2.6, where the spatial comparison between the model output and in-situ measurements is shown. Fig.2.5 corresponds to the correlation coefficient (ρ) while Fig.2.6 represents the RMSE. A good agreement between measured and numerical data is obtained at all locations, except for those tide gauges placed in the Northern Adriatic (stations of Trieste, Venezia, Ravenna and Ancona). As displayed in 2.1, GOS 2.1 achieves slightly higher correlation coefficients and slightly smaller errors than GOS 1.1 although it still does not represent correctly storm surge in the Northern Adriatic. Models in general have difficulty in reproducing sea level in the Adriatic (Marcos et al., 2009). The results found in the northern part of the Adriatic Sea can probably be explained in terms of the relatively shallow shelf present in this area, which makes extremely important the use of an accurate frictional parameter as well as a high resolution bathymetry, aspects that greatly affect the model results. Similar explanation was found by Pascual et al. (2008) in the Northern Adriatic area. Another issue is the Meteorological tsunamis that can affect the Northern Adriatic (Šepić et al., 2012). They are very difficult to accurate reproduce since a very high spatial-temporal resolution and precise forcing are required to obtain good simulations. Except for these stations, results show a good agreement between measured and numerical data. In terms of correlation (see Table.2.1 and Fig.2.5), high correlation indices are obtained between numerical and observed data for both data set. In the Atlantic area, the correlation factor is over 0.8 (over 0.85 in the stations placed along the north coast of Spain), while the correlation found in the Mediterranean Sea is about 0.75. The whole set of tide gauge data (58 stations) has a RMSE lower or around 10 cm (see Table.2.1 and Fig.2.6). These RMSE represent around the 10% of the storm surge variability registered by the tide gauge, which shows the accuracy of the hindcasts performed. These results are similar to the ones found in previous studies (Ratsimandresy et al., 2008), where the highest correlations (over 0.85) are observed in the tide gauges moored along the north and northwest coast of the Iberian Peninsula.

Differences between numerical and observed surge should exist since the signals gathered in each series do not take into account the same processes. While sea level variation in the model is strictly due to wind and pressure, in tide gauges there are local factors or processes (as steric effects, the influence of river outflow, the effects of waves in storm
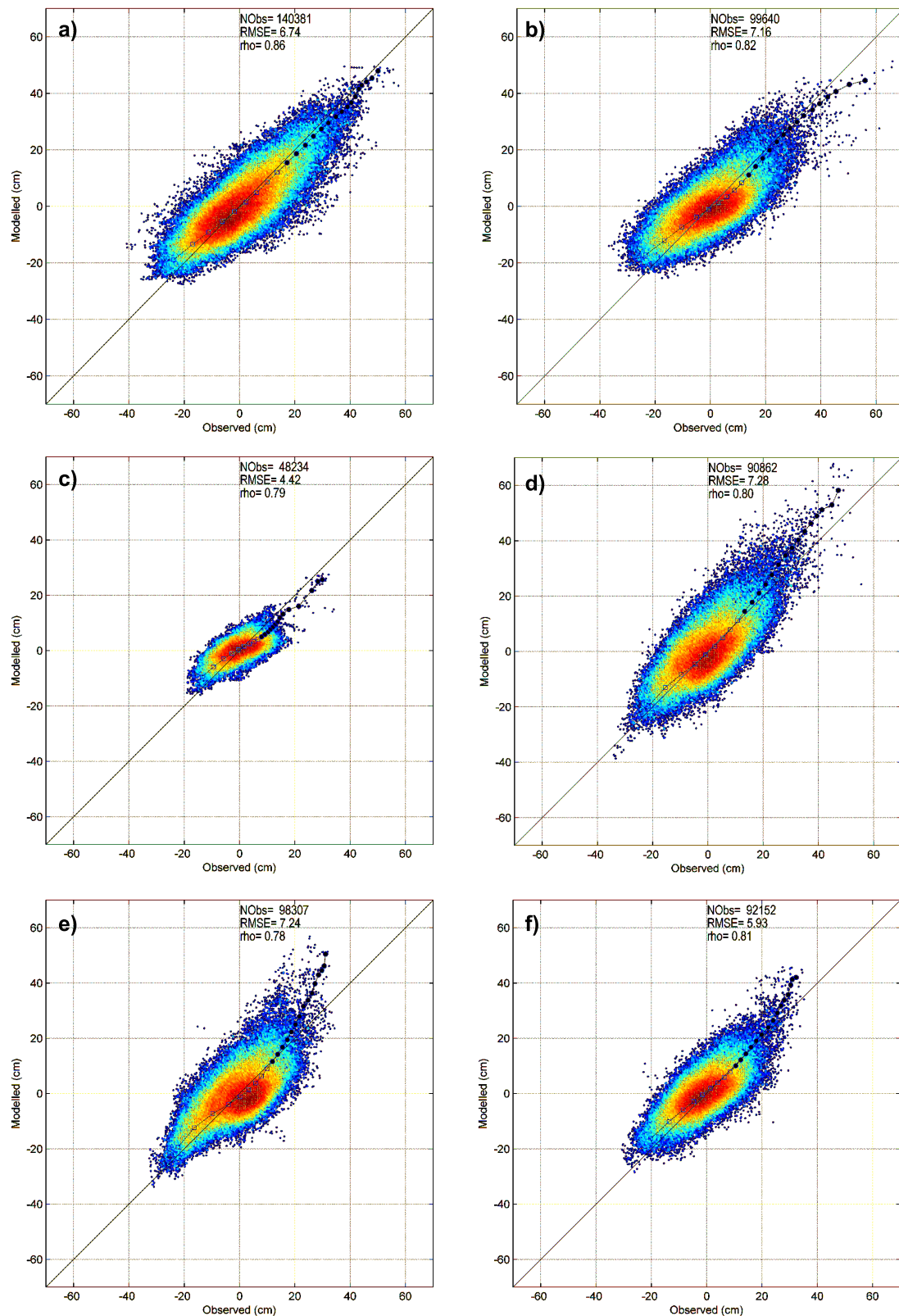
Figure 2.4: Diagnosis comparison between 6 tide gauges and GOS 2.1 dataset. Quantiles (solid circles are quantiles over the 90th percentiles) and statistical indices of observed versus modelled values are shown. Colours represent data density (increasing values from blue to red). a) Santander b) Huelva c) Arinaga d) Genova e) Porto Torres f) Palermo.
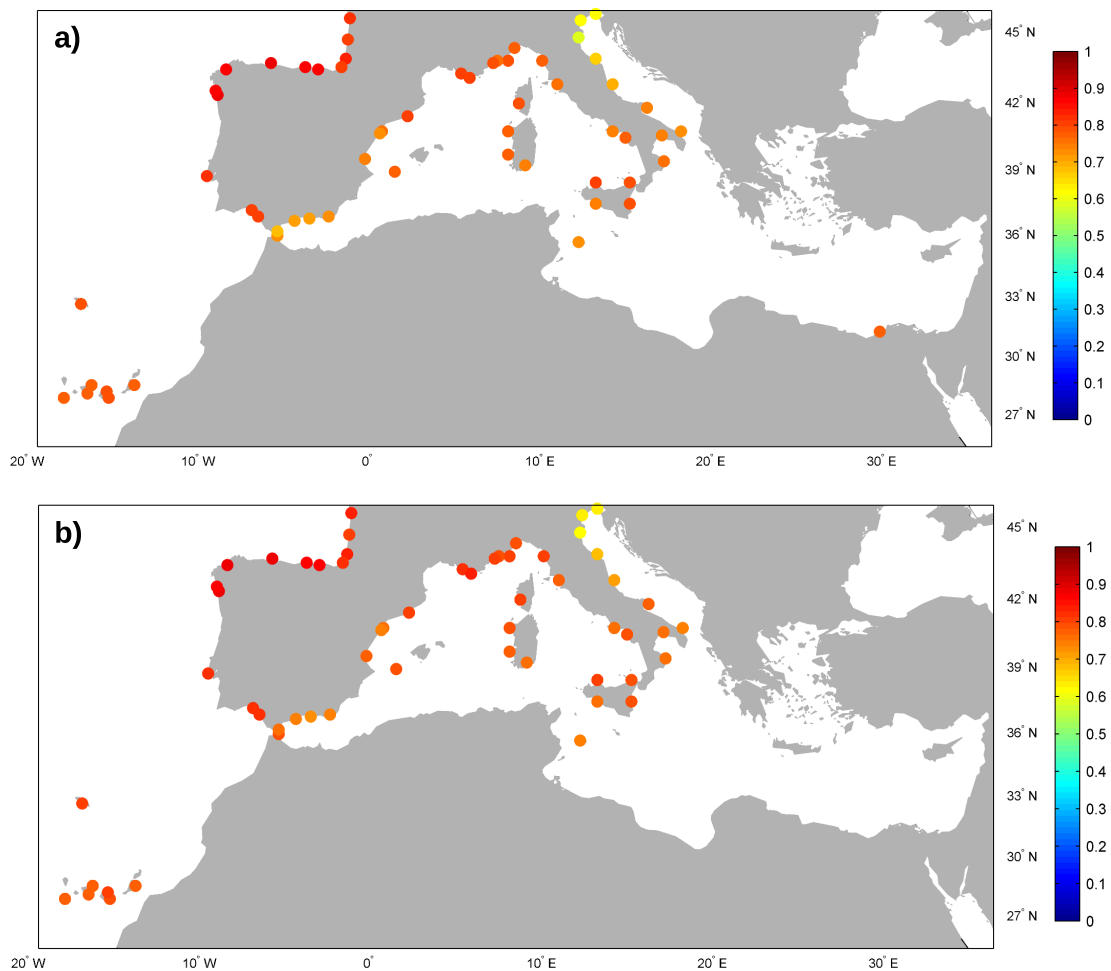
Figure 2.5: Comparisons of the storm surge dataset with in-situ measurements in terms of correlation index (ρ). a) GOS 1.1 b) GOS 2.1.

surge or non-linear interactions between storm surge and tides) that have not been considered in this study.

The statistical validation shows similar results for both storm surge data set. Although GOS 2.1 achieves slightly higher correlation coefficients and slightly smaller errors than GOS 1.1, in general the results show no significant improvements when increasing the resolution of the atmospheric forcing fields from 30 km to 15 km. Thus, in this work, the increase of the atmospheric forcing resolution has negligible effect in the storm surge sea level. Nevertheless, a further analysis should be performed in order to study how the increase of the forcing resolution affects the storm surge results at the local scale (e.g. coastal areas, estuaries or bays).

Figure 2.6: Comparisons of the storm surge dataset with in-situ measurements in terms of root mean square error (RMSE). Units are in centimetres. a) GOS 1.1 b) GOS 2.1.

2.3.2. Satellite altimetry versus modelled data

Additionally, GOS hindcasts are compared to satellite information for the whole spatial domain. This is motivated by the sparse distribution of tide gauges along the analysed coastline and the need of evaluating the model on the open ocean.

The altimeter data used in this study are along-track delayed time products. These data were produced by Ssalto/Duacs and distributed by Aviso, with support from Cnes (`http://www.aviso.oceanobs.com/duacs/`). The Delayed Time component of Ssalto/-Duacs system provides a homogeneous, inter-calibrated and highly accurate long time series of SLA altimetry data from T/P, ERS1/2, GFO, Envisat, Jason-1 and Jason-2 missions. These satellite time series started in 1992 and they are constantly updated. The minimum time lapse of the satellites is around 10 days.

The sea level anomaly (SLA) currently delivered has the classical geophysical and instrumental corrections, including instrumental noise, orbit determination error, atmospheric

attenuation (wet and dry tropospheric and ionospheric effects), and sea state bias (more information in 'User Handbook Ssalto/Duacs: M(SLA) and M(ADT) Near-Real Time and Delayed-Time'). Tides were removed using GOT4.8 tidal model (Ray, 1999). High-frequency signals were also corrected using a combination of a hydrodynamic model (MOG2D-G) for high frequencies (Carrère and Lyard, 2003) and an inverse barometer (IB) for low frequencies, therefore the sea level variation due to atmospheric forcing is not included in the delivered SLA. However, these high-frequency signals are also delivered under the name of Dynamic Atmospheric Correction (DAC) as an auxiliary product (Dynamic Atmospheric Corrections are produced by CLS Space Oceanography Division using the Mog2D model from Legos and distributed by Aviso, with support from Cnes, `http://www.aviso.oceanobs.com/`). This product is currently used in the correction of the altimeter data sets in order to reduce the aliasing effects of high frequency signals (Volkov et al., 2007). In this work, in order to have the sea level variation due to atmospheric forcing included in the altimeter data, DAC product has been added to the along-track DT-SLA (Delayed Time Sea Level Anomaly).

Once the along-track satellite data has the sea level variation due to atmospheric forcing included, the domain is divided in 1-by-1 degree boxes. At each box, all the satellite data placed within it are selected and compared with the closest grid point (in space and time) from GOS database, an example is shown in Fig.2.7.

In order to compare model outputs and satellite data, a statistical analysis is carried out for each box. Since satellite data start in 1992 and the hindcast database ends up in 2009, a period between 1992 and 2009 is selected to perform the validation. The comparison with satellite data is made for both databases. Here the results for GOS 2.1 are presented. The validation of GOS 1.1 provides very similar results (not shown).

An example of some scatterplots, performed for the areas that overlap the tide gauge locations presented in Fig.2.4, can be seen in Fig.2.8. They show the comparison between the satellite and GOS results, taking into account all the data within a 1-by-1 degree box centred at the tide gauge position. Contrasting these scatterplots with the ones obtained from the tide gauge validation (see Fig.2.4), slight differences in RMSE and ρ can be observed, as well as a steeper underestimation of the results. It should be kept in mind that the number of available satellite data is considerably smaller than the tide gauge observations. Therefore, the validation with altimeters is also accurate, as shown in Fig.2.9, where the correlation factor and the RMSE are displayed. These results show a good agreement between the model output and the satellite data. The correlation factor is high through most of the domain (greater than 0.75) except for three areas: Northern Adriatic, Aegean Sea and Gulf of Gabes. Similar to the already discussed case of the North Adriatic, also for these other two shallow semi-enclosed basins, the less
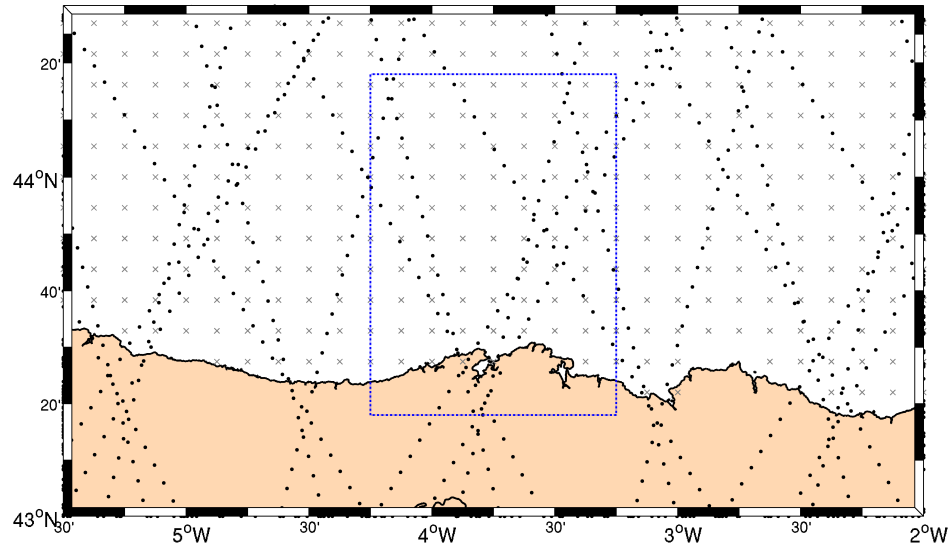
Figure 2.7: Along-track satellite measures (black points) within a 1-by-1 degree box
centred in Santander (Spain). Grey crosses represent GOS grid nodes

accurate results could be related to limitations in data available (e.g., bathymetry) or
description of physical processes (e.g., friction). Lower RMSE are found in the Atlantic,
where the maximum discrepancy is around 8 cm. In the Mediterranean Sea, apart from
the three areas above mentioned, the highest errors observed are about 10 cm. Authors
as Marcos and Tsimplis (2007) or García-Lafuente et al. (2004) have suggested that the
steric signal may be higher in the Mediterranean than in the Atlantic; this would explain
the differences in the RMSE found between the two areas.

Validation with altimeter data has shown the good accuracy of GOS database. As was
already mentioned in section 2.3.1, even though modelled series and satellite series do
not include sea level variations due to exactly the same forcings, high correlations and
low errors are obtained from this comparison.

Validation with altimeters has allowed the identification of some areas where GOS data-
bases do not represent correctly the storm surge level. In these regions, GOS signal
overestimates altimeter data. If the reason of these differences lied in an inadequate
spatial resolution of the atmospheric forcing, storm surge results should lead to an un-
derestimation of the signal, as pointed out by Wakelin and Proctor (2002), where they
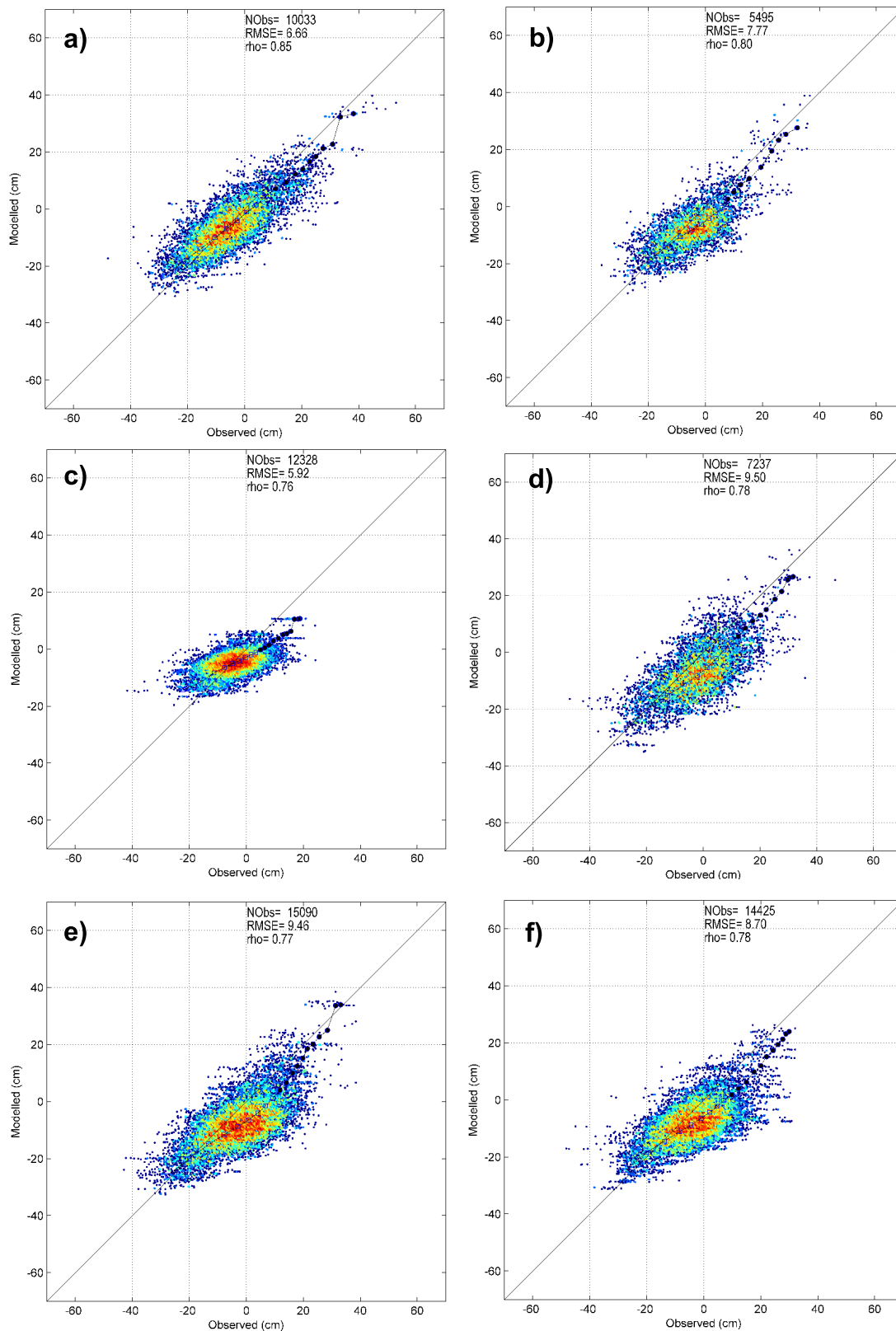
Figure 2.8: Diagnostics plots for the 1-by1 degree boxes associated with tide gauges from Fig. 4 used for the validation of GOS 2.1 dataset. Quantiles (solid circles are quantiles over the 90th percentiles) and statistical indices of observed versus modelled values are shown. Colours represent data density (increasing values from blue to red). a) Santander b) Huelva c) Arinaga d) Genova e) Porto Torres f) Palermo.
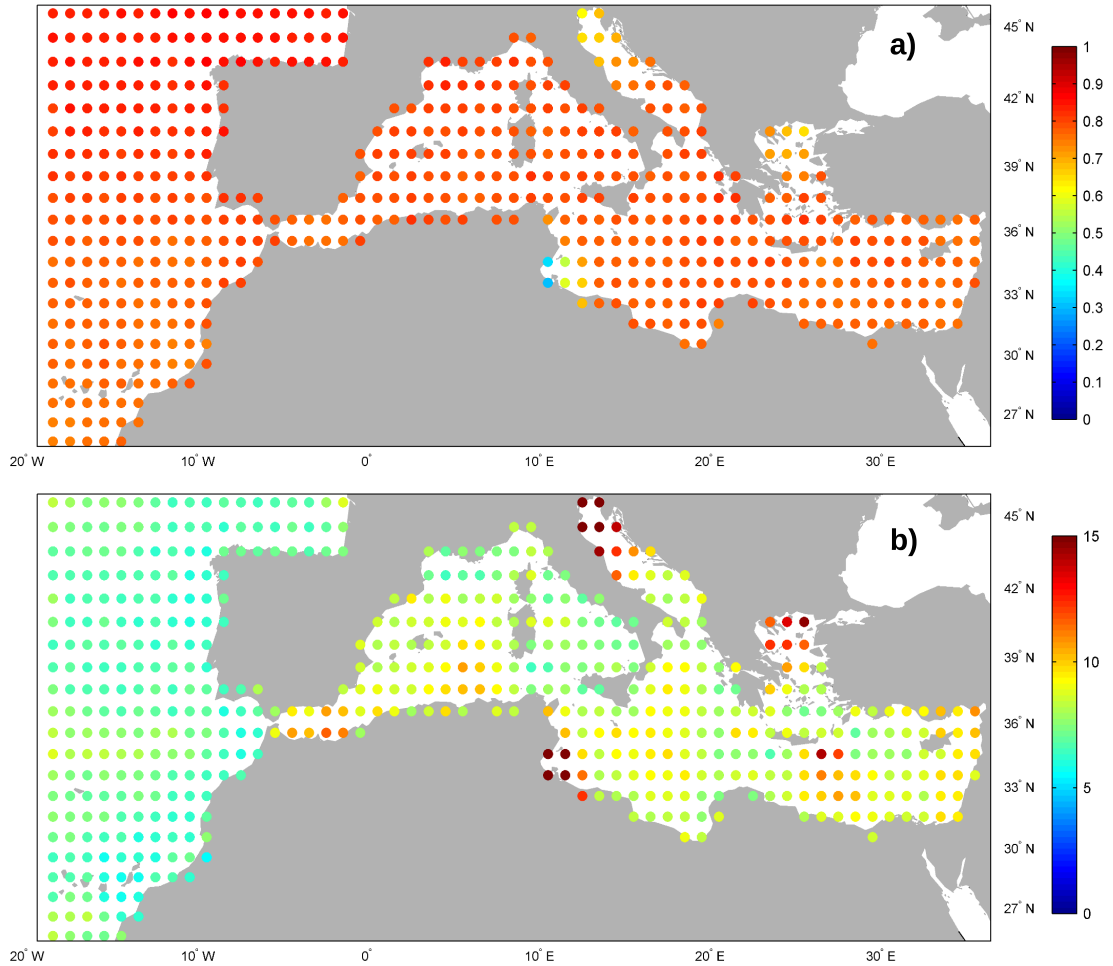
Figure 2.9: Comparison between GOS 2.1 hindcast and altimeter data. a) Correlation index (ρ), b) Root mean square error in cm (RMSE)

conclude that a coarse spatial resolution in the atmospheric forcing results in an underestimation of the amplitude of the surges in the Adriatic Sea. Hence, the overestimation of GOS in these relatively shallow areas, could be more probably explained in terms of the bathymetry or frictional parameters used, as already suggested by Pascual et al. (2008).

2.4. Storm surge variability

In this section, long term variability and trends in storm surge are calculated using GOS databases. For this purpose time series at each grid point are averaged at different time scales. Averages are made monthly and seasonally, and trends are obtained by a linear fit to each grid point.

Some studies carried out so far (Calafat and Gomis, 2009; Gomis et al., 2008; Tsimplis et al., 2005) have pointed out the different results obtained when computing trends from

different periods. For this reason, according to the developed GOS data set, the storm surge behaviour for two time periods is investigated. A long term trend from 1948 to 2009, and a recent trend from 1989 to 2009, are estimated. Storm surge trends for the last 61 years (GOS 1.1) and for the last 21 years (GOS 2.1) are presented in Fig.2.10. The analysis for the last two decades was also done using GOS 1.1; trends are similar (not shown) to the ones obtained with GOS 2.1 (Fig.2.10b), suggesting that trends do not depend on the database but on the period analysed. Trends for the 1948-2009 period (Fig.2.10a) are negative in all domain, showing stronger values in the Atlantic African coast, the Adriatic and the North-East of the Levantine basin, with values around -0.35 mm/yr. Weaker trends are found in the North Atlantic Spanish coast and also along the East part of the Mediterranean African coast, where trends are about -0.1 mm/yr. Fig.2.10b shows trends for the 1989-2009 period, in this case trends are positive all along the domain, showing quite uniform values around 0.5 mm/yr for the Atlantic sector and more variability in the Mediterranean Sea with values ranging between 0.6 and 1.5 mm/yr. Similar results were obtained by Gomis et al. (2008) when computing trends for modelled sea level due to wind and pressure. They showed negative values when computing trends for period 1958-2001 and positive values when computing trends for period 1993-2001. This difference in the sign of the trends also found between GOS 1.1 (1948-2009) and GOS 2.1 (1989-2009) can be correlated with trends obtained from tide gauges by Tsimplis and Baker (2000) and Tsimplis et al. (2005). They displayed negative trends for the period 1960-1994 in most of the Mediterranean tide gauges (typically between -0.5 and -1 mm/yr), while for the last decade tide gauges reported sea level trends between +5 and +10 mm/yr. Therefore, trends in the observed sea level could be partially explained in terms of changes in the atmospheric forcing.

To analyse seasonal variability of storm surge, hourly series are averaged gathering each season of every year in a single value. Periods are defined as: Spring (March 15th – June 15th), summer (June 15th – September 15th), autumn (September 15th – December 15th), and winter (December 15th – March 15th). Fig.2.11 shows mean values for each season for GOS 1.1. As can be seen, the transitional stages, spring and autumn, show a weak climate variability of mean storm surge, with quite uniform values ranging between -1 and +1 cm in most of the domain. Summer and winter present an opposite spatial pattern to each other. In summer, highest values are found in the Eastern Mediterranean basin (3 cm) and slightly smaller along the African Atlantic coast. Lowest values are found in the Adriatic, North Atlantic Spanish coast and Libya and Tunisia coasts (-3 cm). Highest mean storm surge levels during winter season are located at the Gulf of Biscay, north coast of the Iberian Peninsula, the whole Italian coast and the Adriatic Sea and also along the eastern Mediterranean African coast and the Aegean Sea.
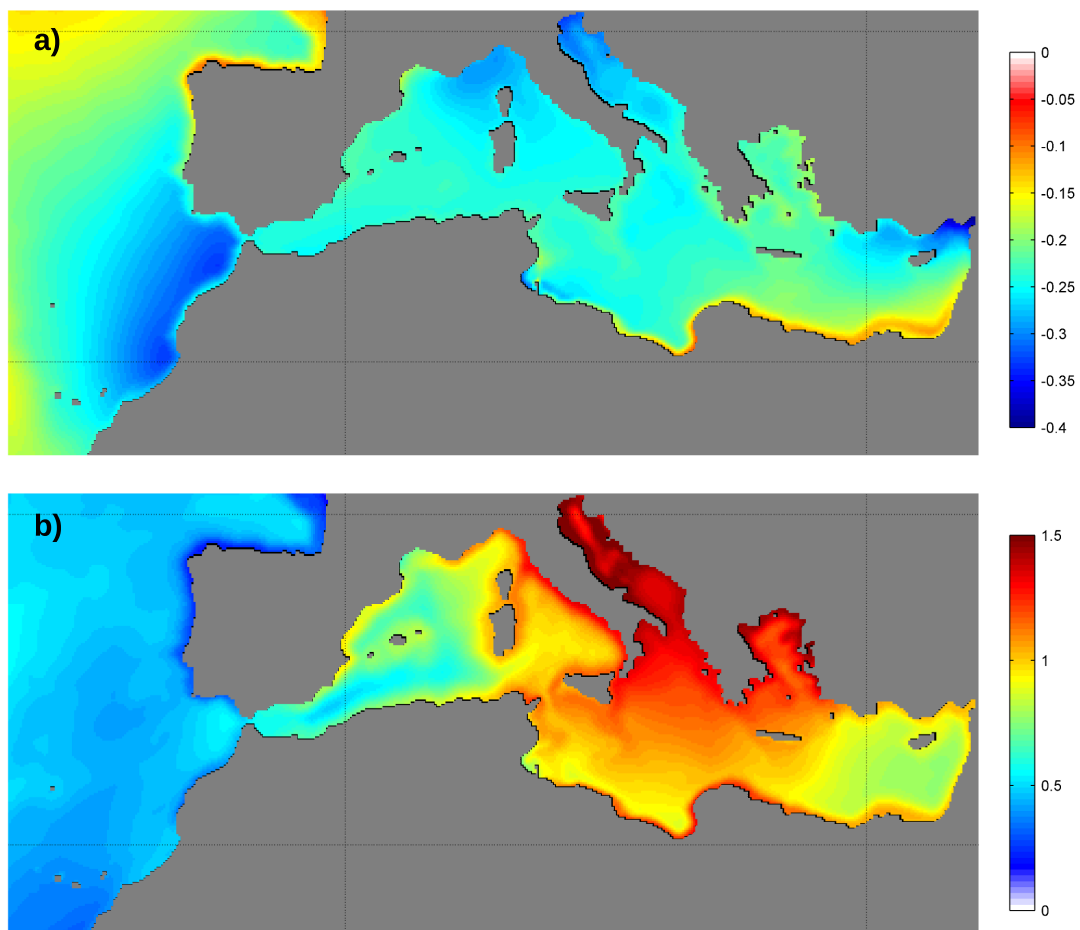
Figure 2.10: a) Estimated long term trends (mm/yr) of storm surge for GOS 1.1 (1948-2009) and b) estimated trend (mm/yr) for the last two decades (1989-2009, GOS 2.1).
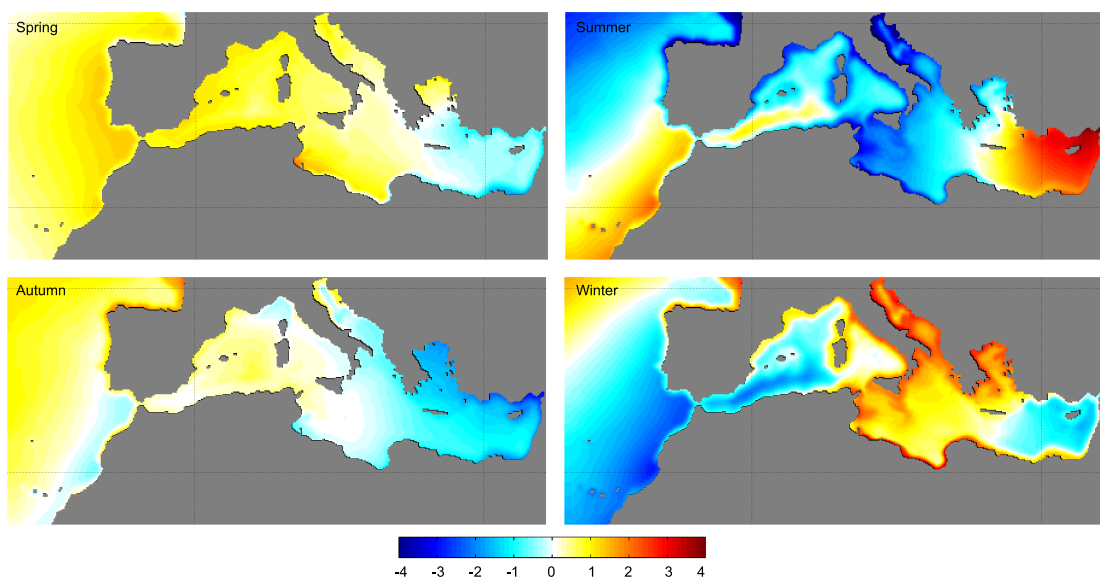
Figure 2.11: Mean seasonal values of storm surge (cm) for the 1948-2009 period (GOS 1.1).

Fig.2.12 shows the seasonal trends for winter and summer periods. As can be observed, winter trends are negative all along the domain. Strong trends are found in the Adriatic and in the central Mediterranean, with values around -1 mm/yr. Smaller but still negative trends are found in the Eastern Mediterranean and in the Atlantic area. Summer trends show positive and negative values. Positive values of around 0.1 mm/yr are found in the North Atlantic and Mediterranean Spanish coast and also along the Tunisian coast. The strongest negative trends (-0.3 mm/yr) are found along the Atlantic African coast. Similar patterns regarding seasonal trends were found by Gomis et al. (2008).
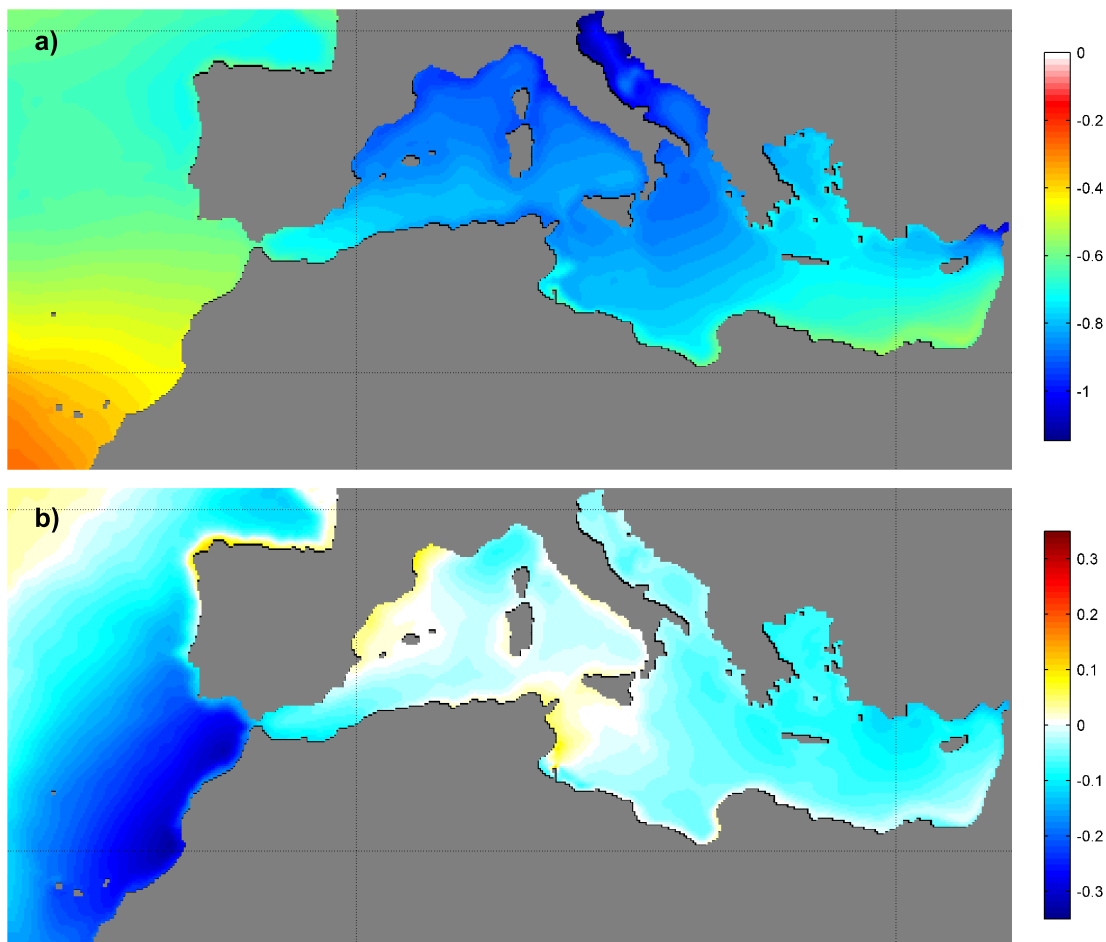
Figure 2.12: Seasonal trends (mm/yr) for the 1948-2009 period (GOS 1.1). a) Winter b) Summer.

2.5. Summary and conclusions

The main objective of this study was the generation of a long-term high-resolution (1/8°) storm surge database for Southern Europe. Studying the sensitivity of the storm surge results to the resolution of the atmospheric fields was also possible through the

two different runs carried out using ROMS model. The difference between the two hindcasts lies in the atmospheric forcing used. These atmospheric fields were the result of two dynamical downscalings: a regional re-forecast coupling the WRF-ARW model to NCEP reanalysis and to ERA-Interim conditions. The model is driven hourly with these high-resolution atmospheric fields (30 and 15 km, respectively). Therefore, two hourly data set of storm surge hindcast are obtained: GOS 1.1, a 62-year (1948-2009) dataset forced with an atmospheric downscaling (30 km) obtained with NCEP reanalysis; and GOS 2.1 a 21-year (1989-2009) dataset forced with an atmospheric downscaling (15 km) obtained with ERA-Interim.

The storm surge numerical results are comprehensively validated using data provided by tide gauges and altimeter data distributed throughout the domain. It is worthy to note that:

1. 58 tide gauges are used for the validation;

2. validation with satellite data has allowed a wide spatial comparison.

The spatial validation has pointed out some areas where the model shows unreliable results that otherwise would have not been noticed due to the lack of tide gauges measures in those areas. The overestimation of the model in these relative shallow and semi-enclosed areas could be explained in terms of the bathymetry or the frictional parameters used. However, a further study is needed in order to address other possible sources (e.g., resonance of the surges).

The statistical analysis carried out shows that, at tide gauge locations, the correlation factor is over 0.8 in the Atlantic area and about 0.75 in the Mediterranean Sea. RMSE are lower or around 10 cm for the whole set of tide gauges.

Accurate results are also obtained when comparing with satellite data. Most of the domain presents a correlation index over 0.75 and a RMSE of 8-10 cm. This validation has shown the good agreement between modelled and measured data and the capability of the model to simulate accurately storm surge sea level.

Regarding the sensitivity of the storm surge results to the resolution of the atmospheric fields, the statistical validation shows similar results for both storm surge data set GOS 1.1 and GOS 2.1. Although the correlation coefficients are slightly higher for GOS 2.1, the results show no significant improvement when increasing the resolution of the atmospheric forcing fields from 30 to 15 km. We should bear in mind that both atmospheric forcings are already high-resolution fields and both have an hourly temporal resolution, thus differences between the two GOS databases should not be as noticeable as the ones

found by other authors (Wakelin and Proctor, 2002) since they compared data with really different temporal and spatial resolutions. Moreover, a further analysis in coastal or estuarine areas should be carried out in order to test how increasing the atmospheric forcing resolution affects the results at local scale.

The analysis of the storm surge variability has identified negative trends for the period 1948-2009 (GOS 1.1) while positive trends are obtained for the last 20 years (GOS 2.1). These results are in agreement with trends found in Mediterranean tide gauges by Tsimplis et al. (2005) and with trends from a numerical model found by Gomis et al. (2008), showing that trends are positive before 1960 and also during the period 1993-2001, while during 1960-1994 sea level trends are negative. The seasonal analysis has also shown that the overall negative trends found in the domain are mainly driven by the winter season.

This work has shown how the new storm surge database can be applied to study variability and trends. Future studies could use the databases to address for example extreme events. Further improvements in terms of bathymetry resolution and, possibly, a downscaling at coastal scale could provide insight on local processes and improve predictability.

Chapter 3

Long-term changes in the frequency, intensity and duration of extreme storm surge events in southern Europe

Abstract

Storm surges are one of the major hazards in coastal regions; positive surge events are added to tidal levels, increasing the risk of coastal flooding by extreme water levels. In this study, changes in the frequency (occurrence rate per year), intensity (magnitude of the extremes) and duration of extreme storm surge events from 1948 to 2013 are investigated using a non-stationary statistical model. To fully model extremes, the time-dependent statistical model combines the Generalized Pareto Distribution (GPD) for studying exceedances over the threshold, and the non-homogeneous Poisson (P) process for studying the occurrence rate of these exceedances. Long-term trends and the association between storm surges and the North Atlantic Oscillation (NAO) are represented in the model by allowing the parameters in the GPD-P model to be time-dependent.

Different spatial patterns in the three analysed properties of storm surges are found in the Atlantic region and the Mediterranean Sea. The up to now uncharted regional patterns of storm surge duration show completely different values between the Atlantic

and the Mediterranean regions, being the duration of storms surges in the Atlantic two times longer than the duration in the Mediterranean. For the last half century, we detect positive and negative spatial trends in terms of intensity of storm surge but only significant decreasing rates, of around 2%, in the number of extreme events per year. Regarding duration, we find positive trends in certain Mediterranean areas, with durations of extreme events increasing at a rate of 0.5-1.5 hours/year. Values for the fifty-year return level are also estimated, showing a large spatial variability with relatively higher values along the coast. A clear sensitivity of extreme storm surges to negative NAO index is detected, specifically in the western Mediterranean basin. Results show that negative NAO phases lead to an increase in the number of extreme events and also in their intensity.

3.1. Introduction

Coastal areas are specially vulnerable to climate variability and changes in sea level. Particularly, extreme sea level events have immediate impacts on the coast (Storch and Woth, 2008). During the past century, storm surge events have caused considerable damage to properties and even loss of life. One of the worst natural disasters in Europe was the 1953 North Sea flood (Baxter, 2005), which led to promote major studies on the strengthening of coastal defences. Over the Mediterranean Sea, there are also numerous low pressure systems, a few of which may develop a dynamical evolution similar to the one of tropical cyclones (medicanes) (see Cavicchia et al. 2014). Such storms produce severe damage in the highly populated coastal areas surrounding the Mediterranean Sea. Therefore, it is important in the general coastal planning and in flood risk assessment, to try to foresee future storm surge impacts on the coast. These extreme events are generally driven by the combination of high tides and storm surges. While astronomical tide is a deterministic component of the sea level, storm surge depends on the atmospheric pressure and wind; hence, in order to study long-term changes in coastal risks, it is necessary to analyse this non-deterministic variable from a statistical point of view.

Various statistical techniques have been used to study changes in extreme sea level events. A basic approach is the percentile time series analysis. This technique has provided interesting information about the different behaviour of high water levels with respect to the mean sea level (e.g. Woodworth and Blackman 2004), however, it does not allow the estimation of return water levels. Focusing on extreme value models, two familiar approximations in extreme value theory are the Generalized Extreme Value (GEV) distribution from block maxima, and the Generalized Pareto (GP) distributions from the excesses over a threshold. A set of methods can be used for the selection of

extreme sea levels. The classical annual maxima method (AMM) has the disadvantage of gathering a small extreme sample that could disregard extremes in the remaining data. The limitation of AMM can be overcome by methods that select maxima from shorter time blocks than a year such as monthly maxima, the r-largest values within a year, or the independent peaks over a threshold. The use of monthly maxima requires modelling the seasonal dependence for the good estimation of return periods (see Méndez et al. 2007) and the r-larger values requires defining a specific number of extremes per period (Coles et al., 2001). These techniques are, however, constrained to choosing the same number of maxima within time blocks, which can lead to a misinterpretation of climatic changes in an environment with a mean sea level rise and large inter-annual variations. Taking this into consideration, in this work we have decided to define extreme events as the exceedances over a high threshold. Two important issues that must be overcome when using the peak over threshold approach are the selection of the threshold and the minimum time span that will be required to assume the independence of consecutive storm events, since both affect the results in terms of the frequency and the exceedance estimates (see, e.g, Arns et al. 2013). Storm surge extremes have been selected from an already validated surge database (GOS database, see Cid et al. 2014) that provides, for southern Europe, a long (66 year length) and spatially uniform set of data, which is adequate to analyse long-term changes in the storm surge extremes.

The above-mentioned statistical techniques have been applied lately to analyse extreme sea level events. For example, Gräwe and Burchard (2012) tested different statistical methods to estimate return periods on simulated storm surges. Merrifield et al. (2013) use the AMM to investigate spatial patterns of the relative contributions from tides and non-tidal residual components. The AMM is also the approach chosen by Bernier and Thompson (2006) to calculate return levels in the north-west Atlantic. The r-largest method has been widely used in European regions (e.g. Tsimplis 1997 in the Aegean and Ionian seas, Butler et al. 2007 in the North Sea, and Marcos et al. 2009 in the Mediterranean Sea). Both methods, the AMM and the r-largest were used by Haigh et al. (2014) to estimate extreme water levels around the coastline of Australia. Finally, the peak-over-threshold (POT) approach has been recently applied to determine return water levels, as for instance, in northern Germany (see Arns et al. 2015); and specifically for storm surges, it was used by Tebaldi et al. (2012) along the US coasts, Hallegatte et al. (2011) in Copenhagen-Denmark and Bernardara et al. (2011) along the French Atlantic coasts.

The IPCC (Intergovernmental Panel on Climate Change) concludes that climate change might affect the frequency, intensity, and length of many extreme events, such as floods and storms (Church et al., 2013), which would also lead to a non-stationary behaviour of storm surges. Therefore, we propose a time-dependent extreme model that combines

the Generalized Pareto Distribution (GPD) for studying exceedances over a threshold (in terms of intensity and duration), and the Poisson (P) process for studying the occurrence rate of these exceedances. Note that a point-process approach in terms of extreme value models is not commonly used to analyse variations of sea surface variables, and moreover, non-stationarity in extremes tends to be overlooked in the extreme value theory. Some exceptions can be found in the literature. The effect of temporal dependence on the frequency of storm surge in the western Mediterranean basin is explored from a non-homogeneous Poisson model in Luceño et al. (2006). The methodology to analyse climate variations at different time scales from a time-dependent monthly GEV model in extreme sea levels is described in Méndez et al. (2007). The seasonal, mean sea level rise and astronomical modulations in high water levels are explored in Menendez et al. (2009) from a time-dependent GEV as a potential extreme forecast tool. Different time-dependent extreme models are applied in Menéndez and Woodworth (2010) to a global tide-gauge dataset to conclude that the highest water levels have been increasing since the 1950s in most regions of the world mainly due to mean sea level rise, although higher regional extremes are also caused by interannual-decadal variations associated with climate fluctuations. Non-stationary extreme models have also been applied to storm surge water levels; Marcos et al. (2011) analysed the extension of GEV model to r-largest values with several time-dependent terms in order to study changes in storm surges under projections of climate scenarios. Mudersbach and Jensen (2010) used an approach based on the GEV distribution and compared the results with common stationary methods. Serafin and Ruggiero (2014) modelled extreme events of total water levels (waves, tides, and non-tidal residuals) using non-stationary extreme value distribution that includes seasonality and climate variability.

The main goal of this work is the analysis of changes in extreme storm surges (i.e. changes in extreme sea levels produced by the effect of wind stress and pressure gradients over the sea surface). Following this purpose, a statistical framework to study extreme surges is established. Extreme events have been chosen using a POT technique, which allows us not to limit the number of extremes to a certain amount, but to consider all the events above a threshold. A spatial description of these storm surge extremes in terms of intensity, duration and frequency is given. In a second step, trends were studied by means of a time-dependent GPD-Poisson model, where time variability is included by adding linear trends on the scale parameter of Pareto and on the Poisson parameter. The use of a time-dependent GPD-P model has enabled us to estimate long-term trends, not only in terms of the magnitude of the extremes but also in the frequency. Specifically, significant trends in the intensity, frequency and duration of the extreme storm surge events, as well as the value of the 50-year return level were estimated at every grid-point of the model domain. Sensitivity of frequency and magnitude of extreme surges

to monthly NAO index was also studied.

Following this purpose, the next section describes briefly the database used for selecting the extremes (Section 3.2). The methodology applied for defining and fitting the extremes is explained in Section 3.3. Section 3.4 describes the extremes in terms of intensity, frequency and duration and also gives the results of implementing the statistical model, in terms of trends, sensitivity to NAO and the estimation of 50-year return levels. Finally, a summary and a discussion are provided in Section 3.5.

3.2. Database description

Extreme events have been selected from a 66-year (1948-2013) high-resolution surge hindcast named GOS 1.1, which describes the sea level variation due to the effect of wind stress and pressure gradients. (Cid et al., 2014). Although the database in Cid et al. (2014) ends in 2009, for this work GOS 1.1 has been updated until December 2013. It has been performed for southern Europe using the Regional Ocean Modelling System (ROMS) of Rutgers University. ROMS is a three-dimensional, free-surface, terrain-following ocean model that solves the Reynolds-averaged Navier–Stokes equations using the hydrostatic vertical momentum balance and Boussinesq approximation with a split-explicit time stepping algorithm (Haidvogel et al., 2008, 2000; Shchepetkin and McWilliams, 2005). It uses a horizontal curvilinear Arakawa C grid and vertical stretched terrain-following coordinates. The model domain (see green box on subplot at Fig.4.2) encloses southern Europe, including the Mediterranean Sea and the Atlantic area in southern Europe, with a horizontal resolution of 1/8° ($\sim$ 14 km). GOS 1.1 was driven with hourly meteorological data of wind and atmospheric pressure from the *Sea-Wind I* hindcast (Menendez et al., 2014). The *SeaWind I* dataset is a high-resolution (30 km) atmospheric dynamical downscaling from NCEP global atmospheric reanalysis focused on offshore surface wind fields. The ROMS model was run in barotropic mode and the inverted barometer effect was imposed at the open boundaries of the domain (north and west edges), using a free surface Chapman condition and 2D Flather condition for momentum. The GOS 1.1 database was exhaustively validated with tide gauges and satellite data, reaching high correlation coefficients and small root mean square errors all over the domain, except for three semi-enclosed areas (northern Adriatic, Gulf of Gabes and Aegean Sea) where the hindcast overestimates satellite measures. An example of the general agreement between measured and modelled data can be seen in Fig.4.2 for Vigo and Barcelona tide gauges. The modelled surge data (red line) are well correlated with the tide gauge measures (blue line), where statistics show a root mean square error of 6.5 cm and a correlation factor of 0.88 (see Cid et al. 2014). A good
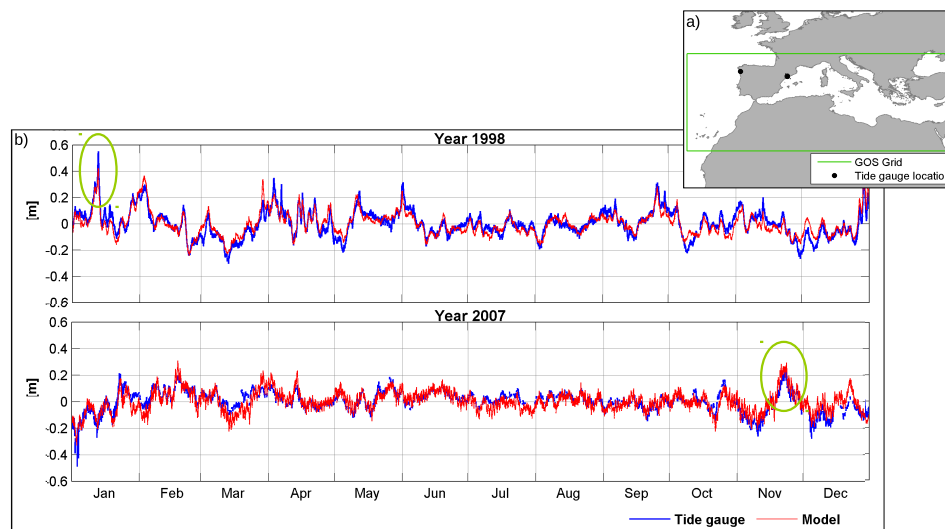
Figure 3.1: Panel a) shows the model domain (green box) and the location (black dot) where data are compared. b) Storm surge comparison (m) at Vigo (top) and Barcelona (bottom) tide gauges for years 1998 and 2007, respectively. Measured data (blue line) vs. modelled data (red line). Green circles encompass instants of high surge levels

agreement is also observed when referring to extreme values, as can be seen from the data within green circles. Note that GOS 1.1 grid-points have a spatial resolution of about 14 km and therefore they do not exactly represent in-situ values in shallow water depths at the coast (i.e. tide gauge records).

3.3. Extreme value model

3.3.1. Selection of the extreme events

Surge time series are extracted from the hourly database at every grid cell of the domain. Following the Peak Over Threshold (POT) technique, all data over the threshold of 99.5%, derived from the entire period, are considered exceedances. The threshold selection is made taking into account that the number of events above the threshold is sufficient not to violate the basis of the model (i.e. an average of around 2 events per year, following the experience of previous works, e.g. Menéndez et al. 2008)

Fig.4.3 represents the applied method to characterise storm surge extremes. Red dots indicate the peaks of 2 events (excesses y_i and y_{i+1}) that happen at time t_i and t_{i+1}; the duration of each extreme event is given by d_i and d_{i+1}, respectively. The statistical model used to estimate trends requires the extremes to be independent. Thereby, the independence between consecutive events is achieved by imposing that extremes must be separated by at least 3 days in between. This value has been chosen taking into account that the average lifetime of the cyclones in the Mediterranean is 28 hours and
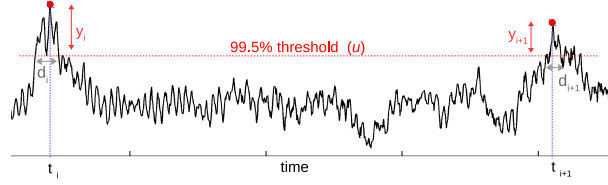
Figure 3.2: Peak over threshold technique. Red dots are extreme events, values over the 99.5%. Each of the selected extremes occurs at a specific time t_i, has a specific duration of d_i and exceeds the threshold by an amount of y_i

the typical values for the North Atlantic are 3 days (Trigo et al., 1999). Therefore, the value of 3 days is selected to ensure independence between storms in the region. The maxima sample data is then introduced in the extreme model. Results of the extreme statistical analysis in terms of number of events per year and duration will be shown in section 3.4.

3.3.2. The time-dependent GPD-Poisson model

As already mentioned, the statistical model chosen to estimate long-term trends in the frequency (extremes occurrence rate), intensity (sea level reached above the threshold) and duration (number of hours where the level is above the threshold) of storm surge events is a time-dependent version of the Peak Over Threshold model (Méndez et al., 2006). This model combines the Generalized Pareto Distribution (GPD) (see Eq.3.1) for studying exceedances over a threshold, and the Poisson Distribution (P) (see Eq.4.1) for studying the occurrence rate of exceedances.

$$G(x; \sigma, \xi) = 1 - (1 + \xi \frac{x}{\sigma})^{-1/\xi} \tag{3.1}$$

$$P(n; \lambda) = e^{-\lambda} \frac{\lambda^n}{n!} \tag{3.2}$$

The basic idea is to choose a high threshold (u) and to study the statistical properties of all the exceedances over u; specifically, the number of events (n) every year, the amounts by which the threshold is exceeded (threshold excesses, i.e. y_i) and the duration over that threshold (d_i).

The number of events (n) over the level u in any given year follows a Poisson distribution with annual mean λ. The intensity and duration of the extremes will be the variables analysed by the GPD distribution. The combination of Poisson model for frequency and the GPD model for intensity (or duration) can be expressed as shown in Eq. 4.2.

$$H(x, n; \sigma, \xi, \lambda) = exp\{-\lambda \left(1 + \xi \frac{x}{\sigma}\right)^{-1/\xi}\} \tag{3.3}$$

where $\lambda > 0$ is the Poisson parameter (mean number of events over a period of time), and $\sigma > 0$ and ξ ($-\infty < \xi < \infty$) are the scale and shape Pareto parameters, respectively. x corresponds to the threshold excess (or the duration) of the selected extreme events.

For this purpose, the GPD-P model is run twice; in one case the variable of the GPD distribution (x) is the sample of the independent peaks (i.e. y_i) and in a second run the GPD variable is the sample of durations of the independent events (i.e. d_i). In both cases the Poisson variable is the occurrence of the extreme events (i.e. t_i).

The main idea of the approach in this work is to consider that the exceedance probability of a certain extreme event varies through time. Consequently, variability is represented in the model by allowing the parameters in the GPD-P to be time-dependent, using linear parametric expressions for the scale Pareto parameter (Eq.3.4) and the Poisson parameter (Eq.3.5).

$$\sigma(t) = \sigma_0 + \sigma_1(t - t_0) \tag{3.4}$$

$$\lambda(t) = \int_{t_0}^{t_f} \nu(t) \, dt \,; \qquad \nu(t) = \nu_0 + \nu_1(t - t_0) \tag{3.5}$$

where $\nu(t)$ represents the rate of occurrence of independent events over the threshold every year. $\sigma(t)$ accounts for the mean value and the variance of the exceedances.

The added value of this extreme model in the estimation of trends on return values is shown in Fig.4.4. In this figure, blue dots represent the excesses of the selected extreme events for a grid cell located at the south-west of Cyprus (31.5° in longitude and 34.23° in latitude), blue line corresponds to scale Pareto parameter, green line is the Poisson parameter and black line is 50-year return level estimated as shown in Eq.3.6.

$$Y_{50}(t) = u - \frac{\sigma(t)}{\xi} \left[1 - (\nu(t) \ T)^{\xi} \right] \tag{3.6}$$

where $\sigma(t)$, ξ and $\nu(t)$ are the GPD-P parameters; T is, in this case, 50 years and $Y_{50}(t)$ is the time-dependent 50-year return level.

A visual inspection of the maxima sample (blue dots) on Fig.4.4 shows a slight increase in magnitude and a clear decrease in the frequency of the events throughout the analysed period (1948-2013). Fig.4.4a shows the stationary approach, where the GPD-P
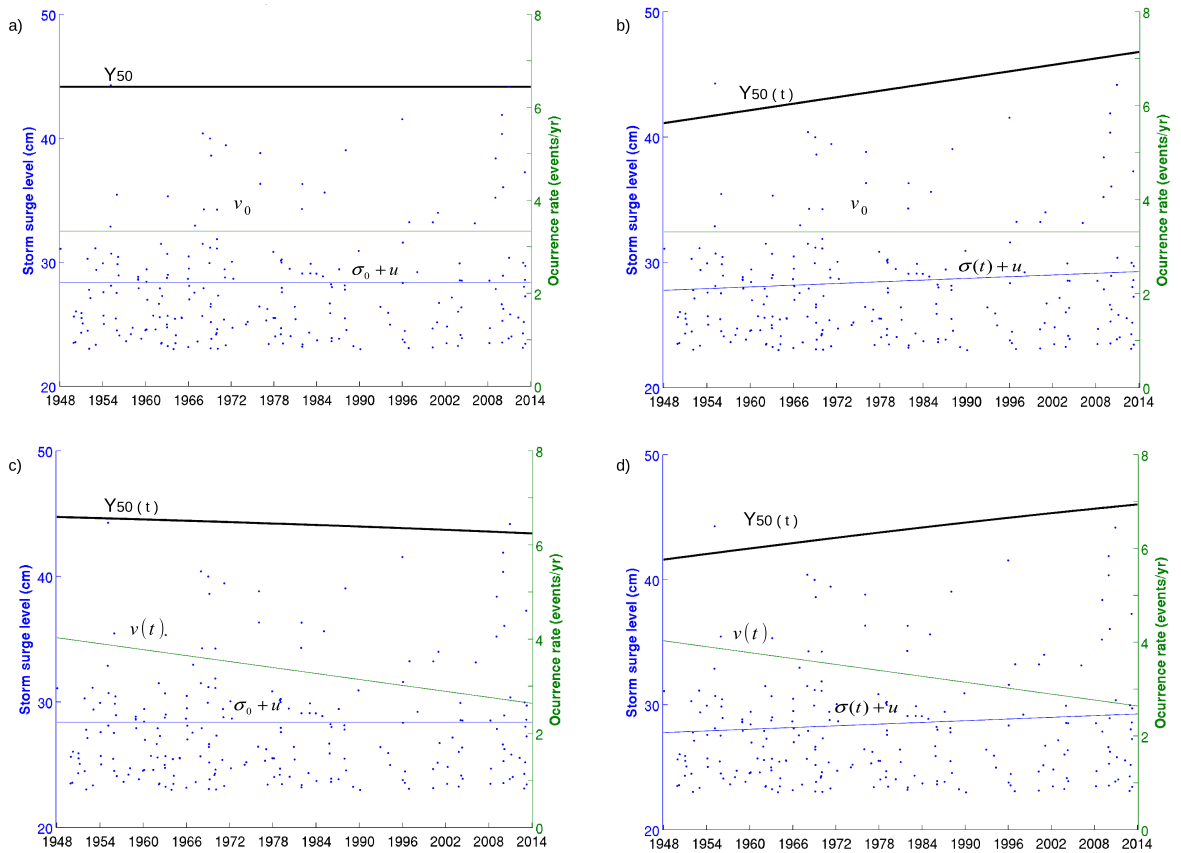
Figure 3.3: Effect of the time-dependent parameters. Blue dots: extreme events; blue line: scale Pareto parameter; green line: Poisson parameter; black line: 50-year return level. a) stationary case. b) time-dependent scale Pareto parameter. c) time-dependent Poisson parameter. d) both Pareto and Poisson parameters are time-dependent.

parameters are constant (u=23 cm; $\hat{\sigma}_t$=$\hat{\sigma}_0$=5.4 cm; $\hat{\nu}_0$=3.3 events/yr.). The estimated flat 50-year return level is 44.15 cm. The increase in the magnitude of the peaks is depicted in Fig.4.4b, where a trend of 0.86 mm/yr in $\hat{\sigma}_t$ indicates that 42.5 cm is a storm event of the 50-year period during the sixties whilst 46 cm is the 50-year return level from the 2000s. Panel c shows the results if we only take into account time dependence in the occurrence rate of extreme events. A decrease in the occurrence rate of events per year is detected, with about 4 events/year until the seventies to within 3 events/yr nowadays. This decrease in the frequency of extreme events also affects the 50-year return level, which results in 44.5 cm during the sixties and a slightly lower value (43.5 cm) at the end of the 2000s. Fig.4.4d highlights the time dependent analysis taking into account significant trends in both, Pareto and Poisson parameters. The combination of an increase in the magnitude of extreme events and a decrease in the occurrence rate leads to a rise of the 50-year return value through time. Therefore, Fig.4.4 evidences the importance of using a point-process approach since resulting trends may have opposite signs depending on the feature (magnitude/frequency) allowed to be time-dependent.

In order to investigate if the estimated trends are partly due to interannual-decadal fluctuations, the statistical relationship between climate indices and storm surge extremes is studied. A linear term is added to the scale parameter of Pareto (Eq.3.7) and the Poisson parameter (Eq.3.8) to estimate the sensitivity of the storm surge exceedances to climate patterns. The North Atlantic Oscillation index (monthly NAO index, available from the Climate Research Unit `http://www.cru.uea.ac.uk/cru/data/nao`) was chosen to be used as a covariate in the model since its phase and strength has been widely linked to storm surges in Europe. Positive NAO phases lead to an increase in the storms magnitude and frequency towards north-east Europe, while negative NAO phases lead to a shift and weakening of the storms towards southern Europe. This causes a negative correlation between the sea level and the NAO index along the Mediterranean and eastern North Atlantic (e.g. Calafat et al. 2012; Woolf et al. 2003). Most of the English Channel is weakly and negative correlated to NAO, but from the Straits of Dover up to the North Sea, strong and positive correlations are found (e.g. Haigh et al. 2010; Woodworth et al. 2007).

$$\sigma(t) = \sigma_0 + \sigma_2 Cov(t); \tag{3.7}$$

$$\lambda(t) = \int_{t_0}^{t_f} \nu(t) \, dt \,; \qquad \nu(t) = \nu_0 + \nu_2 Cov(t); \tag{3.8}$$

where $Cov(t)$ is the covariate defined by the monthly NAO index.

3.3.3. Statistical inference

The maximum likelihood estimation (MLE) method is chosen to estimate the GPD-P model parameters. If the N exceedances x_1, x_2,...,x_N are observed at days t_1, t_2,...t_N over a T-year period, the log-likelihood function for the time-dependent GPD-Poisson model is expressed as shown in Eq.3.9.

$$l_{x,t}(\theta) = \sum_{i=1}^{N} \left\{ log \, \nu(t_i) - \lambda(t_i) - log \, \sigma(t_i) - \left(1 + \frac{1}{\xi}\right) log \left(1 + \xi \frac{x_i}{\sigma(t_i)}\right) \right\} \tag{3.9}$$

where x_i is the threshold excess (or the duration over the threshold) on day t_i and θ is a vector of regression parameters.

Statistical significance of the time-dependent terms compared with the stationary case, is estimated according to likelihood ratio test which relates the deviance function (see Eq.3.10) to the chi-squared distribution (see Coles et al. 2001).

$$Ds = 2\{l(\theta^a) - l(\theta^b)\} \tag{3.10}$$

where $l(\theta^a)$ and $l(\theta^b)$ are two log-likelihood functions that differ only in the number of regression parameters contained in θ.

3.4. Results

3.4.1. Descriptive statistics of the storm surges

The spatial characteristics of the storm surge in southern Europe can be described from the aforementioned variables of the extreme model, i.e. the value of the 99.5% threshold, the mean number of events per year and the duration of each selected event over and above the threshold. Fig.4.6 shows these estimated variables from the latter half of the twentieth century to the present and for each grid point of the GOS dataset.

Fig.4.6a shows the threshold value above which we have considered surge events as extremes. As can be seen, there is a latitudinal gradient; values of the 99.5 percentile are higher than 30 cm at latitudes above 40°N and decrease gradually to the south, reaching values of around 10 cm nearby the Canary Islands. It is also noticeable how surge values are greater throughout the continental shelf due to the wind set-up. This is clearly visible at the French coast, where its wide shelf originates surge levels of above 35 cm. At the Mediterranean sea, the 99.5 percentile is larger at the west basin, and the largest values are located at five semi-enclosed areas (Gulf of Lion, Gulf of Gabes, Adriatic Sea, Gulf of Sirte and Aegean Sea). Fig.4.6b depicts the mean number of extreme events per year; as can be seen, storm surge events over the 99.5 percentile are usual in semi-enclosed geographical areas every year. More than five events per year over the threshold are found in the five mentioned Mediterranean semi-enclosed areas plus the western and easternmost Mediterranean areas (i.e. the Alboran Sea and the eastern Levantine Mediterranean basin). The Atlantic part of the domain experiences less extreme events every year, with values of around two events/year. Fig.4.6c represents the mean duration of the extreme events. There are clearly two different patterns regarding this variable: the Atlantic and the Mediterranean. Storm surges at the Atlantic part of the domain have a duration of around one day while the duration at the Mediterranean is much smaller, with maximum values of 15 hours in the deepest region of the Mediterranean basin. The occurrence rate and duration maps of storm surges have an inverse spatial
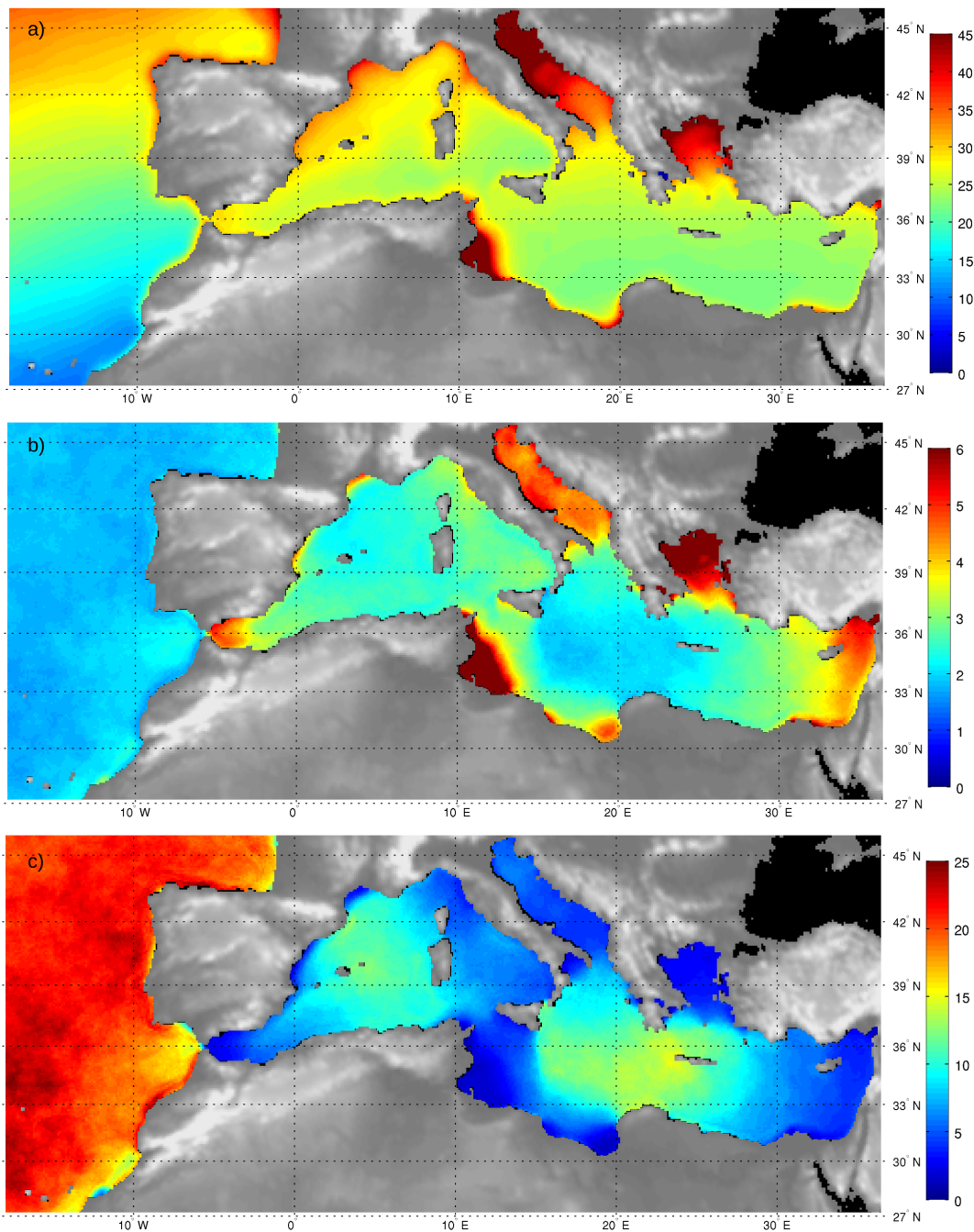
Figure 3.4: Descriptive statistics of storm surge extremes. a) value of the 99.5% threshold (cm). b) mean number of events per year (extremes/year). c) mean of the duration over the threshold (hours).

relationship. This behaviour suggests that the relative small spatial and temporal scale of the meso-scale atmospheric circulation eddies, added to the semi-enclosed character of some coastlines, limit the duration of storm surge events and make them more frequent.

Summing up,

- northern regions show larger magnitudes of high storm surges;

- coasts exposed to the Atlantic Ocean received extreme events of large duration;

- the semi-enclosed areas in the Mediterranean region receive the largest and most frequent storm surge events.

3.4.2. Long-term trends in frequency, intensity and duration of extreme storm surges

Once the GPD-P model is applied, we are able to estimate long-term trends. Fig.4.7 depicts the estimated trends in frequency, intensity and duration. White dots represent areas where trends have a confidence level below the 90%.

Trends in magnitude (see Fig.4.7a, mm/yr) are shown through the linear trend estimated in the time-dependent 50-yr return level. Except for the northern Adriatic, north-west Atlantic, and Gabes and Sirte gulfs, a general increase is estimated in most of the analysed domain. These increases are, however, significant only in the Mediterranean Levantine basin, south Greek coast and north-west Genoa gulf, with trends of around 1 mm/yr, and the Alboran Sea and south coast of Sicily, with increases of about 0.5 mm/yr. Negative trends of 2 mm/yr are estimated at the Gulf of Gabes and Sirte and the north Adriatic. Special caution, however, related to these negative trends must be taken in the north Adriatic and Gulf of Gabes because some uncertainties in the GOS dataset were found during the validation process (Cid et al., 2014).

Trends in frequency are directly given by the non-homogeneous Poisson parameter (Fig.4.7b). In this work, it is expressed as a percentage of change in the number of extreme events per year. Apart from a positive trend in the occurrence rate of events assessed in the south of Greece (increase of 1.5%), only statistically significant decreases are obtained, mainly in semi-enclosed areas at the southern Mediterranean Sea. The largest decreases are found in the middle-south Mediterranean (i.e. Gulf of Sirte and Gulf of Gabes), at diminution rates in the number of events per year of around 2%. Negative trends of about 1% are found in the Alboran Sea, south of Sicily and Levantine Mediterranean basin, and slight decreases are detected in the north Adriatic and Aegean Sea.
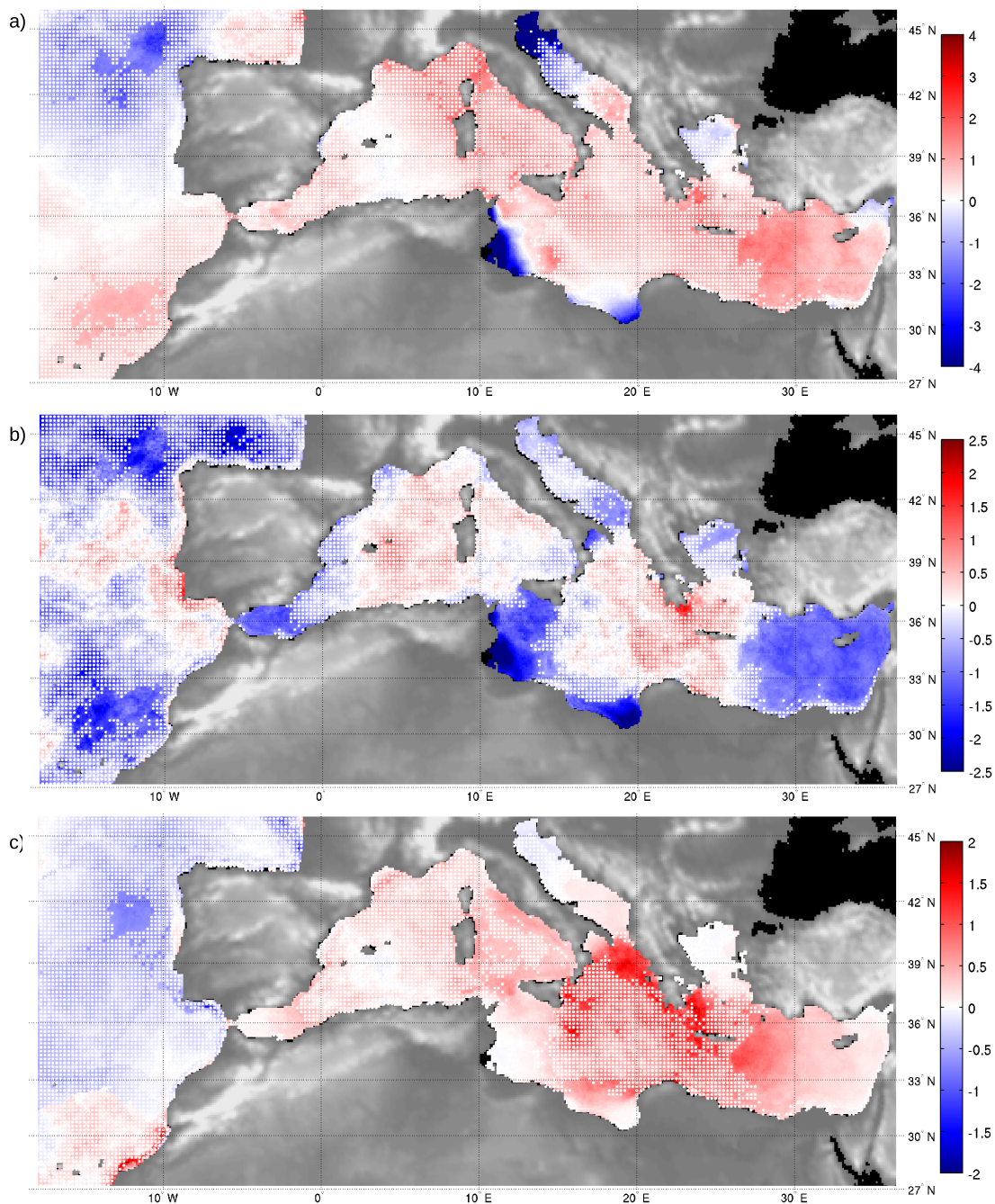
Figure 3.5: Spatial distribution of the long-term trends. White dots represent areas where the statistical significance of the trends is lower than 90%. a) Trends in intensity (mm/yr), obtained from the linear fitting of the yearly 50-year return level. b) Trends in frequency (%), obtained from the time-dependent Poisson parameter and expressed as percentage by using the mean number of events per year. c) Trends in duration (hours/yr), obtained from the second run of the GPD-P model, using the duration of the extremes as the GPD variable

Trends in the duration of extreme events are showed in Fig.4.7c. Results indicate a general decrease in the Atlantic and a general increase in the Mediterranean. The significance of these trends is mainly relevant in the eastern Mediterranean basin. In particular, positive rates of 1.5 h/yr are located at the south of Italy and Greek coasts. Less pronounced trends are found along the Italian Mediterranean coast, with increasing values in the duration of storm surges of rates of 0.5 hours/year. Similar values are reached at Levantine basin, Alboran Sea and along the coasts of Turkey and Egypt.

Overall, some relevant contributions from the analysis of trends for the last half century are:

- Except for some specific regions, most of the Atlantic and Mediterranean southern Europe does not show significant increases or decreases in extreme storm surges. It may indicate that climate variations at lower time scales (seasonal, interannual) are the main drivers of changes in extreme storm surges.

- Only south Greek coasts show an increase of all analysed properties of extreme storm surge. It can be related to the clear significant increases of the magnitude and duration of extreme events in the easternmost Mediterranean basin and may indicate an intensification or changes in circulation patterns of cyclone activity in this region.

- The estimated trends for the last half century reveal a slight but clear decrease in magnitude, occurrence, and duration of extreme storm surge events in the north Adriatic. A detailed analysis should be taken for estimations of changes in Venice lagoon and surroundings due to the complex bathymetry and coastline of this area.

3.4.3. Relationship between NAO and extreme storm surges

Most of the Atlantic and Mediterranean southern European regions do not show significant long-term trends in extreme storm surges. One explanation for this behaviour could be that extreme storm surges have been more affected by inter-annual and decadal variability than by climate variations at longer time scales. This was also described by Wahl and Chambers (2015) for the United States coastline, where they identify regions with considerable multidecadal extreme sea level variations unrelated to changes in mean sea level.

Since storm surges are directly forced by changes in the zonal circulation of the atmosphere and meridional wind components, the relationship between the main coupled ocean-atmosphere mode of variability in the area, the North Atlantic Oscillation (NAO), and extreme storm surges is investigated.

Here, we use the monthly NAO to analyse the relationship between this climate index and extreme surges. Note that we focused on NAO conditions whenever the selected extreme surge events happened and not only during the winter season. A mainly negative relationship is found both in terms of intensity and frequency, which means that extreme storm surges are more intense and more frequent when NAO phase is negative. This is an expected result since negative NAO phases are characterised by a shift of storms tracks towards lower latitudes, and by the high pressure system over the Azores area being weaker than during positive NAO phases, which leads to an increase in the sea level related to the inverse barometer effect. The opposite occurs from the northernmost English Channel to northern European Seas, where positive NAO phases lead to higher sea levels due to more intense storm surge events (Wakelin et al., 2003; Woodworth et al., 2007; Yan et al., 2004).

Although sensitivity to NAO is generally negative, there is a relevant difference of NAO influence patterns in magnitude and frequency of surge extremes. As can be seen from Fig.3.6, where white dots represent areas with less than 90% of statistical significance, most southern Europe shows a significant influence of negative NAO phase in the occurrence of extreme events (see Fig.3.6b) while sensitivity of extremes magnitude is below 90% in most of the Atlantic basin and some areas of the Mediterranean Sea (see Fig.3.6a). The difference in the statistical significance of NAO influence in the properties of the extreme events may be explained in terms of the local-regional scale; the magnitude of the extremes is more affected by the orography or the complex coastline than the occurrence of the event. The highest teleconnections to NAO are found in the western Mediterranean basin. Gulfs of Lion and Genoa and northern Adriatic are the areas where the magnitude of extreme surges is more affected by the NAO index; Alboran Sea and Gulf of Gabes are the areas where the frequency of extremes is more affected by NAO index. These results can be explained by the fact that the occurrence of cyclones in the western Mediterranean basin is partly due to incoming low pressure systems from the Atlantic through the Gulf of Biscay and Iberian peninsula (Trigo et al., 1999) and because the cyclones often remain on the belt-shaped coastal area from the Alboran Sea through the Gulf of Lion and the Gulf of Genoa to the Adriatic Sea (Bartholy et al., 2009).

Fig.3.6 has, therefore, proven that extreme events in southern Europe (their magnitude and their occurrence rate) are significantly affected by NAO, with its negative phase being one of the main drivers of the extreme storm surge events, especially in the western Mediterranean basin.
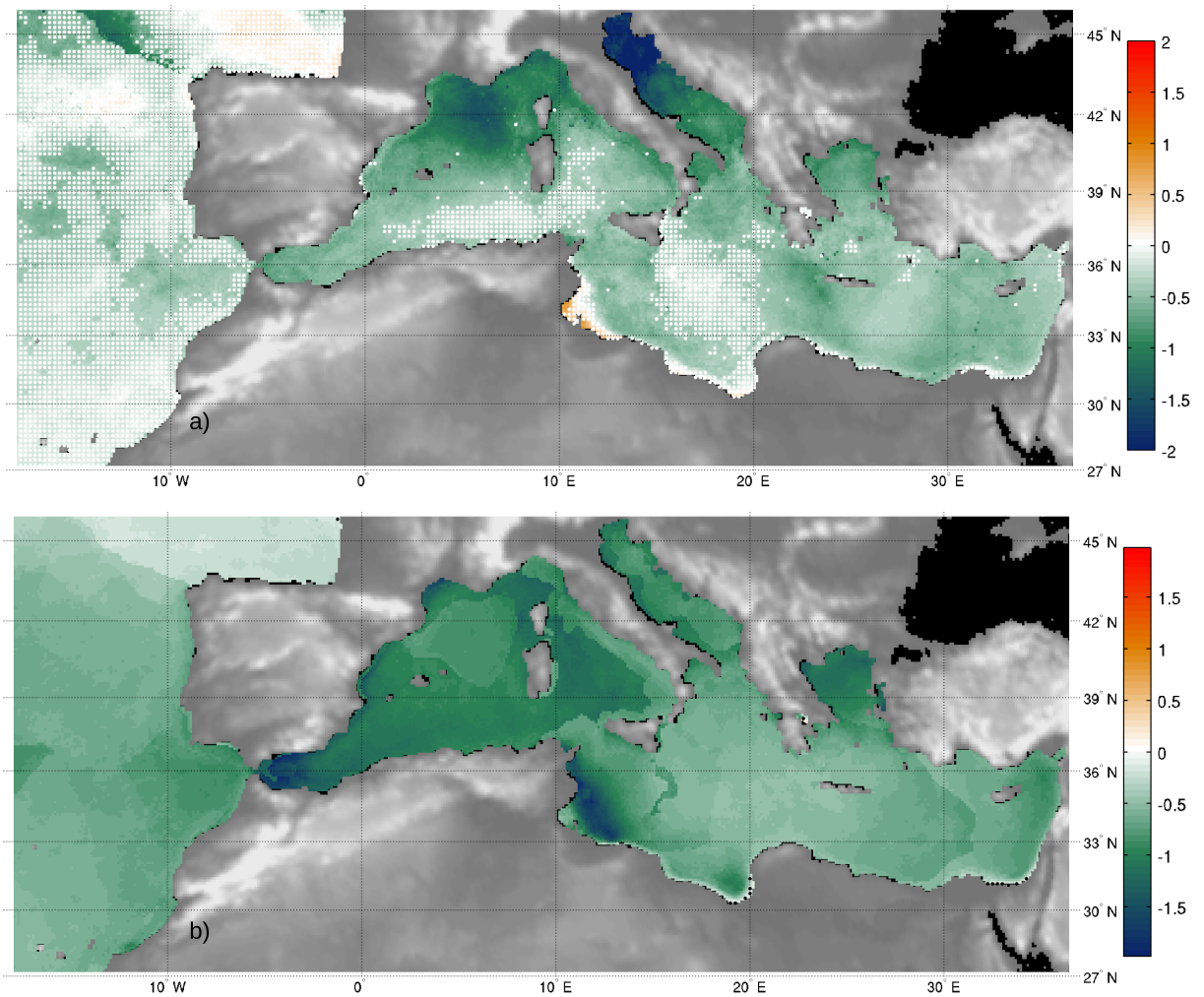
Figure 3.6: a) Sensitivity of the extremes intensity to NAO (cm/unit index). b) Sensitivity of the extremes frequency to NAO (events per year/unit index). White dots represent areas where the significance is lower than 90%.

3.4.4. 50-year return level

Extreme value models enable the estimation of very unusual extreme events from a relatively short data period. This is often referred as return values and return periods, estimations required to design defence structures and to quantify risk.

Fig.4.8 displays the estimated results for the present 50-year return storm surge level, together with the estimated shape parameter of the extreme value distribution for the study region. The shape parameter determines the upper tail of the distribution and consequently describes the behaviour of the most unusual extreme events. In general, negative values are found, indicating a bounded upper tail. This can be a consequence of one of two reasons: either regularly-occurring intense extreme events (e.g. the north-west Iberian Peninsula and the Gulf of Lion), or the scarce occurrence of extreme values (e.g. north Atlantic African shelf and Ionian Sea). There are also regions where the shape
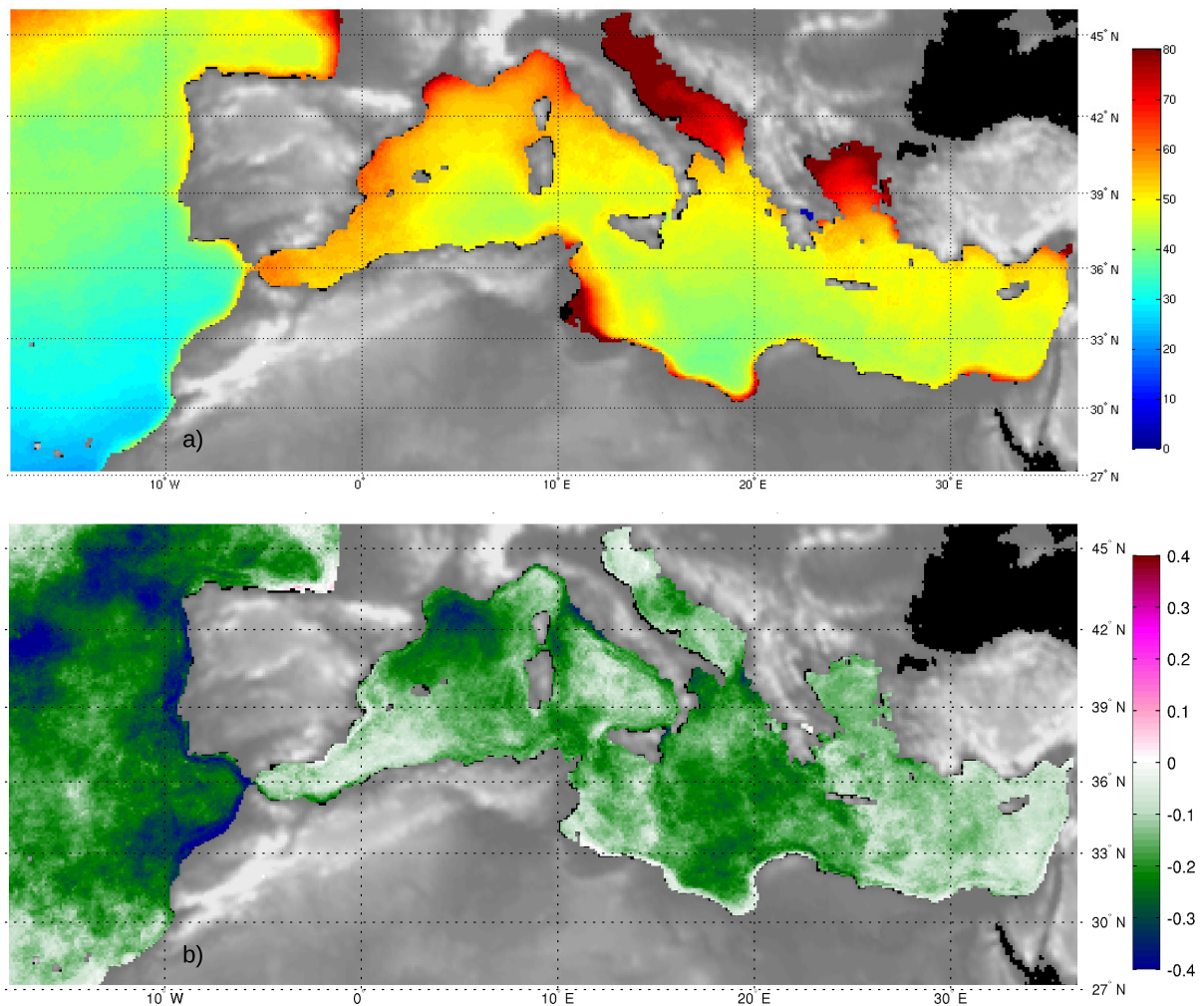
Figure 3.7: a) Current 50-year return level (cm). b) shape pareto parameter (non-dimensional)

parameter is close or equal to zero (e.g. northern Adriatic and eastern Biscay Gulf), indicating an exponential behaviour of the upper tail and, therefore, higher magnitudes for the most unusual extreme events.

Values for the current 50-yr return level were calculated, as shown in Eq.3.6, using the non-stationary Pareto-Poisson model. According to the 99.5% threshold spatial pattern represented in Fig.4.6a, the largest 50-yr return values are found at the northern Adriatic, Aegean Sea, Gulfs of Gabes and Sirte, the Gulf of Lion and along the Egyptian coast, reaching more than 75 cm. A similar north-south spatial gradient is detected, although it is less pronounced. In contrast, the 50-yr return level provides less intense values at the north-west coast of the Iberian Peninsula and larger magnitudes at Alboran Sea and the easternmost Mediterranean basin.

3.5.   Summary and Discussion

In this study, a storm surge hindcast (GOS database) spanning from 1948 to 2013 and a time-dependent Pareto-Poisson model are used to characterise and analyse climate variations in intensity, frequency and duration of extreme storm surge events. Non-stationarity is included into the extreme model by allowing time-dependent parameters through covariate NAO and linear trends.

The climatological analysis of not only the magnitude of the maximum extreme values, but also their duration and frequency of occurrence throughout the time, has allowed a better characterisation of the extreme storm surges. A general north to south gradient is found over the entire domain with respect to the selected 99.5% threshold value (approximately from 30 to 10 cm at the Atlantic and from 30 to 20 at the Mediterranean). This spatial pattern is obviously correlated to the wind speed over this area, as can be checked from Menendez et al. (2014). Higher storm surge values are located in coastal areas due to water piling induced by onshore winds (values of around 35 cm). The mean number of events per year is mainly lower at the Atlantic part of the domain than at the Mediterranean coasts (2 events/year vs. 4-5 events/year). Regarding the duration of the extremes over the threshold, there are clearly two different areas; higher values at the Atlantic with mean durations of 24 hours, and lower values at the Mediterranean Sea with maximum durations of 15 hours. This is because, as pointed out by Trigo et al. (1999), Mediterranean lows are, in general, less intense and are associated with smaller spatial scales and with shorter life cycles than Atlantic synoptic systems. Therefore, durations of storm surges are also smaller in the Mediterranean than in the Atlantic. An inverse relationship between the duration and the number of extreme events has been found. This is, extremes last longer offshore, while close to the coast, and specially along semi-enclosed Mediterranean coasts, extreme events are shorter but present a higher occurrence rate every year.

Regarding trends, results show negative patterns throughout the domain when studying the frequency of storm surge events (mean values between -1 and -1.5%), except for the south coast of Greece where the number of events per year tends to increase at rates of 1.5 %. There are more areas with positive trends in frequency but they do not reach the 90% of significance. Regarding intensity, both positive and negative trends are found; intensity of storm surges has increased mainly at the easternmost Mediterranean basin (1 mm/yr) while decreasing rates at the coast are mostly reduced to semi-enclosed areas such as the Gulf of Sirte (-2 mm/yr), Gulf of Gabes and northern Adriatic. With respect to duration, two different trend patterns are present: positive in the Mediterranean and negative in the Atlantic, although at coastal areas significant trends are only positive within a range of 0.5-1.5 h/yr. In summary, most of the southern European region does

not show significant trends in extreme storm surges; an exception to this are regions as the Alboran Sea, gulfs of Gabes and Sirte, northern Adriatic and the easternmost Mediterranean. The spatial patterns of the trends in duration indicates an increase in the Mediterranean and a decrease in the Atlantic but the mean duration of the extremes is higher in the Atlantic than in the Mediterranean. It is worth noting that decreasing trends found in the northern Adriatic for the 3 analysed variables are in agreement with results from local studies as for example Trieste, where Raicich (2003) found that during the period 1939-2001, strong surges became less frequent. The period of study is a key factor when studying trends; in areas where the inter-annual or decadal variability is of great importance, the sign of trends may even change depending on the temporal coverage of study. For instance, trends in magnitude around the Alboran Sea switch from negative (not shown) to positive (Fig.4.7a) when the study period is 1948-2009 or 1948-2013, respectively. Therefore, the analysis of linear trends is a simplistic approximation and it is totally dependent on the analysed time period. The Alboran sea is an example of an area with a strong interannual-decadal variability.

To test if this interannual-decadal variability of storm surges is related to the North Atlantic Oscillation, we have studied the response of sea level to the NAO index. This relationship has been analysed previously at different time scales, most of them focused on north-west Europe (e.g. Haigh et al. 2010; Woodworth et al. 2007). Studies analysing a bigger domain (e.g. Woolf et al. 2003), found that sea level is generally higher around north-west Europe in NAO positive winters, while it is generally lower around the Azores and southern Europe. We have found an inverse (negative) connection between NAO and extremes, both in terms of intensity and frequency, consistent with the strong and negative correlation found by Calafat et al. (2012) between tide gauge records and NAO when studying sea level decadal variability. For southern Europe and specifically for the atmospheric contribution to sea level, Gomis et al. (2008) found a negative correlation between NAO and surge monthly means. Marcos et al. (2009) also obtained negative correlations between winter NAO and storm surge values for the same domain. The significant connection found in this work between NAO and extremes proves that NAO contributes to changes in the extreme storm surges. Therefore, the latest tendency of the NAO index to positive phases since the 80's, could lead to negative trends in the magnitude and the occurrence rate of extremes, as we have found here. Hence, in this study we provide details of the relationship of the North Atlantic Oscillation with the extreme storm surges at an homogeneous spatial domain and for both, magnitude and occurrence of extreme events.

Other indexes as the Mediterranean Oscillation Index (MOI), Western Mediterranean Oscillation (WEMO), East Atlantic pattern (EA), East Atlantic/Western Russian (EA/WR), Atlantic multidecadal oscillation (AMO), could also have an influence in the Atlantic

and the Mediterranean basin. Thus, a further study including these climatic indexes should be carried out.

The study of the 50-yr return level has shown a general north to south gradient at both the Atlantic and Mediterranean basins. Some exceptions to this are found along coastal areas in the Mediterranean African coast, reaching values up to 70 cm for instance at the Gulf of Lion or Libyan and Egyptian coasts. A similar spatial pattern for the 50-yr return level was obtained by Marcos et al. (2009) where they also found higher values along the Tunisian and Egyptian coasts.

Finally, in this study, we have presented a statistical framework (GPD-P time-dependent model) to study extreme storm surge events, and we have used it to estimate long-term trends; showing that not only the intensity of the extremes affect the value of the 50-year return level but also does the frequency with which the extremes occur. We have also used the North Atlantic Oscillation index as a covariate in the statistical model, addressing the influence of the North Atlantic Oscillation index into the long-term trends. The results found in this work can be of great help in the estimation of the total water level (tide + surge + wave set up) in coastal areas: extremes of storm surges together with wave height extremes, can be a valuable information in the assessment of the flooding risk.

Chapter 4

Global reconstructed daily surge levels from the 20th Century Reanalysis (1871-2010)

Abstract

Studying the effect of global patterns of wind and pressure gradients on the sea level variation (atmospheric surge) is a key issue in understanding the recent climate change effect on the dynamical state of the ocean.

The analysis of the spatial and temporal variability of atmospheric surges from observations is a difficult task to accomplish since observations are not homogeneous in time, scarce in space, and moreover, their temporal coverage is limited. A recent global surge database developed by AVISO (DAC, Dynamic Atmospheric Correction) fulfilled the lack of data in terms of spatial coverage, but not regarding time extent, since it only includes the last two decades (1992-2014).

In this work, we use the 20th Century reanalysis (20CR), which spans from 1871 to 2010, to statistically reconstruct daily maximum surge levels at a global scale. A multivariate linear regression model is fitted between daily mean ERA-interim sea level pressure fields and daily maximum surge levels. Following, the statistical model is used to reconstruct daily surges using mean sea level pressure fields from 20CR. Good agreements are found between DAC levels and the reconstructed surge levels from the 20CR. A time

series comparison with instrumental records from tide gauges is also performed for the beginning of the XX century, showing a high concordance in the selected tide gauges.

Therefore, this work provides to the scientific community, a daily database of maximum atmospheric surges that can be used to improve the knowledge on historical atmospheric surge conditions, allowing the study of their temporal and spatial variability.

4.1. Introduction

The atmospheric surge is one of the main variables that describe the dynamical state of the ocean. It is defined as the sea level variation due to wind stress and sea level pressure gradients over the sea surface. The atmospheric surge magnitude has a large spatial variability and can reach extremely high values associated to tropical and extra-tropical storms (storm surges).

The atmospheric surge is one of the sea level components, and can be extracted from tide gauge records; but since many of the world areas are ungauged, the global coverage is scarce. Besides, areas where instrumental records are available, normally present short time records and hence only recent analysis can be carried out. One option to overcome these shortcomings is the use of numerical models. They enable us to simulate the magnitude of the atmospheric surges at a global scale or in an specific area. In fact, there is a global surge database, the Dynamic atmospheric Correction from AVISO (hereinafter DAC database, `http://www.aviso.altimetry.fr/`), that provides global records from 1992 and onwards (a description of the numerical configuration can be found in Carrère and Lyard 2003). Nevertheless, DAC database is not long enough to address inter-decadal climate variability or likely long-term trends. The numerical modelling at a global scale and for a long period of time requires an extremely high computational effort.

An alternative to numerical models is the statistical modelling; different techniques of statistical reconstruction are widely used in climate or ocean variables. Statistical downscaling techniques can be classified into: transfer functions, weather-type approaches and stochastic weather generators (Giorgi et al., 2001). Regarding marine climate, linear transfer functions (regression models) have been applied to downscale the significant wave height at global (Wang et al., 2012) and at regional scale (Casas-Prat et al., 2014). Also, a weather-type model has been proposed to downscale multivariate wave climate (Camus et al. 2014b, Espejo et al. 2014).

The application of statistical downscaling approaches is usually limited to specific locations. Calafat and Gomis (2009) used a reduced space optimal interpolation analysis

to reconstruct the sea level in the Mediterranean Sea. For atmospheric surges specifically, Dangendorf et al. (2014) compared, in the North Sea, the long-term behaviour of surges to that of reanalysis wind fields by means of a statistical-empirical formulation (Müller-Navarra and Giese, 1999).

The goal of this study is a global reconstruction of the atmospheric surge by means of a statistical model in order to extend the DAC temporal coverage. For achieving this purpose, we define the statistical relationship between the atmospheric surges from DAC database and their drivers (pressure fields from ERA-interim reanalysis, Dee et al. 2011) using multiple linear regression. Once the statistical model is calibrated and validated, we use a global atmospheric database that starts at the end of the XIX century (20th century reanalysis V2, Compo et al. 2011) to reconstruct the atmospheric surge at a global scale and for a long period of time (1871-2010).

The work is structured as follows. Section 4.2 describes the three databases used in this study. The methodology of the statistical model is deeply explained in section 4.3 and its accuracy is shown in section 4.4, where the validation results are depicted. Finally, the global reconstruction of the surges and its comparison with tide gauges is shown in section 4.5. Main conclusions are summarised in section 4.6.

4.2. Databases description

The surge database corresponds to the Dynamic atmospheric Correction (DAC), produced by CLS Space Oceanography Division using the MOG2D model from Legos and distributed by Aviso, with support from Cnes (`http://www.aviso.altimetry.fr/`). MOG2D (2 Dimensions Gravity Waves model) is a finite element, barotropic, non-linear, two-dimensional shallow water hydrodynamic model, derived from Lynch and Gray (1979). The model is forced by pressure and wind fields from the European Centre for Medium-range Weather Forecasts (ECMWF) analysis, with a temporal resolution of 6 hours and including shallow water areas and marginal seas. Barotropic sea level outputs span from September 1992 to present and are provided on a regular grid of 0.25°x0.25° every 6 h.

Regarding the atmospheric forcing, sea level pressure fields (SLP) were selected from two different global atmospheric databases: ERA-Interim reanalysis (Dee et al., 2011) from the ECMWF, which is the DAC forcing field, and the twentieth Century Reanalysis V2 (20CR, Compo et al. 2011).

SLP fields from ERA-Interim, consist of 6-hourly atmospheric data at 0.75° of spatial resolution and spanning from 1 January 1979 to present. In this work, only data covering

DAC period (1992 - 2014) are selected. These data are used to calibrate and validate the statistical model (see Section 4.3).

SLP fields from the 20CR are available every 6 hours at a spatial resolution of 2°, covering the period between 1871 and 2010 (i.e. 140 years). These data are used for the statistical reconstruction of surge levels.

4.3. Statistical modelling methodology

4.3.1. Predictor and predictand definitions

The aim of the statistical reconstruction is to estimate surge levels (predictand) from local atmospheric conditions (predictor) based on a statistical relationship. Specifically, our interest consists in finding the statistical relationship between mean daily atmospheric conditions and maximum daily surge levels. Following this purpose, the predictand is defined as the maximum of the 4 daily DAC values (DAC has a 6-hourly temporal resolution) at each grid point. The spatial resolution of the statistical reconstruction is determined by the 2° resolution of the 20CR. This spatial resolution is considered sufficient to represent the surge variability at a global scale. Therefore, surge levels are selected from DAC database every 2°.

As mentioned in Section 4.2, SLP fields from ERA-interim are used to obtain the statistical relationship between these atmospheric fields and surge levels. Although both, surface wind and pressure fields, are the drivers of the atmospheric surge, in this work we are only extracting SLP fields from the atmospheric reanalysis. This is because in global circulation models, sea wind fields are not as well reproduced as sea level pressure fields (Wang et al., 2010). On the other hand, the geostrophic wind speed is proportional to the square pressure gradient; hence, SLP gradients are calculated and taken into account in the statistical modelling to also have an estimation of the wind speed.

Although SLP from ERA-interim reanalysis has a horizontal resolution of 0.75°, SLP fields and the calculated gradients have been re-arranged in a 2° grid at a daily scale. The final step in the definition of the predictor is the establishment of the spatial coverage. Taking each of the predictand grid points, a local area of 4°x4° enclosing this target point is defined. As a result, the predictor is composed of 9 SLP values and 9 SLP gradients (18 components) centred in the predictand location.

Same process is carried out for the definition of the predictor from 20CR SLP fields, with the only difference that in this case, data are already in a 2° grid.

Therefore, the predictand consists of daily maximum values of surge levels from September 1992 to December 2014 in a 2° global grid; the predictor for the statistical model configuration consists of daily means of SLP fields and square SLP gradients from ERA-interim, covering an area of 4°x4° centred at the predictand location. Once the statistical model is defined, 20CR daily predictors are used to reconstruct surge levels from 1871 to 2010 at each location (10594 locations).

4.3.2. Description of the statistical model

The statistical method chosen to reconstruct surge levels is based on the method used in Camus et al. (2014a) to downscale multivariate wave climate. It comprises a multivariate regression model fitted between daily maximum surge level (predictand) and the principal components(PCs) of the mean daily SLP and gradients (predictor).

First step in the methodology consists in performing a principal component analysis (PCA) of the predictor to reduce the dimensionality of the problem while preserving the maximum variance of the data sample. PCA projects the original data on a new space, searching for the maximum variance of the sample data. The eigenvectors (empirical orthogonal functions, EOFs) of the data covariance matrix define the vectors of the new space. The transformed components of the original data over the new vectors are the principal components (PCs). The original predictor, which varies with space and time $X(x, t)$, can be expressed as a linear combination of EOFs (accounting for the space variability) and PCs (accounting for the time variability). Eq.4.1 shows that at any given time, the predictor can be estimated as the spatial pattern detected (EOF) multiplied by the corresponding coefficient for that instant (PC), adding all the N components (dimensions).

$$X(x, t_i) = EOF_1(x) \times PC_1(t_i) + EOF_2(x) \times PC_2(t_i) + ... + EOF_N(x) \times PC_N(t_i) \quad (4.1)$$

where N is the number of dimensions in the data, specifically in this case $N = 18$.

Prior to PCA, SLP and SLP gradients are standardise to avoid attributes with large values (and larger variances) to dominate the analysis. Then, PCs of the predictor have been calculated for the period 1992 - 2014. Following, we have selected the components that explain the 95% of the variance. The number of PCs explaining the 95% of the variance varies spatially between 4 and 12 (not shown) from the total amount of 18 components. Therefore, although in this case the dimension reduction is not highly

relevant, PCA is carried out anyway so that this methodology could also be applied to wider predictors (i.e higher dimensions).

Next step consists in establishing the relationship between the predictor PCs that explain the 95% of the variance and the surge levels (predictand). The multivariate regression model is fitted in a forward procedure: first predictor PC is obtained from the best fit (smallest sum of squared errors, SSE) among each of the components separately ($PC_{(1)}$ in Eq.4.2). The second predictor PC ($PC_{(2)}$ in Eq.4.2) is chosen from the rest of the PCs so that it gives the best fit with two predictors, the best predictor selected in the previous model plus one of the remaining potential predictors. The cycle continues until a more complex model does not produce a significant improvement (at the 5% level of significance) in the multivariate regression fit. This evaluation is based on the F statistics that compare the SSE of fitting a simpler-parameter model with that of a more complex parameter model (Wang et al., 2010). Therefore, although all PCs explaining the 95% of the variability could be used in the regression model, only those that produce a significant improvement are taken into account.

A leave-one-out-cross-validation process is used to set up the statistical model: The regression model is fitted for all years except one, which is used for validating the surge reconstruction. Then, the regression model is fitted 22 times (there are 22 complete years of surge levels, 1993-2014). Results of the validation process are shown in Section 4.4.

This methodology allows us to estimate surge levels as a linear combination of the most important PCs. As can be seen from Eq.4.2, surge levels at any given location (x_i) can be estimated from a specific number of PCs, which varies throughout the domain.

$$surge(x_i, t) = a_i + b_{1,i} \times PC_{(1)}(x_i, t) + b_{2,i} \times PC_{(2)}(x_i, t) + ... + b_{n,i} \times PC_{(n)}(x_i, t) \quad (4.2)$$

where n is the number of PCs that achieved a statistical improvement of the results (following F statistics) and selected in a forward procedure from the PCs that explained the 95% of the variance. $a_i, b_{1,i}, ..., b_{n,i}$ are the coefficients obtained in the regression model.

Once the statistical model is defined, SLP and gradients from the 20CR reanalysis are standardised and projected into the EOFs detected for ERA-interim to obtain the PCs for the 20CR predictors. Finally, using the coefficients and the PCs identified as in Eq.4.2, daily surge values can be reconstructed for the 1871-2010 period.

4.4. Model validation

The validation of the statistical model shows the quality of the fittings in terms of correlation coefficient (ρ), root mean square error ($RMSE$), and the RMSE relative to the maximum surge variability at each location ($RMSE_{relative}$). Fig.4.1 shows the spatial distribution of the fitting quality. As can be seen from Fig.4.1a, correlation coefficients are above 0.7 all along the domain. Largest differences are located along the North Atlantic coast of South America, the area from the Gulf of Thailand through Indonesia to North Australia, and along the Siberian and Beaufort Seas. An extended area of relative lower correlations (above 0.8) is located along tropical areas. The explanation for this lies in the fact that the ocean dynamics at high latitudes have smaller space and time scales. The predictor used in the proposed statistical model describes better the dynamical response of the atmospheric surge in those areas in comparison with tropical areas. Besides, the small magnitude of the storm surge in tropical areas is more difficult to reproduce. Fig.4.1b shows that the RMSE is generally higher in the Northern Hemisphere (maximum values of ~10 cm), specifically in semi-enclosed areas as the Hudson bay or the North Sea. Also along high latitudes of Russian and Siberian coasts. This is because storm surge generation at shallow waters, especially in semi-enclosed areas, is related to local wind conditions. Therefore, a higher resolution predictor should be required to improve the skill of the statistical model at those areas. Nevertheless, a generalised predictor is used in this study due to the global scale of the atmospheric surge reconstruction. Fig.4.1c displays the RMSE relative to the maximum surge variability detected at each grid point. This reveals areas of maximum relative errors of around 10% along equatorial regions, not detected in Fig.4.1b due to the small magnitude of the surge levels long the tropical areas (see Fig.4.4).

A validation at some specific points is also carried out (red dots in Fig.4.2). Fig.4.3 shows the time series comparison and the scatter plots at these 6 locations, contrasting DAC original data (red lines) with the statistical reconstruction using ERA-interim predictors (blue lines). It can be seen how the equatorial area (point 4) presents the lowest correlations and the highest relative errors, even so, ρ reaches a 0.89 value and the relative error is around 6%. A general good fitting to the bisector can be seen at all grid points. Fig.4.3 confirms that the poorest agreement is located at equatorial areas, but although absolute values are not exactly reproduced at grid point 4, mean levels are well represented. It is also important to notice that the surge magnitude at these tropical zones is about one order of magnitude lower than at the points located in other areas. Time series at the rest of grid points follow DAC original data properly.

Last comparison between DAC original data and the statistical reconstruction using ERA-interim predictors is represented in Fig.4.4. It shows the spatial value of the
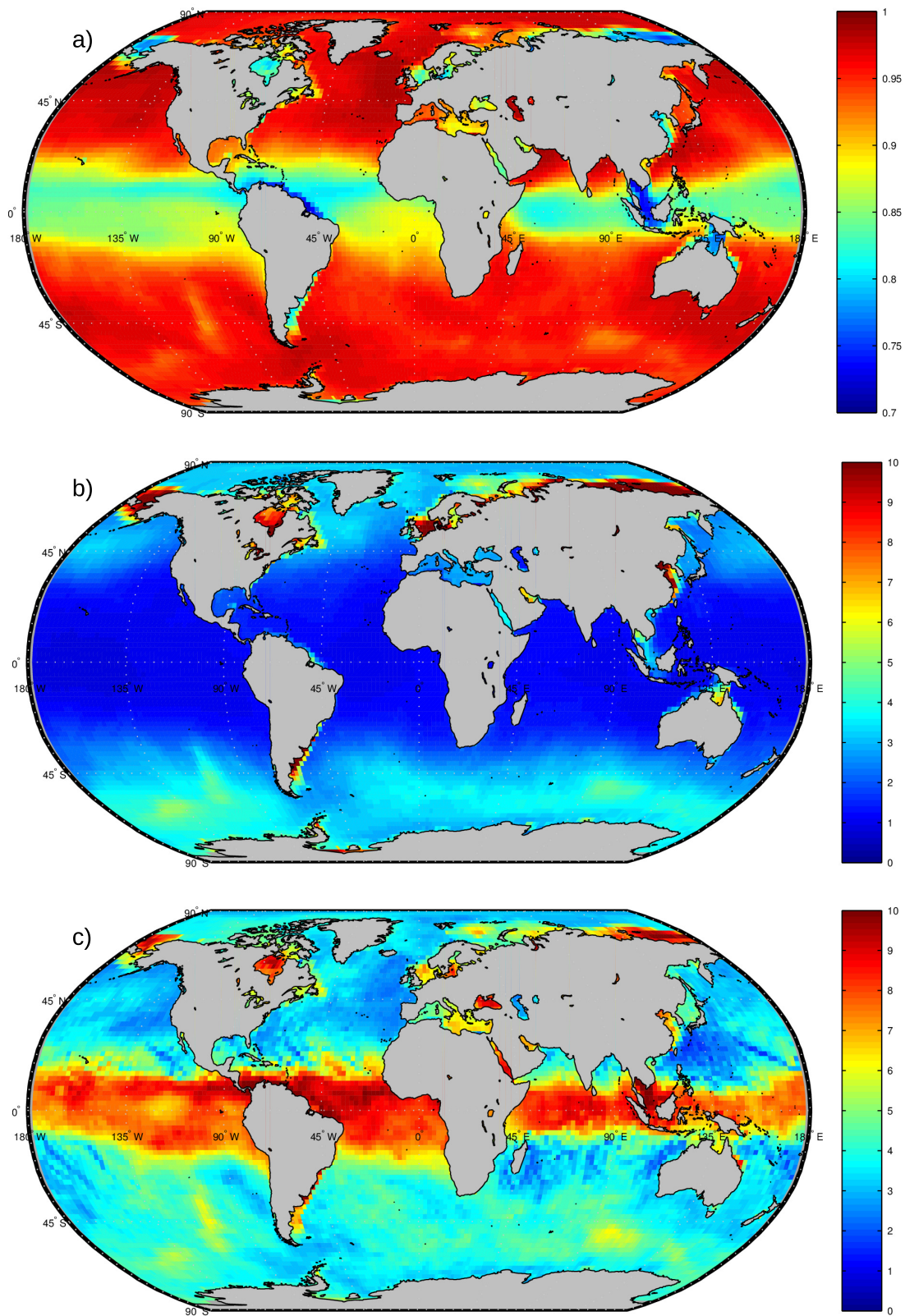
Figure 4.1: Spatial validation of the statistical reconstruction. a) correlation coefficient(ρ). b) RMSE (cm). c) RMSE relative to the maximum surge variability(%).
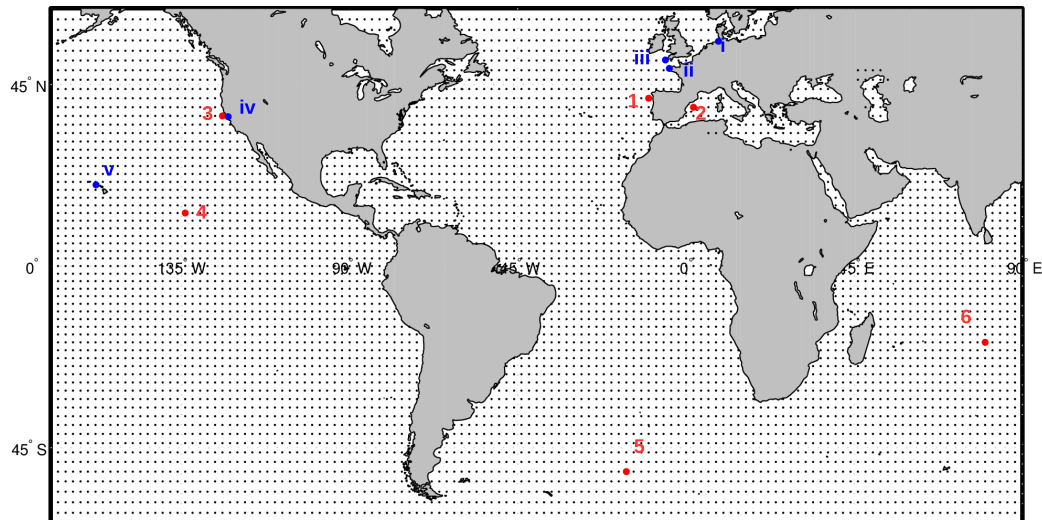
Figure 4.2: Selected points where a point comparison is carried out. Red grid points are used to validate the statistical model and to compare with the 1871-2010 reconstruction. Blue grid points are compared with tide gauges. Black dots show the spatial resolution of 2°.

99.5% percentile obtained from the complete daily surge series. As can be seen, the spatial pattern is almost identical; main differences are found along the North European coastline, where the statistical reconstruction does not reach the values displayed in the original data. As we mentioned previously, the generation of the atmospheric surge at coastal areas is mainly forced by local winds, being the resolution of the predictor not enough to represent local features. Maximum surge values are present in these areas, reaching magnitudes of about 1 m. As already mentioned, smallest surges are located around the equatorial area, where 99.5% is even negative due to the fact that these areas have high mean pressure conditions (permanent anticyclonic conditions). The extratropical Southern Ocean (40°S - 60°S) is an area with relatively higher values, where the 99.5% percentile is above 60 cm. Wind conditions at high latitudes of the Southern Hemisphere are the most energetic at a global scale; the general conditions of low pressures present in this area also contribute to maintain high surge levels.

Figure 4.3: Surge (m) time series comparison and scatter plots at the 6 grid points defined in Fig.4.2. Red line represents original DAC data, blue line corresponds to the statistical reconstruction using ERA-interim predictors. (1): $\rho = 0.98$ $RMSE = 1.66$ cm; (2): $\rho = 0.94$ $RMSE = 2.71$ cm; (3): $\rho = 0.97$ $RMSE = 1.37$ cm; (4): $\rho = 0.89$ $RMSE = 1.01$ cm; (5): $\rho = 0.96$ $RMSE = 3.57$ cm; (6): $\rho = 0.94$ $RMSE = 1.22$ cm
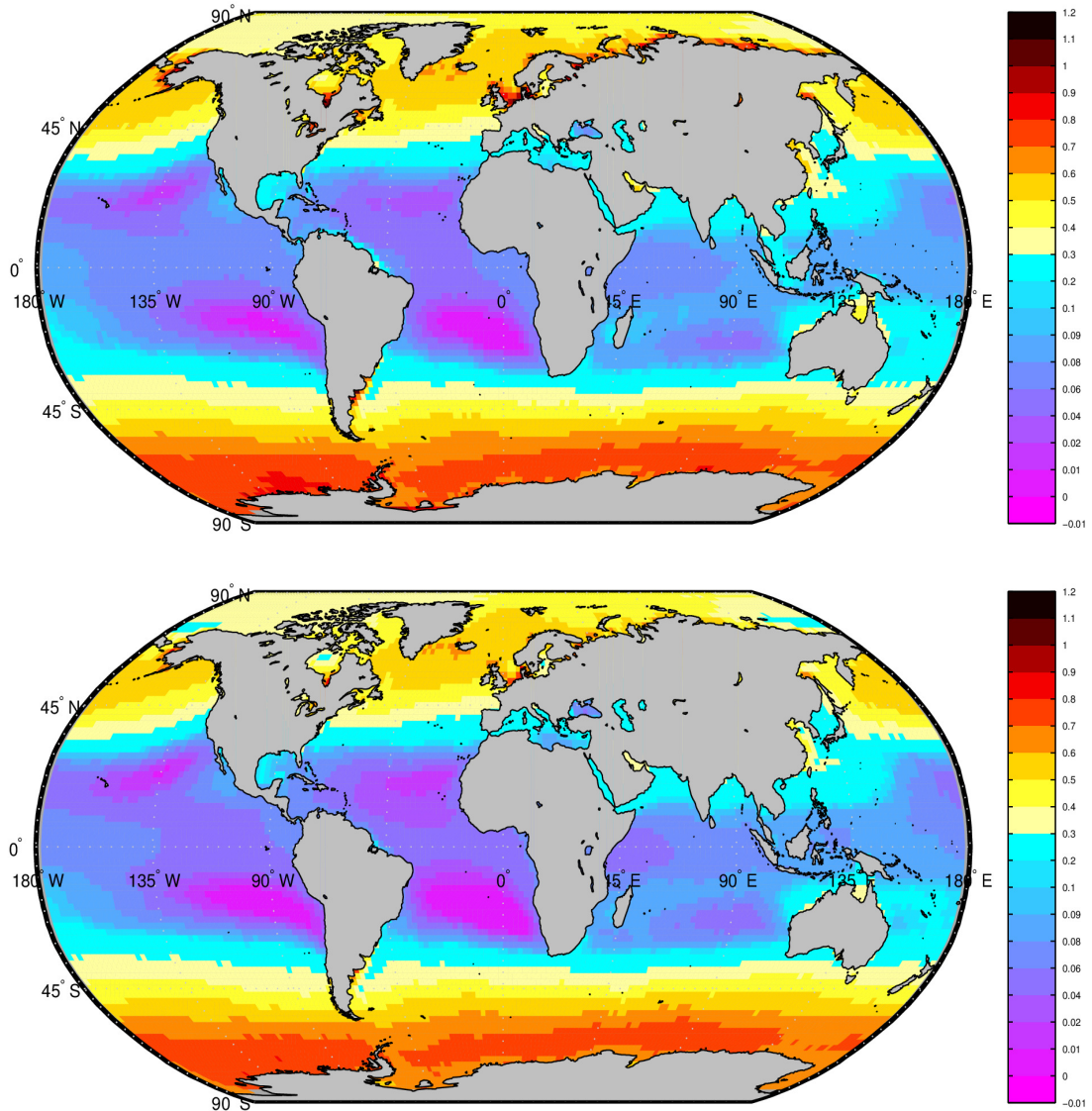
Figure 4.4: Value (m) of the 99.5% percentile for DAC original data (top) and for surge reconstruction using ERA-interim predictors (bottom).

4.5. Global reconstruction of surges (1871-2010)

In this section, a global statistical surge reconstruction is performed using 20CR predictors, obtaining maximum daily surge levels for the period 1871-2010.

4.5.1. Comparison during the control period (1992-2010)

A comparison between DAC original data and the reconstructed 20CR surge is carried out for a control period (1992-2010) where data from both sources coincide. Fig.4.5 shows the spatial comparison, same as in Fig.4.1 but using 20CR predictors instead of those from ERA-interim. The spatial pattern of both figures is very similar for the 3

statistical indicators. Main differences between Fig.4.1 and Fig.4.5 are located in the Southern Hemisphere, specifically in the Pacific Ocean close to Antarctica, where the correlation coefficient decreases from 0.95 (Fig.4.1a) to 0.85 (Fig.4.5a) and the relative error is doubled (even so, barely an 8%). These differences with the statistical validation can only be due to the quality of the 20CR reanalysis. The higher quality of the 20CR upper-air fields over the whole Northern Hemisphere and the mid-latitudes of the Southern Hemisphere has been highlighted when comparing with ERA-40 reanalysis (Compo et al., 2011). Fig.4.6 shows the time series comparison between DAC original data (red lines) and the statistical reconstruction using 20CR predictors (black lines) for the 6 grid points numbered in Fig.4.2. Grid points 4 (equatorial area) and 6 (Indian Ocean) show extreme storm surge events in the reconstruction that are not present in the original data. This can also be seen from the scatter plots; for those points, an overestimation of the reconstructed surge values regarding DAC original data is noticed. The rest of the points show a good agreement, with correlation coefficients and errors of about the same magnitude as in Fig.4.3.

Comparing SLP data from 20CR and ERA-interim (not shown) we verified that the aforementioned extreme surges are due to extreme falls in the SLP of 20CR reanalysis that are not consistent with the SLP in ERA-interim. A brief study has shown us that those drops in the SLP correspond to tropical cyclones (TC), included in 20CR but not in ERA-interim. In the 20CRv2, the estimated minimum central pressure observations for TCs from the International Best Track Archive for Climate Stewardship (IBTrACS) are assimilated into the reanalysis model. This assimilation may justify the more intense minimum pressures found in 20CR, when comparing to ERA-Interim.
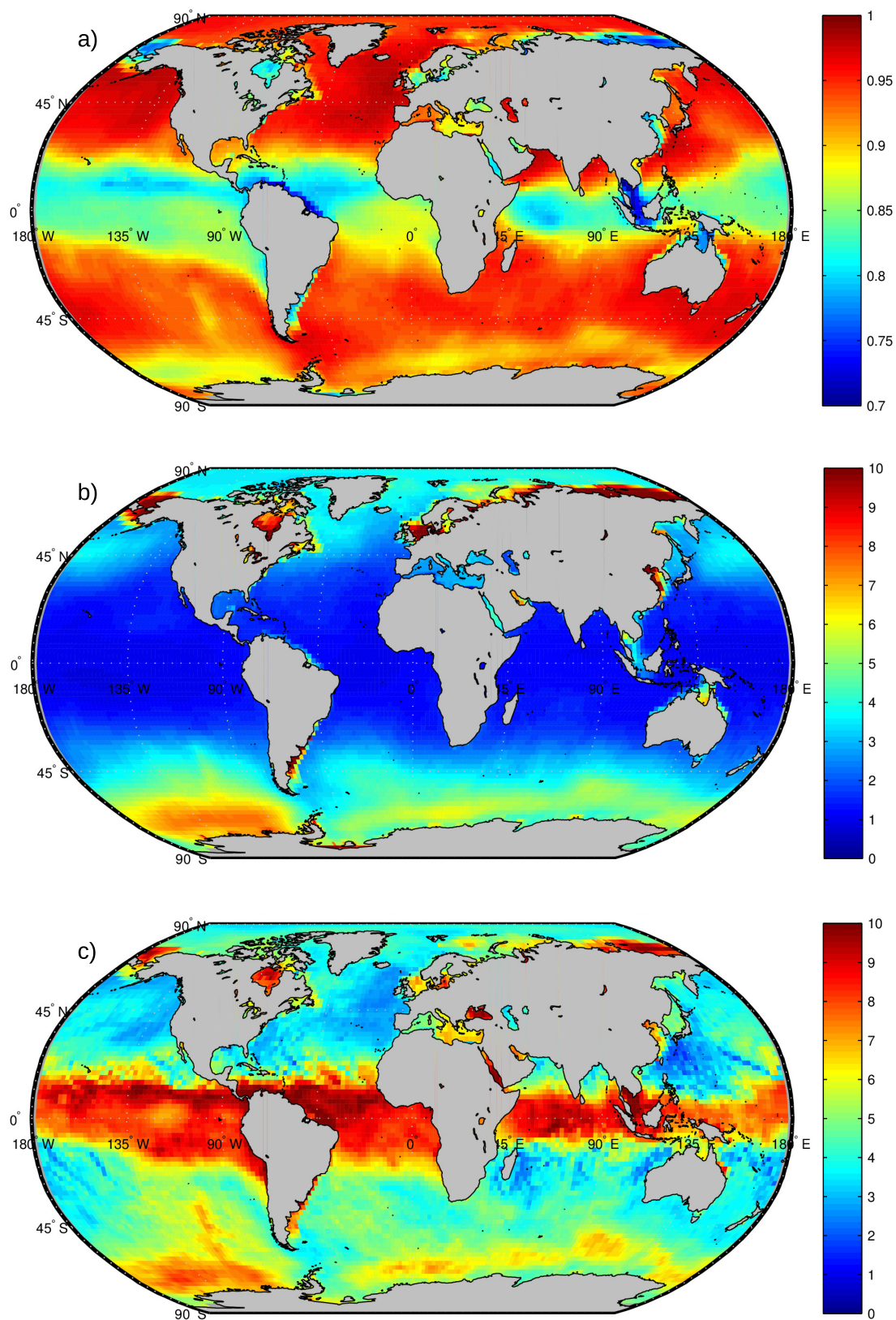
Figure 4.5: Spatial comparison during the control period between DAC levels and the reconstructed surge using 20CR predictors. a) correlation coefficient(ρ). b) RMSE (cm). c) RMSE relative to the maximum surge variability(%).
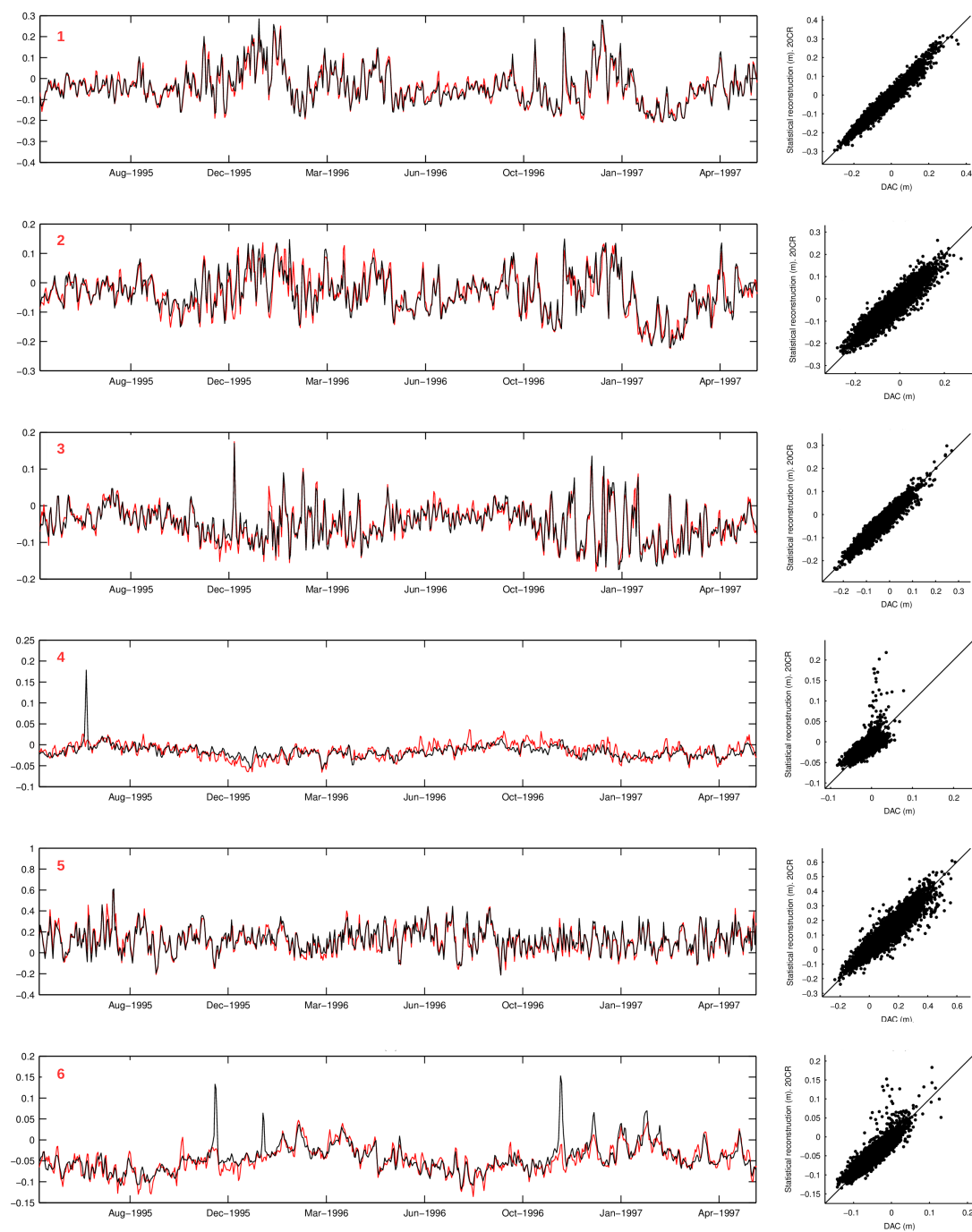
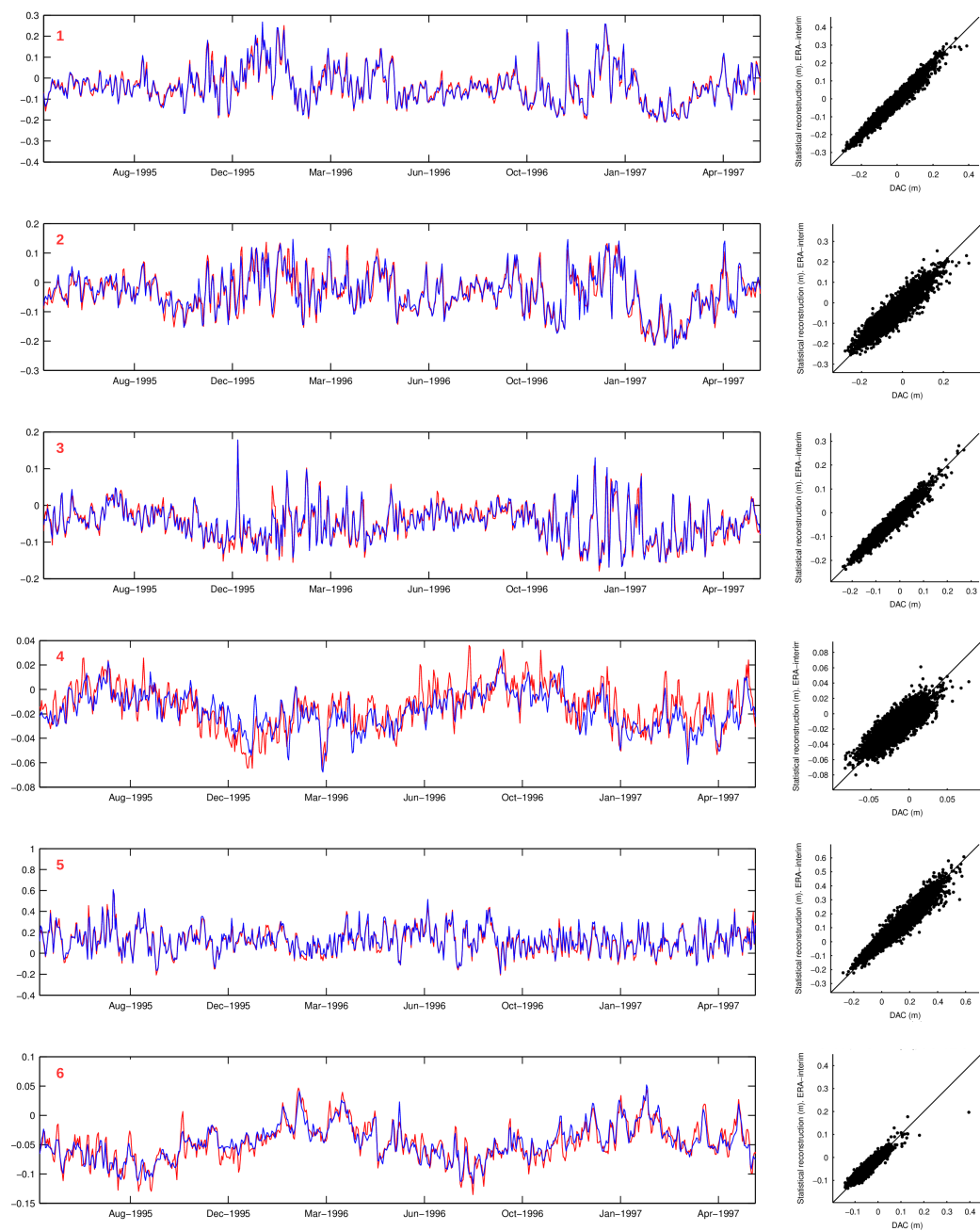*Figure 4.6:* Surge (m) time series comparison at the 6 grid points defined in Fig.4.2. Red line represents original DAC data, black line depicts the surge reconstruction using 20CR predictors. (1): $\rho = 0.97$ $RMSE = 1.84$ cm; (2): $\rho = 0.93$ $RMSE = 2.81$ cm; (3): $\rho = 0.95$ $RMSE = 1.65$ cm; (4): $\rho = 0.81$ $RMSE = 1.43$ cm; (5): $\rho = 0.94$ $RMSE = 4.34$ cm; (6): $\rho = 0.91$ $RMSE = 1.42$ cm

4.5.2.   99.5% percentile of daily surge levels

The value of the 99.5% percentile is calculated for the statistical reconstruction using 20CR predictors (see Fig.4.7). It is done for two periods, one which corresponds to the control period (1992-2010) and that will allow us to compare the results with the original DAC data (Fig.4.4 top panel), and the other one which covers the complete 20CR period (1871-2010). As can be seen from Fig.4.7, the 99.5% spatial pattern for the control period (top panel) is very similar to the one corresponding to DAC (top panel in Fig.4.4). When taking into account the complete period, surge levels decrease generally throughout the domain. The decrease is obvious in the Antarctica surrounding area, where the 99.5% value decreases from around 80 cm to 60 cm. A decrease of 10 cm is found around Canada Arctic coasts. Extra-tropical cyclone activity is estimated to have increased slightly over the period 1871-2010 in the Northern Hemisphere, although this still is a controversial finding (Dangendorf et al., 2014), and significantly for the Southern Hemisphere (Wang et al., 2013). The lower magnitude of the storm surge 99.5% percentile, for the period 1871-2010, is in agreement with these trends in the extra-tropical cyclone activity.
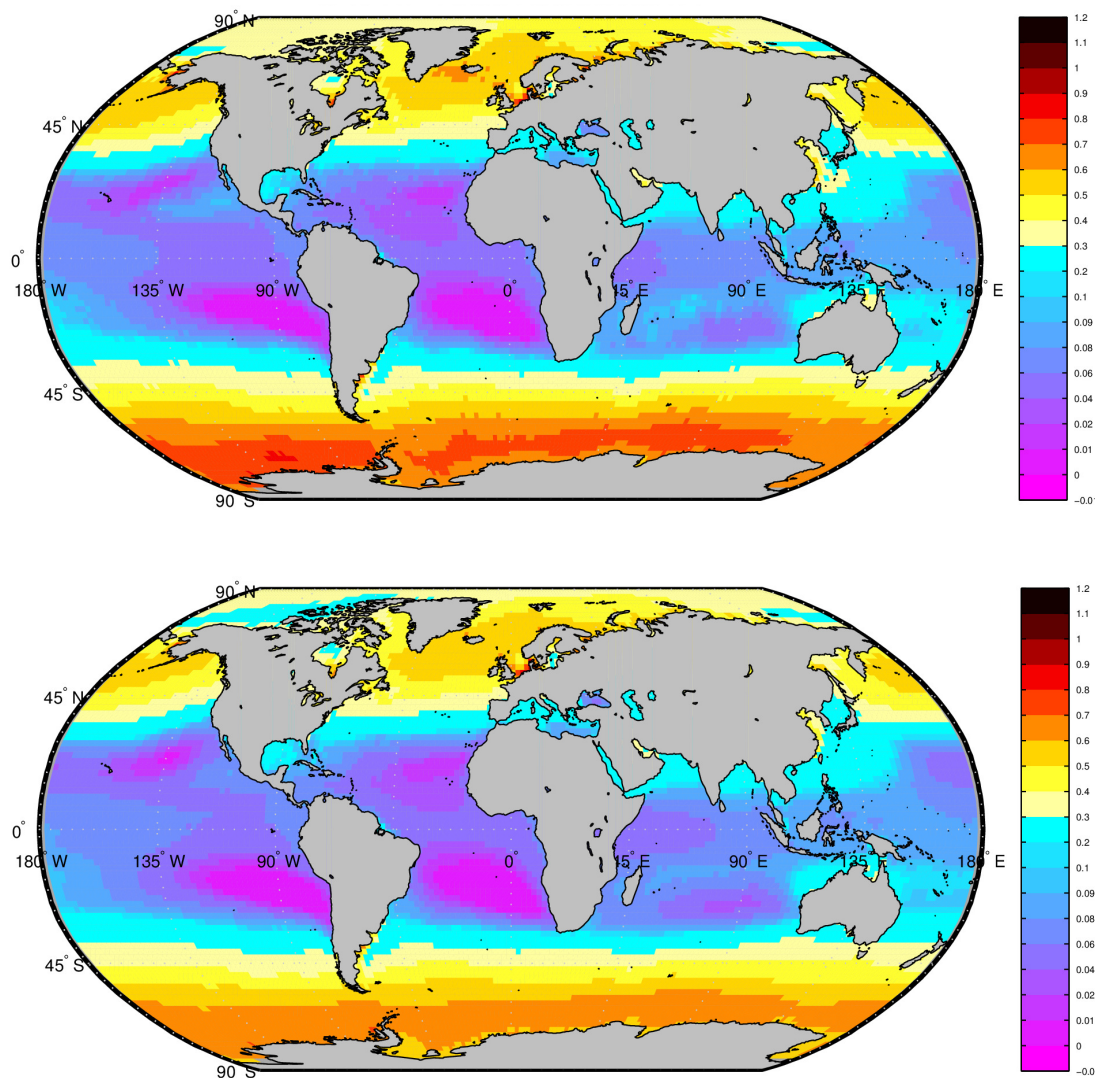
Figure 4.7: 99.5% percentile value (m) of the statistical reconstruction using 20CR for the period 1992-2010 (top) and for the complete 20CR period 1871-2010 (bottom)

4.5.3. Comparison with tide gauges

The surge reconstruction from 20CR predictors has also been compared to measures from tide gauges. For this purpose, five of the longest records from UHSLC (University of Hawaii Sea Level Center) have been selected (blue dots in Fig.4.2. i: Cuxhaven, ii: Brest, iii: Newlyn, iv: San Francisco, v: Honolulu) and used to contrast their daily measures with the reconstructed daily maximums from 20CR, for periods different to the DAC temporal coverage. A time series comparison can be seen, for the end of the nineteen century or the beginning of the twenty century, in Fig.4.8, where red line represents tide gauge measures and black line corresponds to the surge reconstruction. Time series from Brest and Newlyn coincide extremely well, both in the timing and the magnitude, with correlation coefficients of 0.92 and 0.91, and RMSE of 4 and 5 cm,

respectively; Cuxhaven and San Francisco show a slightly lower agreement (ρ is 0.85 in both locations and RMSE is about 18 and 4 cm, respectively); Honolulu shows periods where the concordance is low (ρ is 0.74 and RMSE is 2 cm).

Assuming that DAC is of high quality all over the domain, this is the expected result since Brest and Newlyn are located in areas with remarkably high levels of agreement (see Fig.4.5); Cuxhaven in the North Sea and San Francisco, are placed in areas with slightly smaller correlation coefficients and higher relative errors; Honolulu is located in an area where the lower agreements are found. Besides, DAC performances are also better for coastal tide gauges rather than islands tide gauges (Carrère and Lyard, 2003).

From the comparison with these five tide gauges, it can be seen that the reconstructed surge database is able to represent the measured atmospheric signal, also from periods back at the end of the nineteen century with relatively high accuracy.
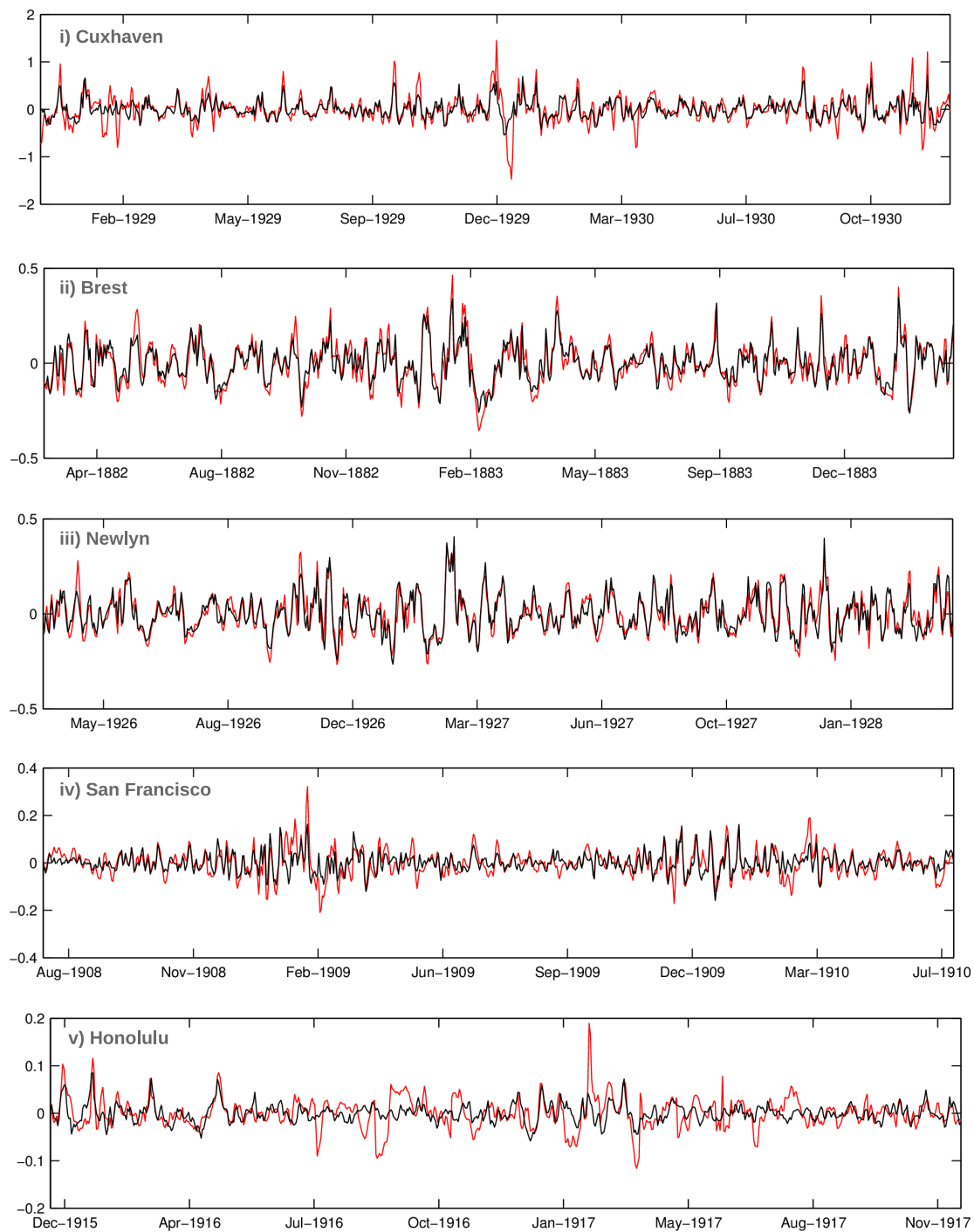
Figure 4.8: Comparison of the reconstructed daily maximum surges (black line) with daily values from tide gauges (red line) at 5 locations (blue dots in Fig.4.2).

4.6. Conclusions

This study provides a global atmospheric surge database that estimates daily maximum surge levels from 1871 to 2010, at a spatial resolution of 2°. It has been carried out using a statistical model, based on multiple linear regression, that relates the mean SLP and gradients from ERA-interim reanalysis with daily maximum surge levels from DAC database. The model is calibrated and validated, and then used to reconstruct daily maximum surge levels, taking the atmospheric SLP fields from the 20CR as predictors.

The validation of the model showed an extremely high performance all over the world, with minimum agreements (maximum $RMSE_{relative}$ of 10% and minimum ρ of 0.7) around equatorial zones and semi-enclosed areas. Two different reasons explain these lower performance areas. In the case of semi-enclosed areas, a finer predictor resolution would be needed to capture the variability of the atmospheric structures and hence to properly reproduce the surge; in equatorial areas, the small surge magnitude and also the large temporal and spatial scales of the ocean dynamics make more difficult for the statistical model to accurately reproduce the surge.

The comparison between the 20CR reconstructed surge and the original data for the control period, shows a decrease in the agreement at the Southern Hemisphere, specially around the Antarctic area. This is explained in terms of the lower quality of the 20 Century Reanalysis in the Southern Hemisphere (Compo et al., 2011). Around tropical zones, we find an overestimation of the reconstructed surge at some areas that have been proved to be located in usual cyclone tracks. This is due to the fact that the 20CR assimilates information about tropical cyclone tracks that are not gathered in the ERA-interim reanalysis, since the detected minimum pressures are more noticeable in 20CR than in ERA-interim.

The comparison with tide gauges has also proven the ability of the model to reproduce the surge signal far from the control period.

It is important to note, that at high latitudes there is a variable ice coverage that would eliminate the surge signal, but since DAC database provides sea level data throughout all the domain, the statistical model presented here also finds the relationship between the atmospheric forcing and the oceanic response at those areas.

All in all, we have proved here the good ability of the statistical model to reproduce daily maximum surges. The global obtained database provides daily surge values for 140 years, and can be freely used for the scientific community to study, for instance, long term variability of atmospheric surges. An interesting application would also be the use of these data as hydrodynamic boundary conditions for numerical downscaling studies.

Future work regarding the improvement of the predictor's resolution will be carried out at specific areas to show how this affects the predicted surge. This methodology could also be applied to regional climate projections of surge levels for different climate change scenarios.

Chapter 5

Conclusions and future research

5.1. Summary of contributions

The overall aim of this thesis was to broaden our knowledge of the atmospheric surge. In the thesis, this general objective was accomplished by fulfilling three specific goals:

1. **Studying the atmospheric surge from a numerical modelling perspective**. We developed two atmospheric surge datasets and presented the results of its validation with tide gauges and satellite data. We obtained the influence that the atmospheric forcing resolution has on the surge results, and also used the developed databases to study variability and trends.

2. **Studying the extremes of the atmospheric surge from a time-dependent statistical model**. We presented a statistical framework for analysing changes in extreme storm surges, not only in its magnitude but also in its frequency and duration. A POT technique was used to select the extreme events, which were characterise in terms of intensity, frequency and duration; and then, long-term trends were studied using a time-dependent GPD-Poisson model. This model also enabled us to estimate the 50-year return level and the sensitivity of the extremes to the monthly NAO index.

3. **Studying the atmospheric surge from a statistical modelling perspective**. We developed a global atmospheric surge database, spanning from 1871 to 2010, by means of a statistical model. Using multivariate linear regression we defined the statistical relationship between the atmospheric forcing (sea level pressure fields) and the surge. Once the statistical model is settled, a different atmospheric forcing (20th Century Reanalysis) was used to reconstruct the surge from the end of the XIX century to 2010 at a global scale.

5.2.   Conclusions

In this section we summarise the main conclusions obtained in this thesis.

1. **Studying the atmospheric surge from a numerical modelling perspective**.

   - The validation of the atmospheric surge database with 58 tide gauges and satellite data allowed for a wide spatial comparison. At tide gauge locations, the correlation factor is over 0.8 in the Atlantic area and around 0.75 in the Mediterranean Sea. Root mean square errors are lower or about 10 cm for all locations.

   - The use of satellite data in the validation process allowed us to identify specific zones where the simulated surge shows unreliable results, that otherwise would have not been notice since they are ungauged areas.

   - These zones have a common feature regarding its spatial characteristics, since they all are relatively shallow semi-enclosed areas. In these zones, local characteristics become very important, as for instance the strong south-east sirocco wind channelled by orography in the Adriatic, that leads to sea level variations not represented at the regional scale. Therefore, there are areas where it is needed to take into account local features to properly represent the sea level dynamics.

   - In this study we compare the GOS signal, which is strictly the atmospheric sea level component, to the non-tidal residual from tide gauges, which gathers sea level variations from other sources (i.e. steric component and mass component). These signals may be higher in the Mediterranean Sea, leading to lower agreements as we saw from the statistical validation.

   - Despite the aforementioned, a further study regarding the sensitivity of the bathymetry resolution and the influence of the model parameters on the results, should be analysed.

   - We found that the resolution of the atmospheric forcing did not influence significantly the surge results, i.e. no significant improvement was found when increasing the atmospheric forcing resolution from 30 to 15 km. Although as already said, a further analysis in coastal or estuarine areas should be carried out to test its influence at local scale.

   - The analysis of the storm surge variability showed trends of opposite signs, depending on the time period of study. For the period 1948-2009, only negative trends were identified, while for the last 20 years, obtained trends have a positive sign.

2. **Studying the extremes of the atmospheric surge from a time-dependent statistical model**.

  - The use of a time-dependent GPD-P model allowed the analysis of climate variations of the intensity, frequency and duration of storm surge extremes.

  - The magnitude of the threshold value shows a general north to south gradient (higher at the north and lower magnitudes at the south). The mean number of events per year is mainly lower at the Atlantic part of the domain than at the Mediterranean. The duration of extreme surges is longer at the Atlantic than at the Mediterranean.

  - We found that most of the southern European region does not show significant trends in none of the above variables. An exception to this are the Alboran Sea, the easternmost Mediterranean sea, northern Adriatic and the gulfs of Gabes and Sirte.

  - When comparing the trends obtained in this study with those obtained from other authors, we found that there are a wide variety of methods and time ranges used to estimate them. Therefore, to conclude with strong statements regarding trends is complex issue, since it is highly dependent on the time period of analysis.

  - We obtained negative teleconections between NAO index and extreme events, both in terms of the magnitude and the number of extreme surges. The sensitivity of the extremes frequency to NAO index is higher than the magnitude.

  - We checked the relationship between NAO index and the magnitude and frequency of extreme surges but there are other climatic indexes, as for instance the Mediterranean Oscillation Index (MOI) or the East Atlantic pattern (EA), that could explain part of the surge variability in southern Europe, thus including these indexes in the analysis would be an interesting study.

  - Finally, the estimation of the 50-year return level showed a similar spacial pattern to the one obtained from the estimation of the threshold, although magnitudes are obviously higher.

3. **Studying the atmospheric surge from a statistical modelling perspective**.

  - The statistical model showed a high performance all over the world, specially at extra-tropical areas. Around equatorial and semi-enclosed zones, agreements are lower (even so, minimum correlation coefficients are about 0.7 and maximum relative errors of 10%) due to the fact that at semi-enclosed areas

the predictor resolution should be finer to capture the atmospheric variability; at equatorial areas, the surge magnitude is that low that the statistical model has difficulties in reproduce the surge signal accurately.

- The 20th Century Reanalysis shows lower quality at the Southern Hemisphere, for this reason, when comparing the reconstructed 20CR surge and the original data for the control period, agreements are lower.

- There is an overestimation of the surge at some tropical areas. We found that these zones are located in frequent cyclone tracks and that the 20CR is better at assimilating information of tropical cyclones than ERA-interim.

- The estimation of the 99.5% percentile showed that the highest surge magnitudes are located at northern European coasts (above 1 m).

- The comparison with tide gauges has shown that the statistical model gives accurate surge results for times far from the control period, as it was depicted for 5 tide gauges that start at the end of the XIX century or the begining of the XX century.

- Although the reliability of the 20th Century Reanalysis is a controversial topic before the mid of the XX century, in this first attempt at validating the surge results with tide gauges, we have found good agreements in the five locations spread along the Northern Hemisphere.

5.3.   Future research

The studies carried out within this thesis have lead to future research topics, some of them are summarised here:

- Regarding the numerical modelling, it would be interesting to analyse the reason or reasons why the simulated surge is generally less accurate in the Mediterranean Sea than in the Atlantic area. Also, the study of the effect that local characteristics (e.g. local winds or high resolution bathymetries) have on the surge results. This could shed light on how important are the local features in regional scale analyses.

- Regarding the extreme analysis, we have studied the relationship between the NAO index and the frequency and magnitude of storm surges, but there is a need of a deeper study regarding general climate patterns and its influence on the surge, so we could explain for instance, why the frequency of extreme surges is higher in the Mediterranean Sea.

■ Regarding the statistical modelling, future research testing the influence of the predictor resolution should be explored, not only at semi-enclosed zones but also at coastal areas where the surge magnitude is higher. On the other hand, it would be interesting to analyse how reliable surge results are before the mid XX century and how this reliability varies spatially along the world. Finally, the use of the statistical model to predict the surge from climate change projections is already an ongoing work.

Bibliography

Arns, A., Wahl, T., Haigh, I., Jensen, J., Pattiaratchi, C., 2013. Estimating extreme water level probabilities: A comparison of the direct methods and recommendations for best practise. Coastal Engineering 81, 51–66. URL: `http://www.sciencedirect.com/science/article/pii/S0378383913001270`, doi:`10.1016/j.coastaleng.2013.07.003`.

Arns, A., Wahl, T., Haigh, I.D., Jensen, J., 2015. Determining return water levels at ungauged coastal sites: a case study for northern Germany. Ocean Dynamics 65, 539–554. URL: `http://link.springer.com/10.1007/s10236-015-0814-1`, doi:`10.1007/s10236-015-0814-1`.

Backhaus, J.O., 1985. A three-dimensional model for the simulation of shelf sea dynamics. Deutsche Hydrographische Zeitschrift 38, 165–187. doi:`10.1007/BF02328975`.

Bartholy, J., Pongrácz, R., Pattantyús-Ábrahám, M., 2009. Analyzing the genesis, intensity, and tracks of western Mediterranean cyclones. Theoretical and Applied Climatology 96, 133–144. doi:`10.1007/s00704-008-0082-9`.

Baxter, P.J., 2005. The east coast Big Flood, 31 January-1 February 1953: a summary of the human disaster. Philosophical transactions. Series A, Mathematical, physical, and engineering sciences 363, 1293–1312. doi:`10.1098/rsta.2005.1569`.

Bernardara, P., Andreewsky, M., Benoit, M., 2011. Application of regional frequency analysis to the estimation of extreme storm surges. Journal of Geophysical Research: Oceans 116, C02008. doi:`10.1029/2010JC006229`.

Bernier, N.B., Thompson, K.R., 2006. Predicting the frequency of storm surges and extreme sea levels in the northwest Atlantic. Journal of Geophysical Research: Oceans 111, C10009. doi:`10.1029/2005JC003168`.

Bromirski, P.D., Flick, R.E., Cayan, D.R., 2003. Storminess variability along the California coast: 1858-2000. Journal of Climate 16, 982–993. URL: `http://journals.ametsoc.org/doi/abs/10.1175/1520-0442(2003)016%`

`3CO982%3ASVATCC%3E2.0.CO%3B2`, doi:`10.1175/1520-0442(2003)016<0982:` `SVATCC>2.0.CO;2`.

Brown, J.M., Souza, A.J., Wolf, J., 2010. An 11-year validation of wave-surge modelling in the Irish Sea, using a nested POLCOMS-WAM modelling system. Ocean Modelling 33, 118–128. doi:`10.1016/j.ocemod.2009.12.006`.

Butler, A., Heffernan, J.E., Tawn, J.a., Flather, R.a., Horsburgh, K.J., 2007. Extreme value analysis of decadal variations in storm surge elevations. Journal of Marine Systems 67, 189–200. doi:`10.1016/j.jmarsys.2006.10.006`.

Calafat, F.M., Chambers, D.P., Tsimplis, M.N., 2012. Mechanisms of decadal sea level variability in the eastern North Atlantic and the Mediterranean Sea. Journal of Geophysical Research: Oceans 117, C09022. doi:`10.1029/2012JC008285`.

Calafat, F.M., Gomis, D., 2009. Reconstruction of Mediterranean sea level fields for the period 1945-2000. Global and Planetary Change 66, 225–234. doi:`10.1016/j.` `gloplacha.2008.12.015`.

Camus, P., Méndez, F.J., Losada, I.J., Menéndez, M., Espejo, A., Pérez, J., Rueda, A., Guanche, Y., 2014a. A method for finding the optimal predictor indices for local wave climate conditions. Ocean Dynamics 64, 1025–1038. doi:`10.1007/` `s10236-014-0737-2`.

Camus, P., Menéndez, M., Méndez, F.J., Izaguirre, C., Espejo, A., Cánovas, V., Pérez, J., Rueda, A., Losada, I.J., Medina, R., 2014b. A weather-type statistical downscaling framework for ocean wave climate. Journal of Geophysical Research: Oceans 119, 7389–7405. doi:`10.1002/2014JC010141`.

Carrère, L., Lyard, F., 2003. Modeling the barotropic response of the global ocean to atmospheric wind and pressure forcing - comparisons with observations. Geophysical Research Letters 30, 1275. doi:`10.1029/2002GL016473`.

Carretero Albiach, J.C., Alvarez Fanjul, E., Gómez Lahoz, M., Perez Gomez, B.n., Rodríguez Sanchez-Arevalo, I., 2000. Ocean forecasting in narrow shelf seas: Application to the Spanish coasts. Coastal Engineering 41, 269–293. doi:`10.1016/` `S0378-3839(00)00035-1`.

Casas-Prat, M., Wang, X.L., Sierra, J.P., 2014. A physical-based statistical method for modeling ocean wave heights. Ocean Modelling 73, 59–75. URL: `http://www.` `sciencedirect.com/science/article/pii/S1463500313001893`, doi:`10.1016/j.` `ocemod.2013.10.008`.

Cavicchia, L., von Storch, H., Gualdi, S., 2014. Mediterranean Tropical-Like Cyclones in Present and Future Climate. Journal of Climate 27, 7493–7501. doi:`10.1175/ JCLI-D-14-00339.1`.

Church, J., Clark, P., Cazenave, A., Gregory, J., Jevrejeva, S., Levermann, A., Merrifield, M., Milne, G., Nerem, R., Nunn, P., Payne, A., Pfeffer, W., Stammer, D., Unnikrishnan, A., 2013. Sea level change, in: Climate Change 2013: The Physical Science Basis. Contribution of Working Group I to the Fifth Assessment Report of the Intergovernmental Panel on Climate Change, pp. 1137–1216.

Cid, A., Castanedo, S., Abascal, A.J., Menéndez, M., Medina, R., 2014. A high resolution hindcast of the meteorological sea level component for Southern Europe: the GOS dataset. Climate Dynamics 43, 1–18. doi:`10.1007/s00382-013-2041-0`.

Coles, S., Bawa, J., Trenner, L., Dorazio, P., 2001. An introduction to statistical modeling of extreme values. volume 208. Springer Series in Statistics.

Compo, G.P., Whitaker, J.S., Sardeshmukh, P.D., Matsui, N., Allan, R.J., Yin, X., Gleason, B.E., Vose, R.S., Rutledge, G., Bessemoulin, P., BroNnimann, S., Brunet, M., Crouthamel, R.I., Grant, a.N., Groisman, P.Y., Jones, P.D., Kruk, M.C., Kruger, a.C., Marshall, G.J., Maugeri, M., Mok, H.Y., Nordli, O., Ross, T.F., Trigo, R.M., Wang, X.L., Woodruff, S.D., Worley, S.J., 2011. The Twentieth Century Reanalysis Project. Quarterly Journal of the Royal Meteorological Society 137, 1–28. doi:`10. 1002/qj.776`.

Dangendorf, S., Müller-Navarra, S., Jensen, J., Schenk, F., Wahl, T., Weisse, R., 2014. North sea storminess from a novel storm surge record since AD 1843. Journal of Climate 27, 3582–3595. doi:`10.1175/JCLI-D-13-00427.1`.

Dee, D.P., Uppala, S.M., Simmons, a.J., Berrisford, P., Poli, P., Kobayashi, S., Andrae, U., Balmaseda, M.a., Balsamo, G., Bauer, P., Bechtold, P., Beljaars, a.C.M., van de Berg, L., Bidlot, J., Bormann, N., Delsol, C., Dragani, R., Fuentes, M., Geer, a.J., Haimberger, L., Healy, S.B., Hersbach, H., Hólm, E.V., Isaksen, L., Kå llberg, P., Köhler, M., Matricardi, M., Mcnally, a.P., Monge-Sanz, B.M., Morcrette, J.J., Park, B.K., Peubey, C., de Rosnay, P., Tavolato, C., Thépaut, J.N., Vitart, F., 2011. The ERA-Interim reanalysis: Configuration and performance of the data assimilation system. Quarterly Journal of the Royal Meteorological Society 137, 553–597. doi:`10.1002/qj.828`.

Eric Jones, J., Davies, A.M., 2006. Application of a finite element model (TELEMAC) to computing the wind induced response of the Irish Sea. Continental Shelf Research 26, 1519–1541. doi:`10.1016/j.csr.2006.03.013`.

Espejo, A., Camus, P., Losada, I.n.J., Méndez, F.J., 2014. Spectral Ocean Wave Climate Variability Based on Atmospheric Circulation Patterns. Journal of Physical Oceanography 44, 2139–2152. URL: `http://journals.ametsoc.org/doi/abs/10.1175/JPO-D-13-0276.1`, doi:`10.1175/JPO-D-13-0276.1`.

Ferrarin, C., Roland, A., Bajo, M., Umgiesser, G., Cucco, A., Davolio, S., Buzzi, A., Malguzzi, P., Drofa, O., 2013. Tide-surge-wave modelling and forecasting in the Mediterranean Sea with focus on the Italian coast. Ocean Modelling 61, 38–48. doi:`10.1016/j.ocemod.2012.10.003`.

Flather, R., Smith, J., Richards, J., 1998. Direct Estimates of Extreme Storm Surge Elevations from a 40-Year Numerical Model Simulation and from Observations. The Global Atmosphere and Ocean System 6, 165–176.

Flather, R., Williams, J., 2000. Climate change effects on storm surges: methodologies and results.

Flather, R.a., 2000. Existing operational oceanography. Coastal Engineering 41, 13–40. doi:`10.1016/S0378-3839(00)00025-9`.

García-Lafuente, J., Del Río, J., Alvarez Fanjul, E., Gomis, D., Delgado, J., 2004. Some aspects of the seasonal sea level variations around Spain. Journal of Geophysical Research C: Oceans 109, 1–9. doi:`10.1029/2003JC002070`.

Giorgi, F., Christensen, J., Hulme, M., von Storch, H., Whetton, P., Jones, R., Mearns, L., Fu, C., Arritt, R., Bates, B., Benestad, R., Boer, G., Buishand, A., Castro, M., Chen, D., Cramer, W., Crane, R., Crossly, J., Dehn, M., Dethloff, K., Dippner, J., Emori, S., Francisco, R., Fyfe, J., Gerstengarbe, F., Gutowski, W., Gyalistras, D., Hanssen-Bauer, I., Hantel, M., Hassell, D., Heimann, D., Jack, C., Jacobeit, J., Kato, H., Katz, R., Kauker, F., Knutson, T., Lal, M., Landsea, C., Laprise, R., Leung, L., Lynch, A., May, W., McGregor, J., Miller, N., Murphy, J., Ribalaygua, J., Rinke, A., Rummukainen, M., Semazzi, F., Walsh, K., Werner, P., Widmann, M., Wilby, R., Wild, M., Xue, Y., 2001. Regional Climate Information- Evaluation and Projections. URL: `http://epic.awi.de/4973/`.

Gomis, D., Ruiz, S., Sotillo, M.G., Álvarez Fanjul, E., Terradas, J., 2008. Low frequency Mediterranean sea level variability: The contribution of atmospheric pressure and wind. Global and Planetary Change 63, 215–229. doi:`10.1016/j.gloplacha.2008.06.005`.

Gräwe, U., Burchard, H., 2012. Storm surges in the Western Baltic Sea: The present and a possible future. Climate Dynamics 39, 165–183. doi:`10.1007/s00382-011-1185-z`.

Haidvogel, D.B., Arango, H., Budgell, W.P., Cornuelle, B.D., Curchitser, E., Di Lorenzo, E., Fennel, K., Geyer, W.R., Hermann, a.J., Lanerolle, L., Levin, J., McWilliams, J.C., Miller, a.J., Moore, a.M., Powell, T.M., Shchepetkin, a.F., Sherwood, C.R., Signell, R.P., Warner, J.C., Wilkin, J., 2008. Ocean forecasting in terrain-following coordinates: Formulation and skill assessment of the Regional Ocean Modeling System. Journal of Computational Physics 227, 3595–3624. doi:`10.1016/j.jcp.2007.06.016`.

Haidvogel, D.B., Arango, H.G., Hedstrom, K., Beckmann, A., Malanotte-Rizzoli, P., Shchepetkin, A.F., 2000. Model evaluation experiments in the North Atlantic Basin: Simulations in nonlinear terrain-following coordinates. Dynamics of Atmospheres and Oceans 32, 239–281. doi:`10.1016/S0377-0265(00)00049-X`.

Haigh, I., Nicholls, R., Wells, N., 2010. Assessing changes in extreme sea levels: Application to the English Channel, 1900-2006. Continental Shelf Research 30, 1042–1055. doi:`10.1016/j.csr.2010.02.002`.

Haigh, I.D., Wijeratne, E.M.S., MacPherson, L.R., Pattiaratchi, C.B., Mason, M.S., Crompton, R.P., George, S., 2014. Estimating present day extreme water level exceedance probabilities around the coastline of Australia: Tides, extra-tropical storm surges and mean sea level. Climate Dynamics 42, 121–138. doi:`10.1007/s00382-012-1652-1`.

Hallegatte, S., Ranger, N., Mestre, O., Dumas, P., Corfee-Morlot, J., Herweijer, C., Wood, R.M., 2011. Assessing climate change impacts, sea level rise and storm surge risk in port cities: A case study on Copenhagen. Climatic Change 104, 113–137. doi:`10.1007/s10584-010-9978-3`.

Jacob, D., Podzun, R., 1997. Sensitivity studies with the regional climate model REMO. Meteorology and Atmospheric Physics 63, 119–129. doi:`10.1007/BF01025368`.

Jordà, G., Gomis, D., Álvarez Fanjul, E., Somot, S., 2012. Atmospheric contribution to Mediterranean and nearby Atlantic sea level variability under different climate change scenarios. Global and Planetary Change 80-81, 198–214. doi:`10.1016/j.gloplacha.2011.10.013`.

Kalnay, E., Kanamitsu, M., Kistler, R., Collins, W., Deaven, D., Gandin, L., Iredell, M., Saha, S., White, G., Woollen, J., Zhu, Y., Chelliah, M., Ebisuzaki, W., Higgins, W., Janowiak, J., Mo, K.C., Ropelewski, C., Wang, J., Leetmaa, A., Reynolds, R., Jenne, R., Joseph, D., 1996. The NCEP/NCAR 40-year reanalysis project. Bulletin of the American Meteorological Society 77, 437–471. doi:`10.1175/1520-0477(1996)077<0437:TNYRP>2.0.CO;2`.

Lionello, P., 2012. The Climate of the Mediterranean Region From the Past to the Future. 1 st editi ed., Elsevier. doi:`10.1016/B978-0-12-416042-2.00009-4`.

Losada, I.J., Reguero, B.G., Méndez, F.J., Castanedo, S., Abascal, a.J., Mínguez, R., 2013. Long-term changes in sea-level components in Latin America and the Caribbean. Global and Planetary Change 104, 34–50. doi:`10.1016/j.gloplacha.2013.02.006`.

Lowe, J.a., Gregory, J.M., Flather, R.a., 2001. Changes in the occurrence of storm surges around the United Kingdom under a future climate scenario using a dynamic storm surge model driven by Hadley Centre climate models. Climate Dynamics 18, 179–188. doi:`10.1007/s003820100163`.

Luceño, A., Menéndez, M., Méndez, F.J., 2006. The effect of temporal dependence on the estimation of the frequency of extreme ocean climate events. Proceedings of the Royal Society A: Mathematical, Physical and Engineering Sciences 462, 1683–1697. doi:`10.1098/rspa.2005.1652`.

Lynch, D.R., Gray, W.G., 1979. A wave equation model for finite element tidal computations. Computers & Fluids 7, 207–228. URL: `http://www.sciencedirect.com/science/article/pii/0045793079900379`, doi:`10.1016/0045-7930(79)90037-9`.

Marcos, M., Jordà, G., Gomis, D., Pérez, B.n., 2011. Changes in storm surges in southern Europe from a regional model under climate change scenarios. Global and Planetary Change 77, 116–128. doi:`10.1016/j.gloplacha.2011.04.002`.

Marcos, M., Tsimplis, M.N., 2007. Variations of the seasonal sea level cycle in southern Europe. Journal of Geophysical Research: Oceans 112, 2007. doi:`10.1029/2006JC004049`.

Marcos, M., Tsimplis, M.N., Shaw, A.G.P., 2009. Sea level extremes in southern Europe. Journal of Geophysical Research: Oceans 114, 1–16. doi:`10.1029/2008JC004912`.

Méndez, F.J., Menéndez, M., Luceño, A., Losada, I.J., 2006. Estimation of the long-term variability of extreme significant wave height using a time-dependent Peak Over Threshold (POT) model. Journal of Geophysical Research: Oceans 111, C07024. doi:`10.1029/2005JC003344`.

Méndez, F.J., Menéndez, M., Luceño, A., Losada, I.J., 2007. Analyzing monthly extreme sea levels with a time-dependent GEV model. Journal of Atmospheric and Oceanic Technology 24, 894–911. doi:`10.1175/JTECH2009.1`.

Menendez, M., García-Díez, M., Fita, L., Fernández, J., Méndez, F.J., Gutiérrez, J.M., 2014. High-resolution sea wind hindcasts over the Mediterranean area. Climate Dynamics 42, 1857–1872. doi:`10.1007/s00382-013-1912-8`.

Menendez, M., Mendez, F.J., Losada, I.J., 2009. Forecasting seasonal to interannual variability in extreme sea levels. ICES Journal of Marine Science 66, 1490–1496. doi:`10.1093/icesjms/fsp095`.

Menéndez, M., Méndez, F.J., Losada, I.J., Graham, N.E., 2008. Variability of extreme wave heights in the northeast Pacific Ocean based on buoy measurements. Geophysical Research Letters 35, L22607. doi:`10.1029/2008GL035394`.

Menéndez, M., Woodworth, P.L., 2010. Changes in extreme high water levels based on a quasi-global tide-gauge data set. Journal of Geophysical Research: Oceans 115, 1–15. doi:`10.1029/2009JC005997`.

Merrifield, M.a., Genz, A.S., Kontoes, C.P., Marra, J.J., 2013. Annual maximum water levels from tide gauges: Contributing factors and geographic patterns. Journal of Geophysical Research: Oceans 118, 2535–2546. doi:`10.1002/jgrc.20173`.

Mudersbach, C., Jensen, J., 2010. Nonstationary extreme value analysis of annual maximum water levels for designing coastal structures on the German North Sea coastline. Journal of Flood Risk Management 3, 52–62. URL: `http://doi.wiley.com/10.1111/j.1753-318X.2009.01054.x`, doi:`10.1111/j.1753-318X.2009.01054.x`.

Müller-Navarra, S.H., Giese, H., 1999. Improvements of an empirical model to forecast wind surge in the German Bight. Deutsche Hydrographische Zeitschrift 51, 385–405. URL: `http://link.springer.com/10.1007/BF02764162`, doi:`10.1007/BF02764162`.

Pascual, A., Marcos, M., Gomis, D., 2008. Comparing the sea level response to pressure and wind forcing of two barotropic models: Validation with tide gauge and altimetry data. Journal of Geophysical Research: Oceans 113, C07011. doi:`10.1029/2007JC004459`.

Pawlowicz, R., Beardsley, B., Lentz, S., 2002. Classical tidal harmonic analysis including error estimates in MATLAB using TDE. Computers and Geosciences 28, 929–937. doi:`10.1016/S0098-3004(02)00013-4`.

Raicich, F., 2003. Recent evolution of sea-level extremes at Trieste (Northern Adriatic). Continental Shelf Research 23, 225–235. doi:`10.1016/S0278-4343(02)00224-8`.

Ratsimandresy, a.W., Sotillo, M.G., Carretero Albiach, J.C., Álvarez Fanjul, E., Hajji, H., 2008. A 44-year high-resolution ocean and atmospheric hindcast for the Mediterranean Basin developed within the HIPOCAS Project. Coastal Engineering 55, 827–842. doi:`10.1016/j.coastaleng.2008.02.025`.

Ray, R.D., 1999. A Global Ocean Tide Model From TOPEX/POSEIDON Altimetry: GOT99.2. Technical Report. NASA Goddard Space Flight Center. doi:`1999-209478`.

Sebastião, P., Guedes Soares, C., Alvarez, E., 2008. 44 years hindcast of sea level in the Atlantic Coast of Europe. Coastal Engineering 55, 843–848. doi:`10.1016/j.coastaleng.2008.02.022`.

Serafin, K.A., Ruggiero, P., 2014. Simulating extreme total water levels using a time-dependent, extreme value approach. Journal of Geophysical Research: Oceans 119, 6305–6329. URL: `http://doi.wiley.com/10.1002/2014JC010093`, doi:`10.1002/2014JC010093`.

Shchepetkin, A.F., McWilliams, J.C., 2005. The regional oceanic modeling system (ROMS): A split-explicit, free-surface, topography-following-coordinate oceanic model. Ocean Modelling 9, 347–404. doi:`10.1016/j.ocemod.2004.08.002`.

Skamarock, W.C., Klemp, J., Dudhia, J., Gill, D., Barjer, D., Duda, M., Huang, X., Wang, W., Powers, J., 2008. A description of the advanced research WRF verson 3. NCAR Tech Note NCAR/TN-475+STR.

Smith, W.H., Sandwell, D.T., 1997. Global Sea Floor Topography from Satellite Altimetry and Ship Depth Soundings. Science 277, 1956–1962. URL: `http://www.sciencemag.org/content/277/5334/1956.abstract`, doi:`10.1126/science.277.5334.1956`.

Storch, H., Woth, K., 2008. Storm surges: Perspectives and options. Sustainability Science 3, 33–43. doi:`10.1007/s11625-008-0044-2`.

Tebaldi, C., Strauss, B.H., Zervas, C.E., 2012. Modelling sea level rise impacts on storm surges along US coasts. Environmental Research Letters 7, 014032. doi:`10.1088/1748-9326/7/1/014032`.

Trigo, I.F., Davies, T.D., Bigg, G.R., 1999. Objective climatology of cyclones in the Mediterranean region. Journal of Climate 12, 1685–1696. doi:`10.1175/1520-0442(1999)012<1685:OCOCIT>2.0.CO;2`.

Tsimplis, M., 1997. Extreme Sea-level Distribution and Return Periods in the Aegean and Ionian Seas. Estuarine, Coastal and Shelf Science 44, 79–89. doi:`10.1006/ecss.1996.0126`.

Tsimplis, M., Baker, T., 2000. Sea level drop in the Mediterranean Sea: an indicator of deep water salinity and temperature changes? Geophysical Research Letters 27, 1731–1734.

Tsimplis, M.N., Álvarez Fanjul, E., Gomis, D., Fenoglio-Marc, L., Pérez, B., 2005. Mediterranean Sea level trends: Atmospheric pressure and wind contribution. Geophysical Research Letters 32, 1–4. doi:`10.1029/2005GL023867`.

Volkov, D.L., Larnicol, G., Dorandeu, J., 2007. Improving the quality of satellite altimetry data over continental shelves. Journal of Geophysical Research 112, C06020. doi:`10.1029/2006JC003765`.

Šepić, J., Vilibić, I., Strelec Mahovi, N., 2012. Northern Adriatic meteorological tsunamis: Observations, link to the atmosphere, and predictability. Journal of Geophysical Research: Oceans 117, C02002. doi:`10.1029/2011JC007608`.

Wahl, T., Chambers, D.P., 2015. Evidence for multidecadal variability in US extreme sea level records. Journal of Geophysical Research: Oceans 120, 1527–1544. URL: `http://doi.wiley.com/10.1002/2014JC010443`, doi:`10.1002/2014JC010443`.

Wakelin, S.L., Proctor, R., 2002. The impact of meteorology on modelling storm surges in the Adriatic Sea. Global and Planetary Change 34, 97–119. doi:`10.1016/S0921-8181(02)00108-X`.

Wakelin, S.L., Woodworth, P.L., Flather, R.A., Williams, J.A., L., W.P.W.S.W.P.W.S., L., W.P.W.S.W.P.W.S., A., F.R., A., W.J., Wakelin, S.L., Woodworth, P.L., Flather, R.A., Williams, J.A., 2003. Sea-level dependence on the NAO over the NW European Continental Shelf. Geophysical Research Letters 30, 1403. URL: `http://doi.wiley.com/10.1029/2003GL017041`, doi:`10.1029/2003GL017041`.

Wang, S., McGrath, R., Hanafin, J., Lynch, P., Semmler, T., Nolan, P., 2008. The impact of climate change on storm surges over Irish waters. Ocean Modelling 25, 83–94. doi:`10.1016/j.ocemod.2008.06.009`.

Wang, X.L., Feng, Y., Compo, G.P., Swail, V.R., Zwiers, F.W., Allan, R.J., Sardeshmukh, P.D., 2013. Trends and low frequency variability of extra-tropical cyclone activity in the ensemble of twentieth century reanalysis. Climate Dynamics 40, 2775–2800. URL: `http://link.springer.com/10.1007/s00382-012-1450-9`, doi:`10.1007/s00382-012-1450-9`.

Wang, X.L., Feng, Y., Swail, V.R., 2012. North Atlantic wave height trends as reconstructed from the 20th century reanalysis. Geophysical Research Letters 39, n/a–n/a. URL: `http://doi.wiley.com/10.1029/2012GL053381`, doi:`10.1029/2012GL053381`.

Wang, X.L., Swail, V.R., Cox, A., 2010. Dynamical versus statistical downscaling methods for ocean wave heights. International Journal of Climatology , n/a–n/aURL: `http://doi.wiley.com/10.1002/joc.1899`, doi:`10.1002/joc.1899`.

Woodworth, P.L., Blackman, D.L., 2004. Evidence for systematic changes in extreme high waters since the mid-1970s. Journal of Climate 17, 1190–1197. doi:`10.1002/joc.761`.

Woodworth, P.L., Flather, R.a., Williams, J.a., Wakelin, S.L., Jevrejeva, S., 2007. The dependence of UK extreme sea levels and storm surges on the North Atlantic Oscillation. Continental Shelf Research 27, 935–946. doi:`10.1016/j.csr.2006.12.007`.

Woolf, D., Shaw, A., Tsimplis, M., 2003. The influence of the North Atlantic Oscillation on sea-level variability in the North Atlantic region. doi:`10.1080/10236730310001633803`.

Woth, K., Weisse, R., Von Storch, H., 2006. Climate change and North Sea storm surge extremes: An ensemble study of storm surge extremes expected in a changed climate projected by four different regional climate models. Ocean Dynamics 56, 3–15. doi:`10.1007/s10236-005-0024-3`.

Yan, Z., Tsimplis, M.N., Woolf, D., 2004. Analysis of the relationship between the North Atlantic oscillation and sea-level changes in northwest Europe. International Journal of Climatology 24, 743–758. doi:`10.1002/joc.1035`.